united nations
educational, scientific
and cultural
organization

international atomic
energy agency

the
abdus salam
international centre for theoretical physics

SMR: 1343/1

EU ADVANCED COURSE IN COMPUTATIONAL NEUROSCIENCE

An IBRO Neuroscience School

(30 July - 24 August 2001)

"Dissection of Nonlinear Neuronal Dynamics"

presented by:

John RINZEL

Centre for Neural Science
New York University
4 Washington Place, Rm. 809
New York, NY 10003
U.S.A.

Refces for Trieste Lectures

Rinzel, J & Ermentrout GB: Analysis of neural excitability & oscillations. In: Methods in Neuronal Modeling (eds. Koch + Segev) MIT Press, 2nd ed, 1998. *

Koch, C: Biophysics of Computation. Oxford Univ Press, 1998. (cellular neurophysics, biophysics & modeling).

Johnston, D & Wu, S: Foundations of Cellular Neurophysiology. MIT Press, 1995.

Strogatz, SH: Nonlinear Dynamics & Chaos. Addison-Wesley, 1994

Software (for integrating & analyzing ode models)

XPPAUT — ftp.math.pitt.edu/pub/bardware

also "Mesh3" — is the Rinzel/Ermentrout chapter

also XPPTut is tutorial (interactive) for XPPAUT

* Contains many other useful chapters.

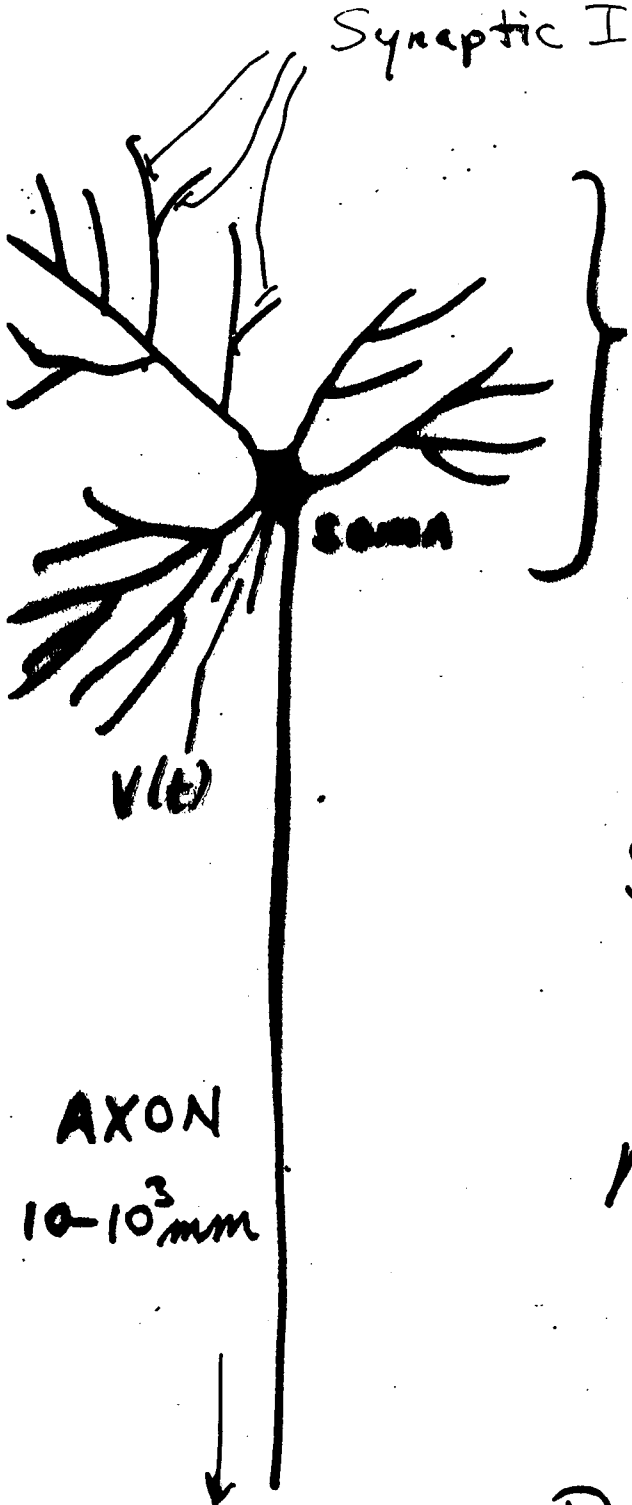

"Classical" neuron

Signals: $V_m \sim 100$ mV
ionic currents
O(msec)

Membrane with pores—
variable over
surface.

Dendrites — graded
potentials.

Axon — characteristic
impulses.

Neglect spatial
structure for
this lecture

Outline

- Hodgkin & Huxley & membrane current
- Action Potentials (in the phase plane)
- Bursting Oscillations
- Collective Rhythms

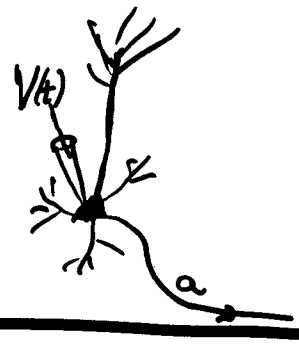

Excitability

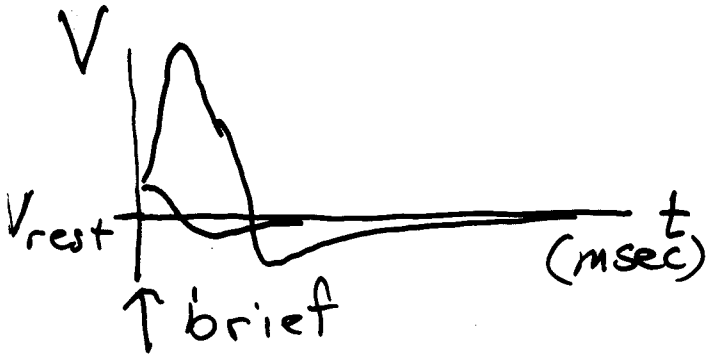

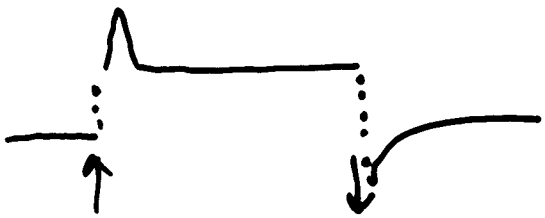

Bistability

Repetitive Firing

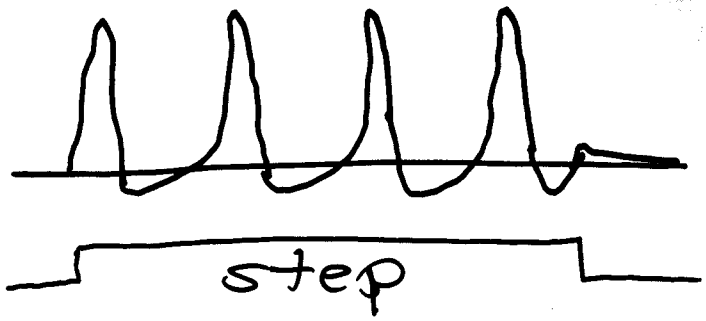

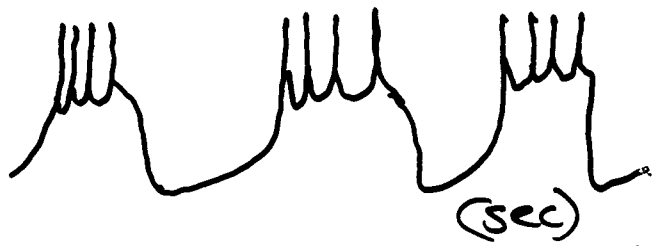

Bursting (endogenous)

umd

Excitability

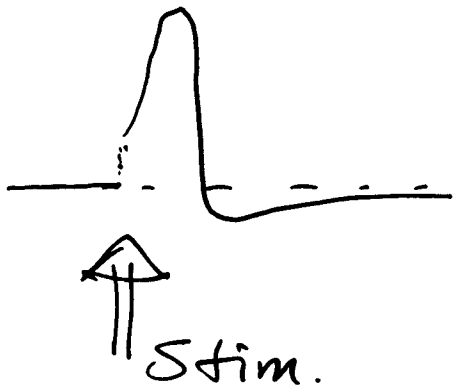

and

Rhythmicity

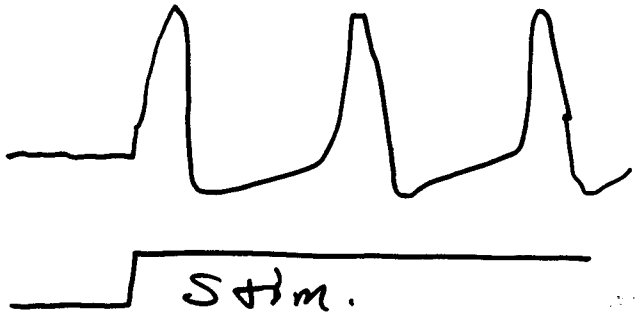

||

fast autocatalytic/
regenerative process

⊕

slow negative feedback

perhaps multiple time scales.

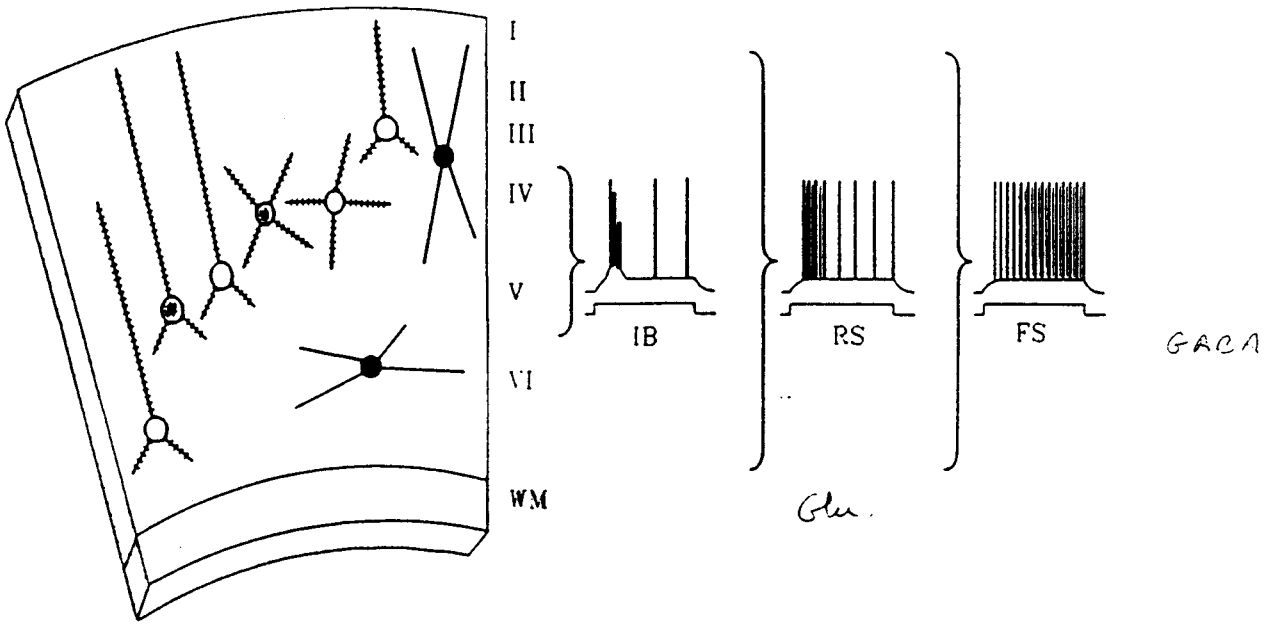

Fig. 4. *Schematic summary of correlations between intrinsic physiology and anatomy of rodent neocortical neurons. RS neurons (open symbols) are spiny cells, either pyramidal or stellate, distributed through layers II through VI. FS neurons (filled symbols) are aspiny or sparsely spiny non-pyramidal cells, with presumed GABAergic inhibitory function, also distributed through layers II through VI. IB neurons (shaded symbols) are restricted to layers IV and V, and are also spiny cells of pyramidal or stellate morphology. Neurons of layer I have not been studied physiologically. Braces on the right summarize the laminar distributions of the three neuron types, and illustrate a typical firing pattern of each. WM, white matter.*

shown that cells generating monosynaptic, GABA-mediated IPSPs onto follower neurons have significantly faster spikes than those cells generating monosynaptic EPSPs[12] (Fig. 2). It is still quite possible that there exist types of neocortical GABAergic neurons that are not FS cells, as suggested for the hippocampus[21]. However, the data strongly suggest that every FS neuron encountered in the neocortex is a GABAergic inhibitory cell.

The data are too scant to ascertain whether classification into three types of neurons on the basis of intrinsic physiological properties is generally applicable to all cortical areas and all species. Analogous neuronal classes have been described for the dorsal cerebral cortex of turtles, where pyramidal-shaped cells generate RS-like or IB-like activity and non-pyramidal interneurons generate FS-like activity[22]. Thus it is likely that this separation arose early in forebrain evolution, and may now be widespread. All three classes have been repeatedly observed in rodent neocortex (i.e. mice, rats and guinea-pigs), as described above. Mountcastle's original description of FS and RS neurons applied to monkey neocortex, and human neocortex also has both FS and RS cells (Ref. 23; McCormick, D. A., unpublished observations). The prevalence of IB cells across species is less well described. They have not been observed in extensive investigations of layer V neurons in cat sensorimotor cortex *in vitro*[18]; however, these studies targeted only the largest (presumed Betz) cells by using microelectrodes with large tip diameters. An earlier study of cat pyramidal tract cells *in vivo* described some features of the rhythmic IB cells seen in rodents (see Fig. 6C in Ref. 6). There are at least two preliminary reports of IB neurons in human neocortex[23,24]. Figure 4 schematically depicts the general distribution of neuron classes in neocortex, based largely upon studies in rodents.

There are several morphological classes of neocortical neurons whose intrinsic physiological properties have not yet been examined[2]. These include the small population of non-GABAergic, non-pyramidal neurons (notably peptidergic bipolar cells) and the assorted enigmatic neurons of layer I, many of which are GABAergic. Also, neurons of layer VI have been only sparsely studied. Finally, it would be of great interest to know whether the diversity of anatomy and biochemistry among GABAergic neurons[2] is paralleled by a diversity of intrinsic firing patterns[21].

Significance of diverse intrinsic firing patterns in neocortex

The intrinsic physiological properties of a neuron's membrane play a central role in determining (1) how it transforms the information it receives into an output pattern, (2) how these transformations are modulated by humoral or environmental factors, and (3) whether (and with what pattern) the neuron generates spontaneous activity. Since these properties can vary widely from neuron to neuron, knowledge of the quirks of each cell type is an essential step in unraveling the functions of a neural circuit[25]. In the neocortex, it is evident that RS cells will attenuate prolonged excitatory stimuli while favoring the transmission of phasic ones; by contrast, FS cells offer a wide-band responsiveness and, if necessary, sustained high-frequency output. The complexities of IB cell behavior suggest more varied possibilities. Near threshold for firing they have very high gains,

Electrical Activity of Cells

- $V = V(x,t)$, distribution within cell (uniform or not?, propagation?)
- coupling to other cells
- nonlinearities
- time scales

$$C_m \frac{\partial V}{\partial t} + I_{ion}(V) = \frac{1}{r_i}\frac{\partial^2 V}{\partial x^2} + I_{app} + \text{coupling}$$

capacitive (under $C_m \frac{\partial V}{\partial t}$); channels (under $I_{ion}(V)$); cable properties (under $\frac{1}{r_i}\frac{\partial^2 V}{\partial x^2}$); other cells (under coupling)

"coupling": $\sum_j \frac{1}{r_{c,j}}(V_j - V)$ — "electrical, gap junctions"

(j = other cells)

: $\sum_j g_{syn,j}(V_j(t))(V_{syn} - V)$ — chemical synapse

$$I_{ion} = I_{ion}(V, \underset{\sim}{w}) \qquad \text{generally nonlinear}$$

$$= \sum_k g_k(V, \underset{\sim}{w})(V - V_k)$$

k ← channel types

$$\frac{\partial \underset{\sim}{w}}{\partial t} = G(V, \underset{\sim}{w})$$

- Time Scales
- Excitability: fast autocatalytic + slow neg fdbk
- Explore parameter space — XPP helpful — before [illegible] [illegible]
- Minimal models
- Think generally — I.e. relative [illegible]

HH recipe

- V-clamp → I_{ion} components
- predict I-clamp behavior?

B PHARMACOLOGICAL BLOCKAGE

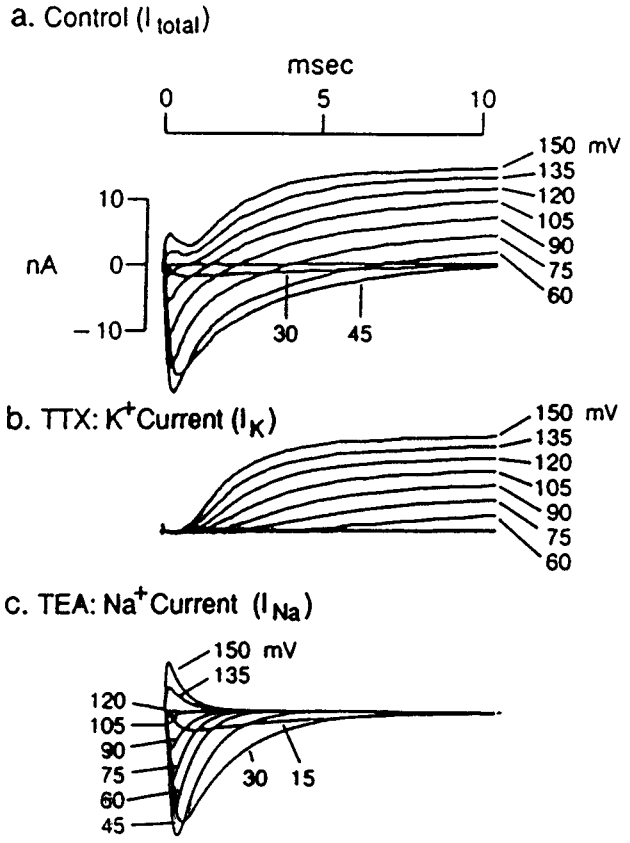

Figure 7. *B*, Separation of ionic currents by use of nerve poisons. *a*, Response in normal seawater; different amplitudes of voltage steps are indicated on the right (in mV). *b*, Response due to I_K when I_{Na} is blocked by tetrodotoxin (TTX). *c*, Response due to I_{Na} when I_K is blocked by tetraethylammonium (TEA). (From Hille, 1977).

ing into the cell) followed by an outward movement of positive current (see Figure 9; solid line).

At this point, we need to define a bit of terminology that will be useful. In simple terms, ionic current through excitable membranes is controlled by two factors: (1) an ion-selective pore through which only certain ions can flow, and (2) a gate or gates that open(s) and close(s) the pore to allow ionic flux. The turning on of a current is known as the *activation* of the current and the opposite of activation is known as *deactivation*. These processes occur when an *activation gate* opens or closes. If a current turns on and then off despite a constant change in membrane potential, it is said to *inactivate*. The reverse of inactivation is *deinactivation*. Inactivation and

Generally — Ionic currents written in HH-form : current of type "j":

$$I_{ion,j} = \bar{g}_j m_j^p h_j^q (V - V_j)$$

$V_j = z_j \frac{RT}{F} \ln \frac{[j]_{out}}{[j]_{in}}$

m_j — activ^n gates — fraction "ON"

h_j — inactiv^n gates — fraction "ON"
(in this case, the "ON" inactivation gates close the "j" channels)

Na^+: $V_{Na} \approx +55_m$
K^+: $V_K \approx -70_m$

Kinetic description : gate "X" —

x = fraction X-gates that are "ON"
$1-x$ = " " "OFF"

OFF $\underset{\beta(V)}{\overset{\alpha(V)}{\rightleftharpoons}}$ ON

$$\dot{x} = \alpha(V)(1-x) - \beta(V)\, x$$

α, β have units $1/msec$

$\bar{g}_j$ = cond^{tc} per area if all j-ch^s are open, units in S/cm^2

$= \hat{g}_j \rho_j$ $\quad \hat{g}_j$ single ch. cond^{tc}

ρ_j — density of ch^s

V_j = reversal potential for ions carrying current "j".

Gating variables — equilibrium fns.

$$\dot{m} = \alpha_m (1-m) - \beta_m m$$

$$= \frac{m_\infty(v) - m}{\tau_m(v)}$$

$$m_\infty(v) = \frac{\alpha_m(v)}{\alpha_m(v) + \beta_m(v)} \qquad \tau_m(v) = \frac{1}{\alpha_m(v) + \beta_m(v)}$$

Often written as

$$m_\infty(v) = \frac{1}{1 + e^{\frac{\theta - v}{k}}}$$

θ — position

$4k$ — slope^{-1}

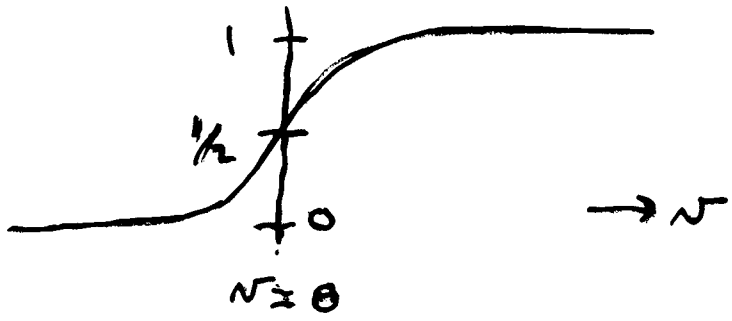

$k < 0 \Rightarrow$

$$\tau_m(v) = \frac{1}{2} \frac{1}{\cosh\left(\frac{\theta - v}{k}\right)}$$

HH Eqns

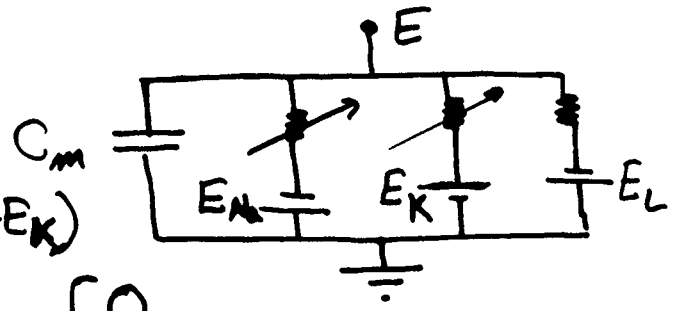

$$C_m \frac{dE}{dt} + \bar{g}_{Na} m^3 h (E - E_{Na}) + \bar{g}_K n^4 (E - E_K) + g_L (E - E_L) + I_{app} = \begin{cases} 0 \\ \frac{d}{4R} \frac{\partial^2 E}{\partial x^2} \end{cases}$$

– cable w/o space clamp

$$\frac{dm}{dt} = \phi \frac{m_\infty(E) - m}{\tau_m(E)}$$

$$\frac{dh}{dt} = \phi \cdots$$

$$\frac{dn}{dt} = \phi \cdots$$

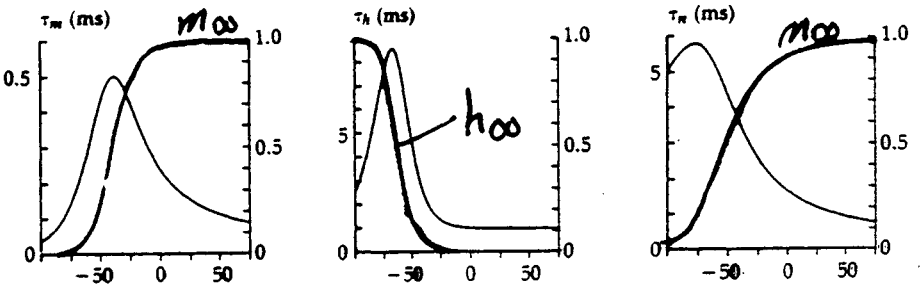

$\phi \sim$ Temperature

Reconstruct action potential

Time course
Velocity
Threshold
Refractory period
Repetitive firing
Ion fluxes
⋮

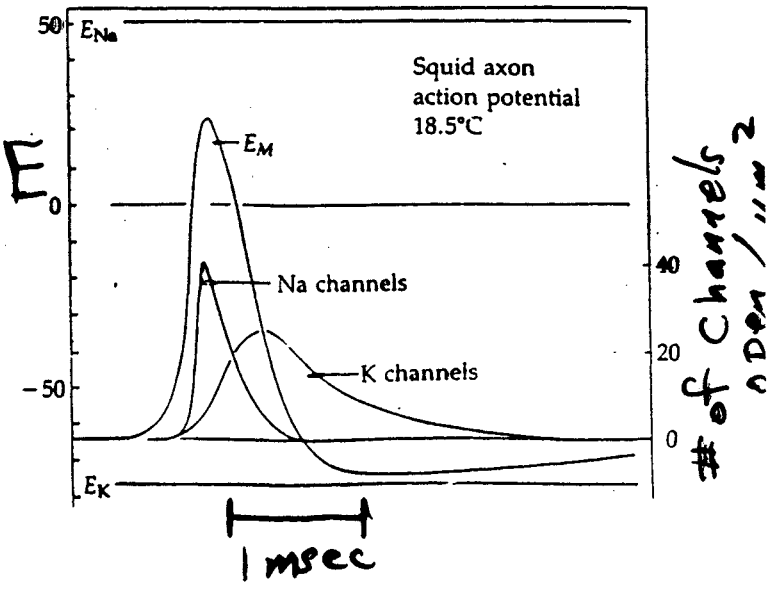

Bullfrog sympathetic ganglion "B" cell

(Yamada, Koch, Adams – 1989)

30 μm

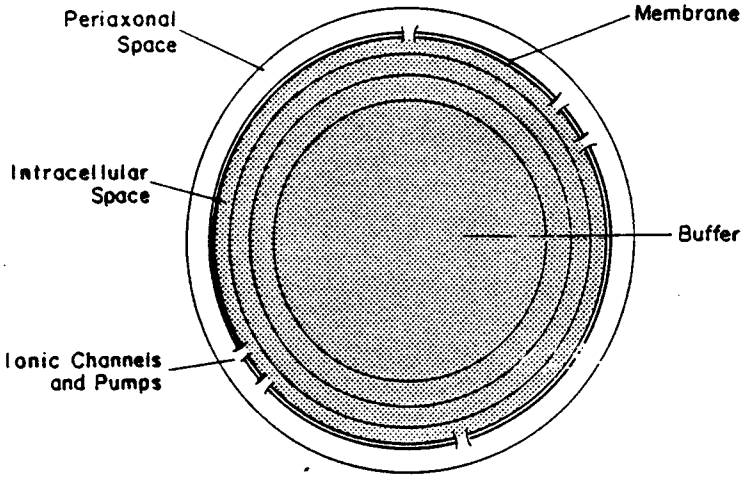

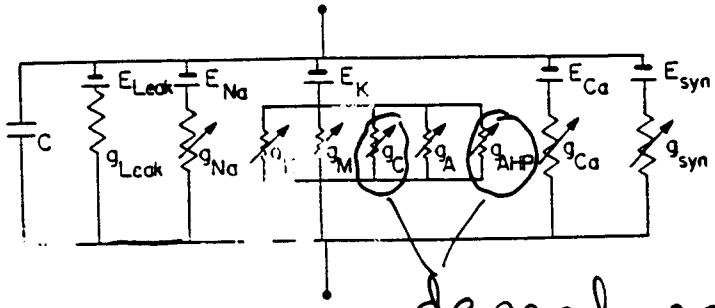

depend on $[Ca^{2+}]_{int}$

"HH" circuit

+ $[Ca^{2+}]_{int}$

+ $[K^+]_{ext}$

vmd

Review of channel types, properties, + where found.

R. R. Llinás: The intrinsic electrophysiological properties of mammalian neurons: insights into CNS function.

Science 242 (1988) 1654-1663.

Cortical pyramidal neuron.

- Complex branching geometry
- Non uniformly distrib^{d} channel densities

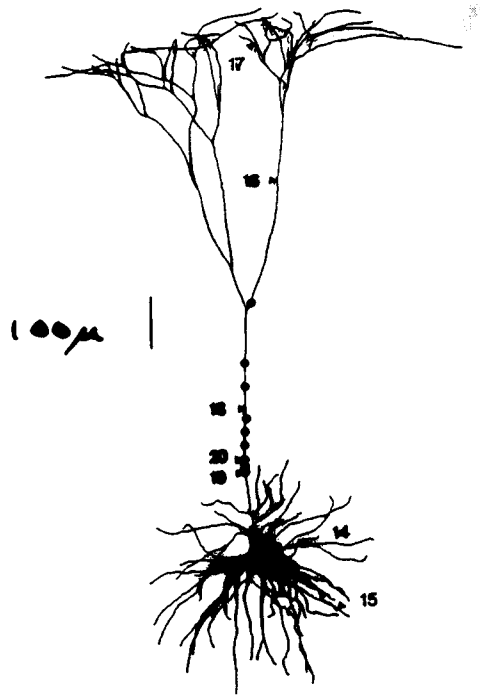

(Koch, Douglas, Wehmeier '90)

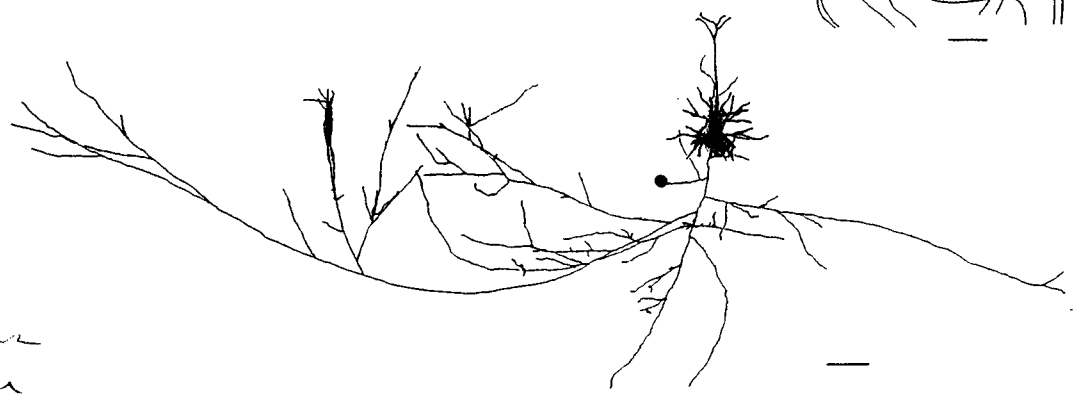

Many examples non-uniform properties in neurobiology — anatomy & physiology

Pyramidal neuron & axonal arbor
(Schwark & Jones, '89)

I-V relations: $I_{ss}(V)$, $I_{inst}(V)$

steady state — instantaneous

$$I_{ss}(V) = \bar{g}_{Na} m_\infty^3(V) h_\infty(V)(V-V_{Na}) + \bar{g}_K n_\infty^4(V)(V-V_K) + \bar{g}_L(V-V_L)$$

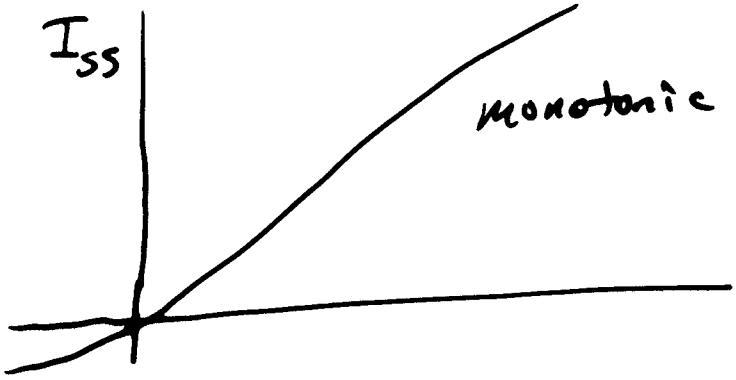

$$I_{inst.}(V) = \bar{g}_{Na} m_\infty^3(V)\, h\,(V-V_{Na}) + \bar{g}_K n^4 (V-V_K) + \bar{g}_L(V-V_L)$$

fast — slow — fixed at holding values

e.g. rest.

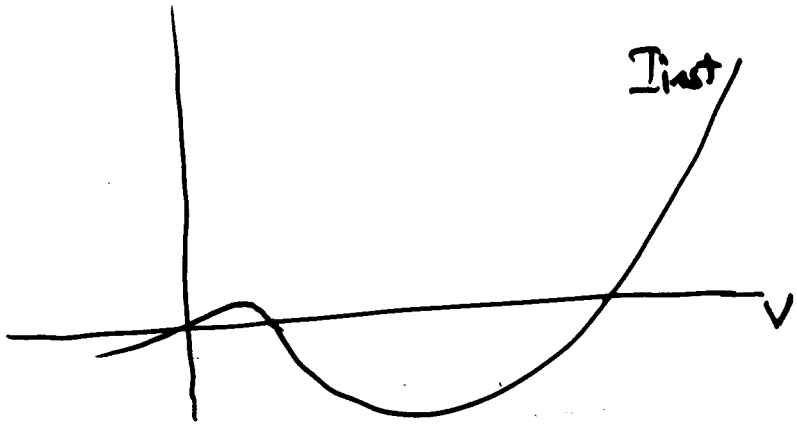

h, n at rest values

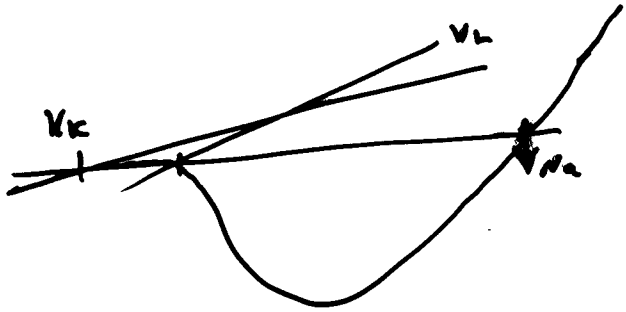

Dissecting the AP

$$C_m \frac{dV}{dt} = -I_{inst}(V; h, n) + I$$

h, n slow m fast

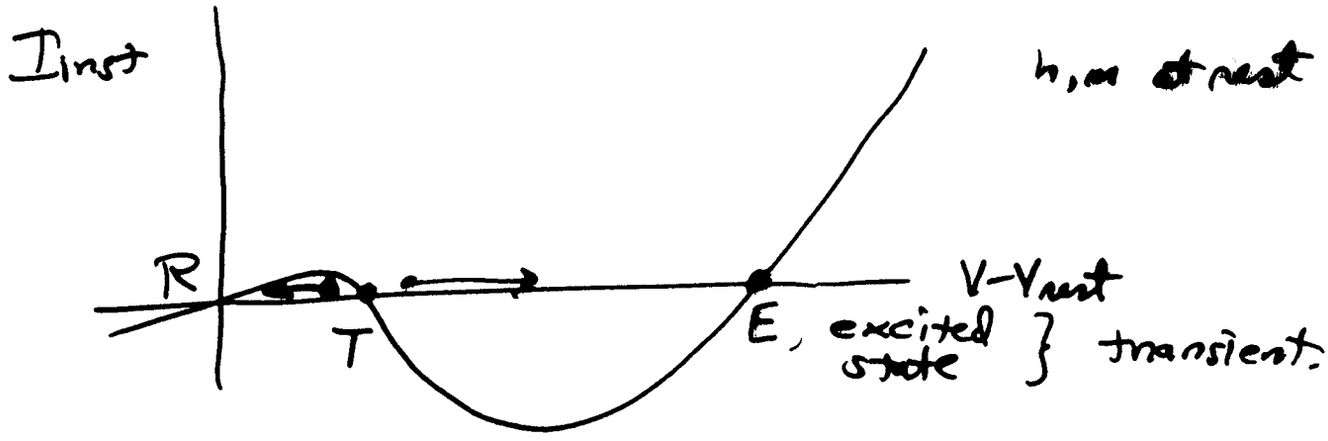

V → depolarizes → E ⇒ h ↓, n ↑

⇒ Iinst ↑

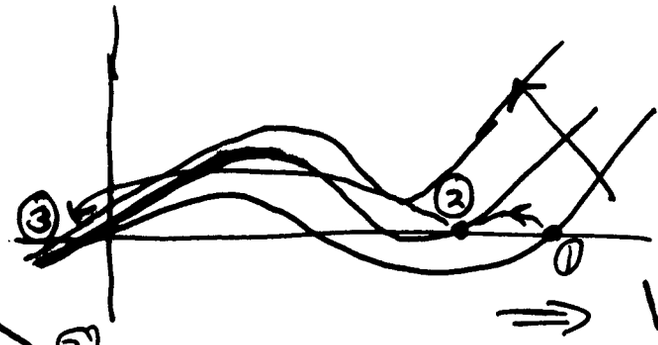

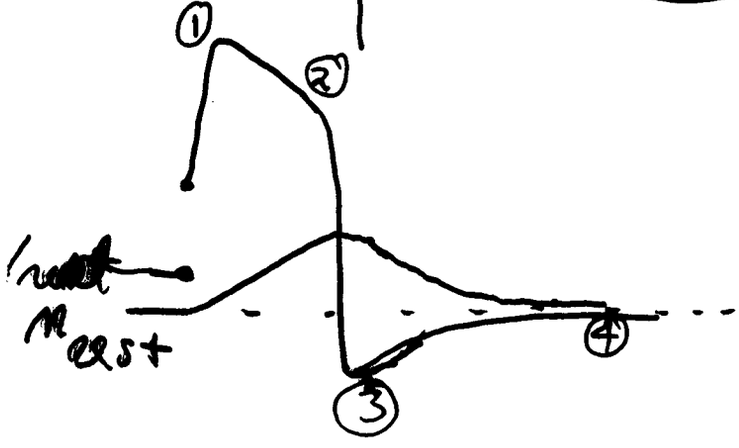

w/ V hyperpolarized

h ↑, n ↓

⇒ Iinst ↓

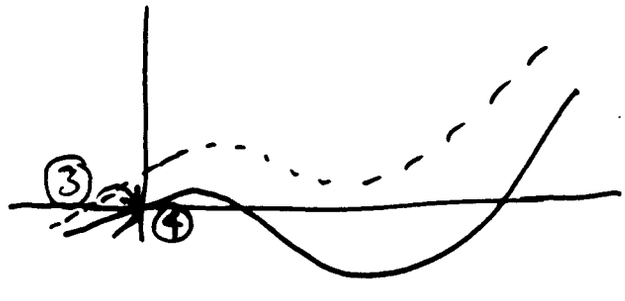

2 variable model system

Morris-Lecar ('81) – barnacle muscle

I_{Ca} – fast, non-inactivating

I_K – delayed rectifier

pseudo inactiv^n: $(1-w)$

$$C\frac{dV}{dt} = -\bar{g}_{Ca}\, m_\infty(V)(V-V_{Ca}) - \bar{g}_K\, w\,(V-V_K) - g_L(V-V_L) + I$$

$$\frac{dw}{dt} = \phi\,\frac{w_\infty(V)-w}{\tau_w(V)}$$

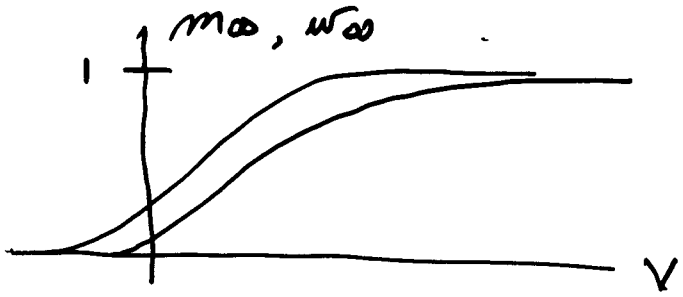

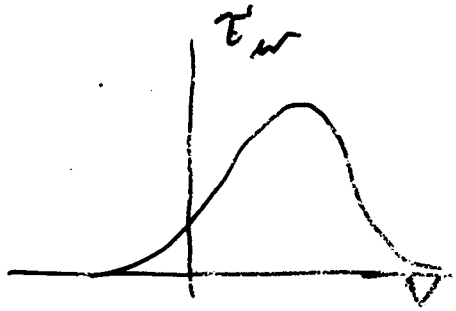

CNS92
3 MAY

Phase Plane & Attractors

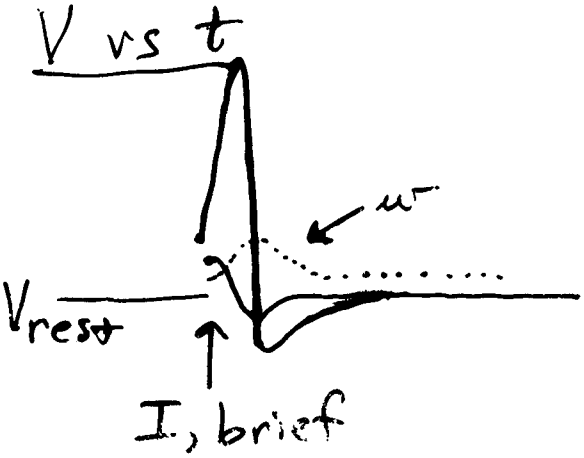

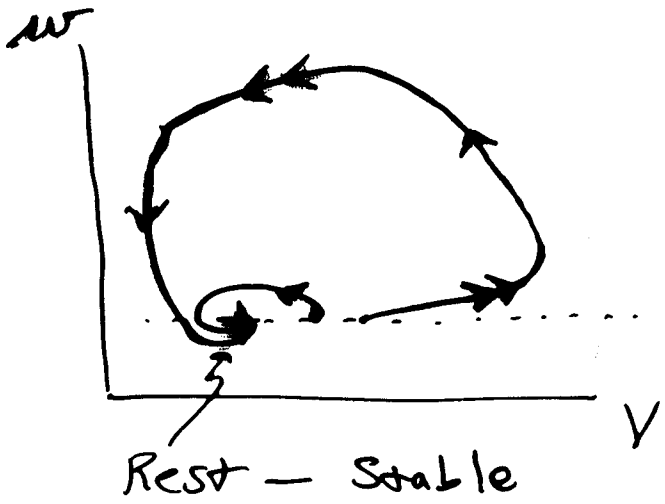

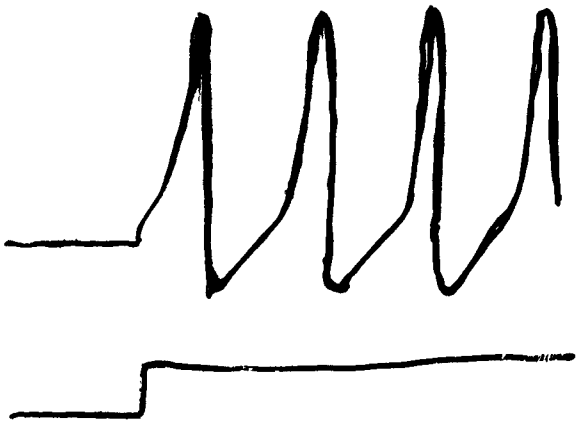

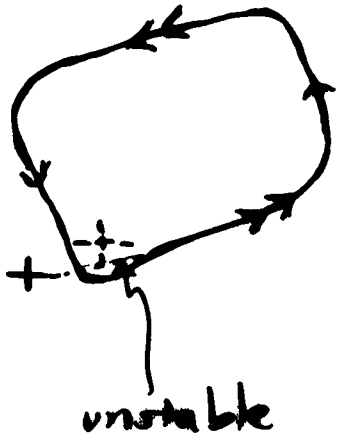

Effect of Perturbations

P.P. Analysis

threshold
adaptation
max Rate

time scale in PP—
draw w/ dots

CNS 92
A31
2

Recovery process — $w \propto g_K$

is slow — consider as param.

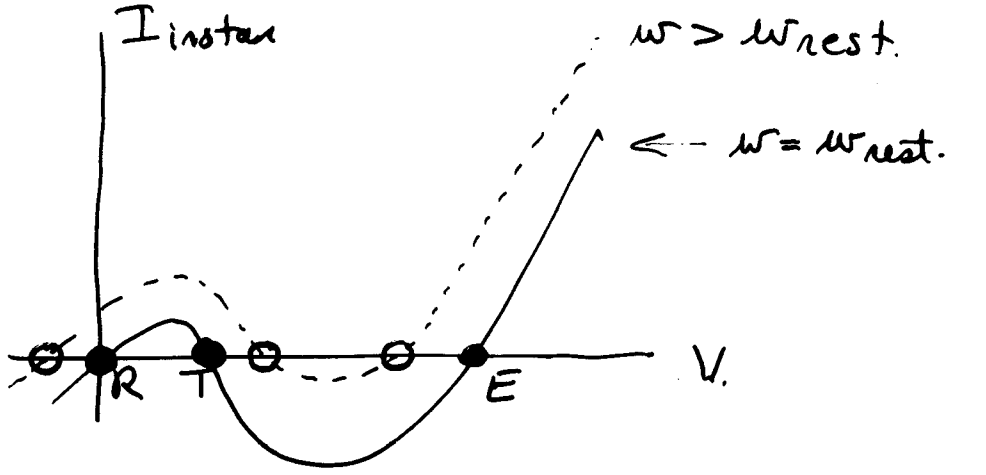

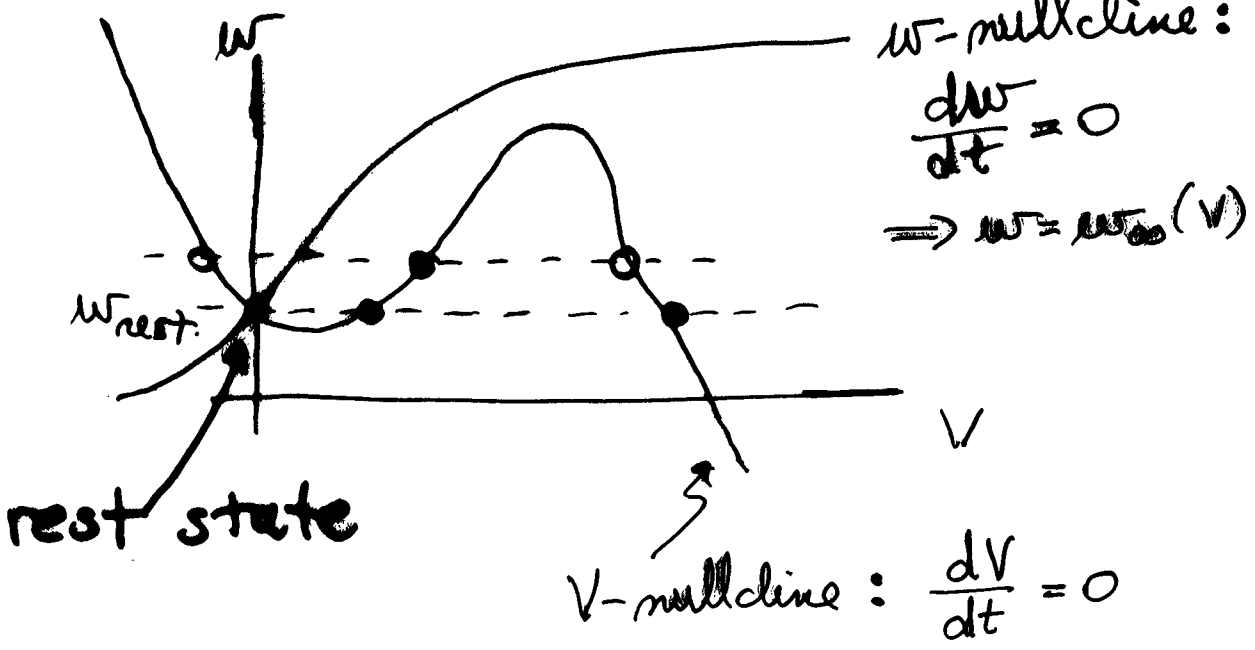

Steps to construct phase plane portrait

$$C\dot{V} = -I_{ion}(V, w) + I$$
$$\dot{w} = \phi \frac{w_\infty(V) - w}{\tau_w(V)}$$

(Morris-Lecar model)

① Determine nullclines + plot them

(1.a) $\dot{w} = 0 \Rightarrow w = w_\infty(V)$

(1.b) $\dot{V} = 0 \Rightarrow I_{ion}(V, w) = I$

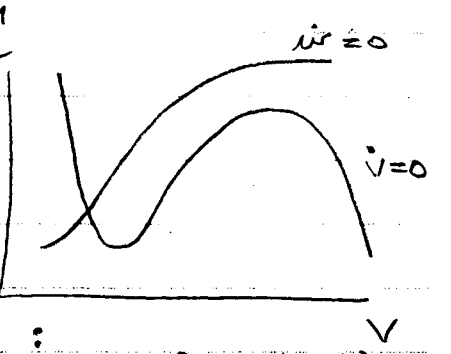

Get this 2 ways —

- explicit expression for w:

$$w = \frac{I - \bar{g}_{Ca} m_\infty(V)(V - V_{Ca}) - g_L(V - V_L)}{\bar{g}_K (V - V_K)}$$

- Determine zero-crossings of $I_{ion}(V, w) - I$ with w treated as parameter.

② Find steady states — where V and w nullclines intersect. Stability?

③ Some features of flow field:

(3a) Flow is vertical on $\dot{V}=0$, horizontal on $\dot{w}=0$ (to know the direction, say on $\dot{V}=0$, evaluate $\dot{w} \Rightarrow$ flow is up or down).

(3b) Evaluate flow (to get direction) above + below the nullclines — e.g. for large w, $\dot{w} < 0 \Rightarrow w$ decreasing for points above the w-nullcline

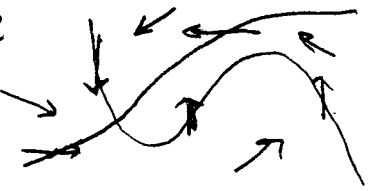

④ Consider some special cases — eg. ϕ small, when flow is very horizontal + traj^s attracted to right and left branches of V-nullcline

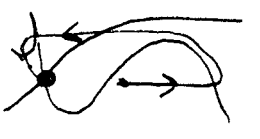

Trajectory — curve $(v(t), w(t))$ in v–w plane

initial cond^{n} — $(v_0, \bar{w})$ at $t = 0+$

Rest — globally attracting

M–L model

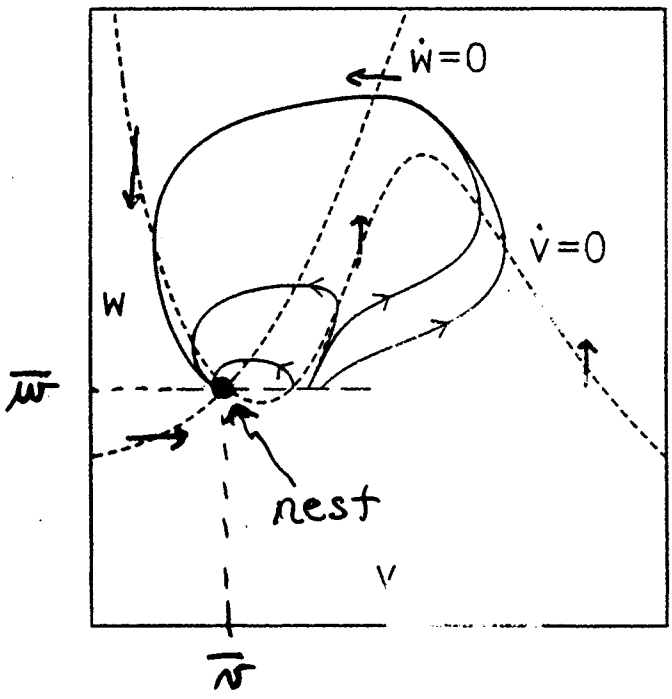

$\dot{V}=0$

3 Branches: "R, T, E"

Excitable

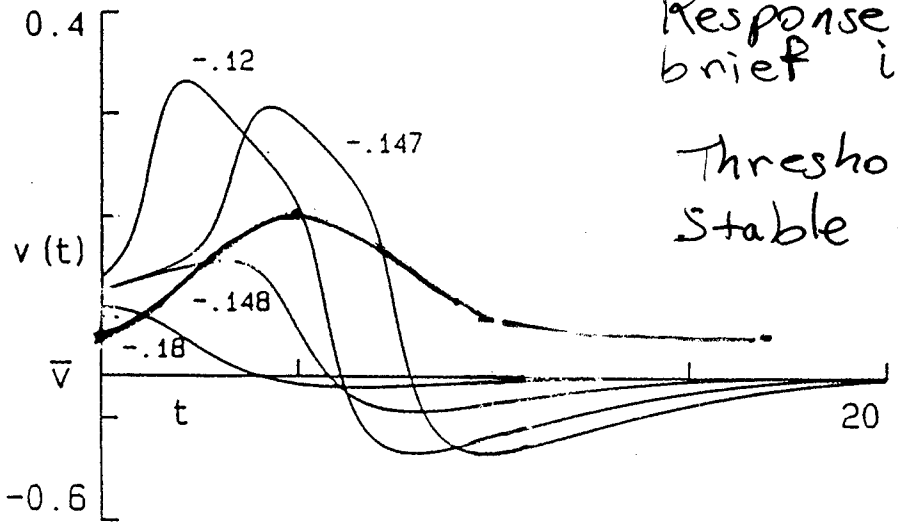

Response to brief $i(t)$.

Threshold.

Stable rest.

WH 91-4 CNS.c

3

Small $\phi \Rightarrow$ w, very slow

$\left|\frac{dw}{dv}\right| \downarrow$ — traj $\hat{=}$ more horiz.
except near $\dot{v}=0$.

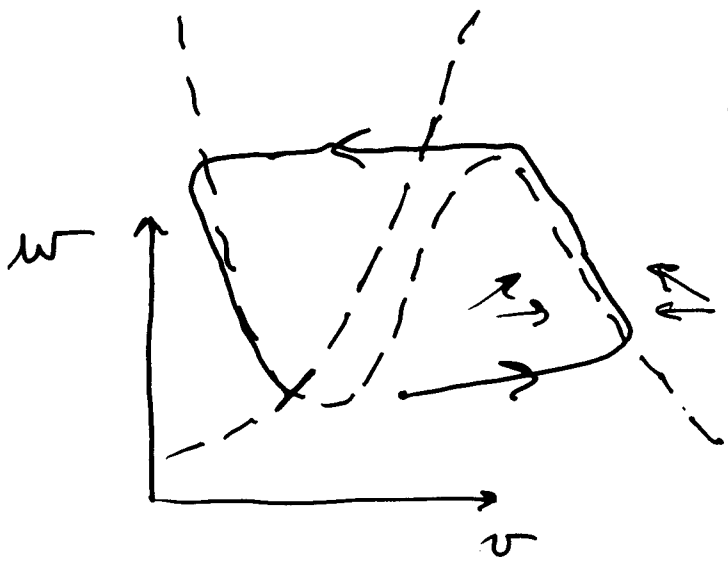

no change in nullclines

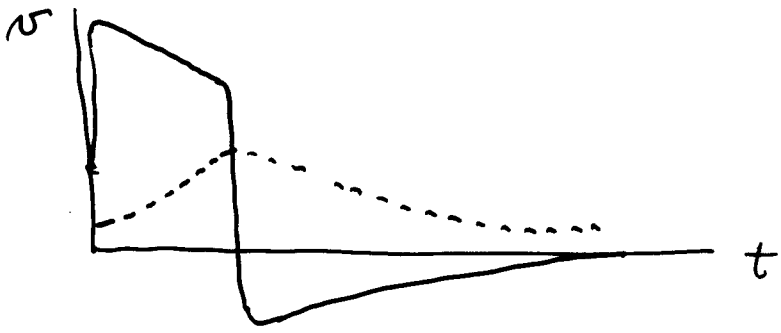

"relaxation" limit

cardiac impulse

singular perturbation methods

— traj either on right or left branch w/ rapid jumps

WH
9/15

Threshold — all-or-none or graded responses?

FHN phase plane (1961)

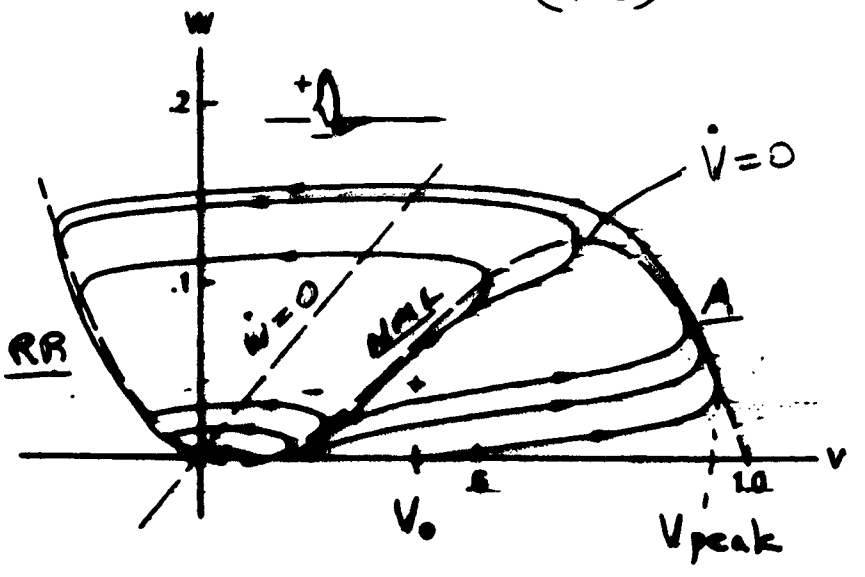

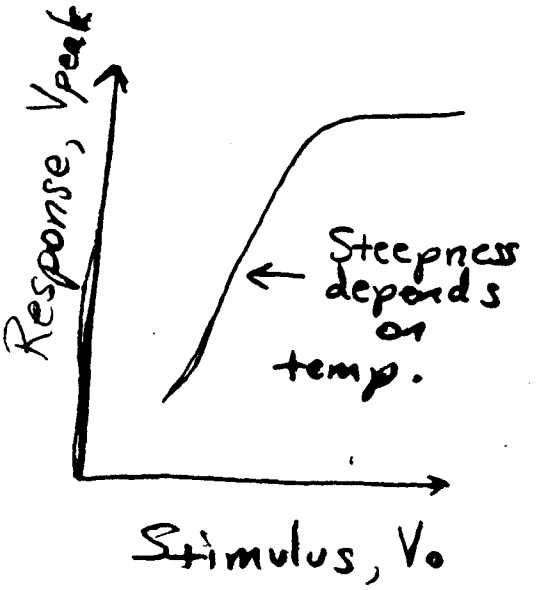

Full HH model:

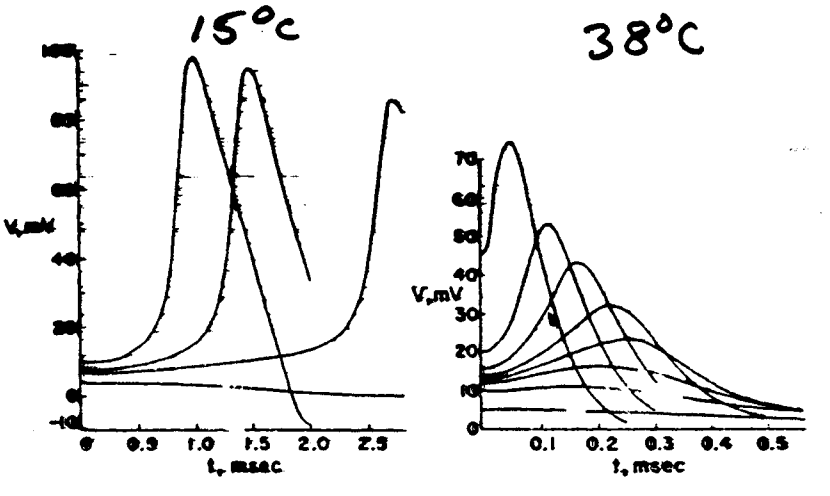

FIG. 3.—Calculated responses, V, at times, t, after initial pulse stimuli as shown at $t = 0$. *Left*, 15°C, *right*, 38°C.

Space-clamped squid axon

Cole, Guttman, + Bezanilla (1970)

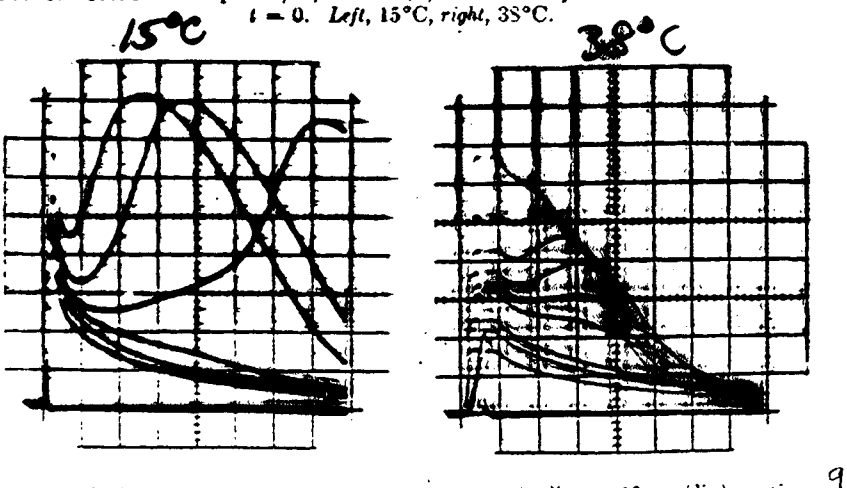

FIG. 4.—Oscilloscope records of membrane responses (ordinates 10 mv/div) vs. time

WN 91-7 1

Anodal Break Excitation (PIR)

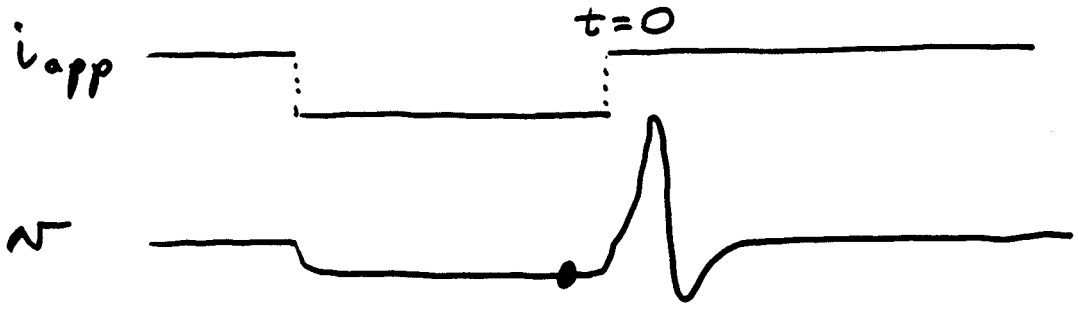

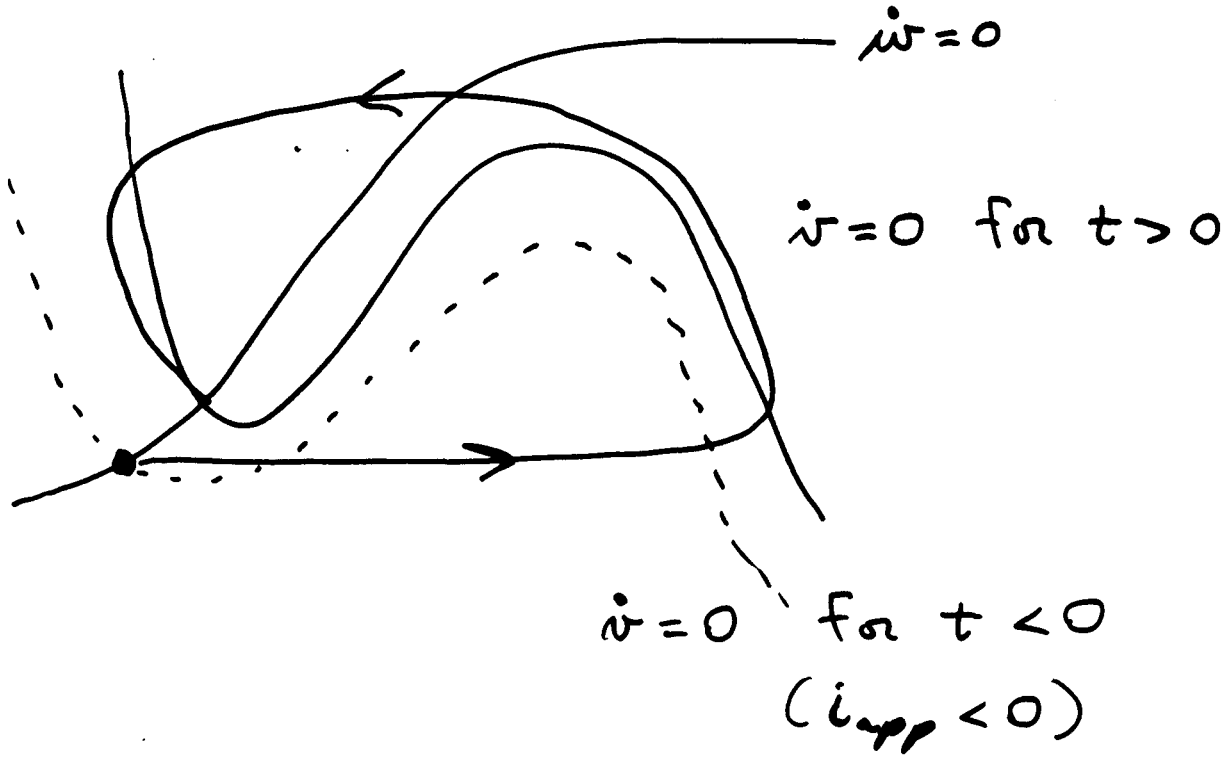

i_K – deactivated

WH
91-6

Action Potential w/o I_K ?

$$C\frac{dV}{dt} = -\bar{g}_{Na} m^3 h (V - V_{Na}) - g_L (V - V_L) + I_{appl}$$

m^3: fast autocatalytic

h: slower negative feedback

If I_{Na} not completely inactivated at rest.

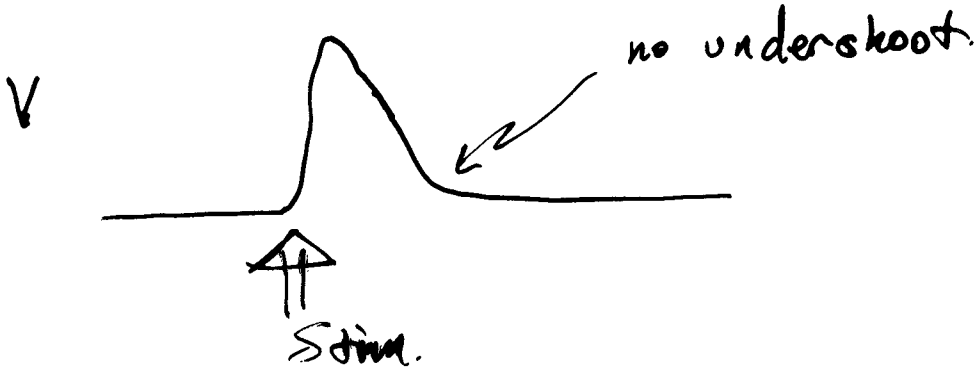

Some myelinated nerves.

Repetitive Activity

i_{app} - adequate

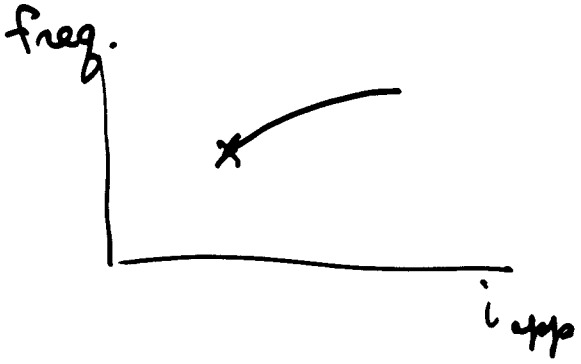

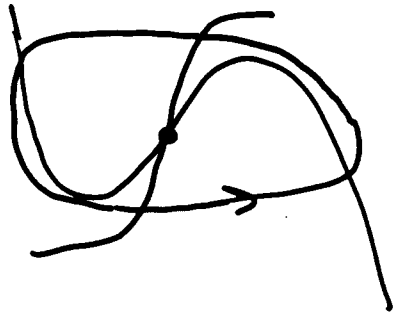

"rest" — unstable

↑

only if on middle branch (math)

Condition for instability*:

damped
$i < i_1$

growing
$i > i_1$

(Hopf)

$$\frac{1}{C_m}\frac{\partial i_{ion}}{\partial v} < -\frac{\phi}{\tau_w}$$

"negative" resistance — destabilizing

* near "rest"
i_{ss} - monotone

Concepts not just for 2 variable models!!

Relate V-nullcline to I_{inst} vs V

WH 91-12

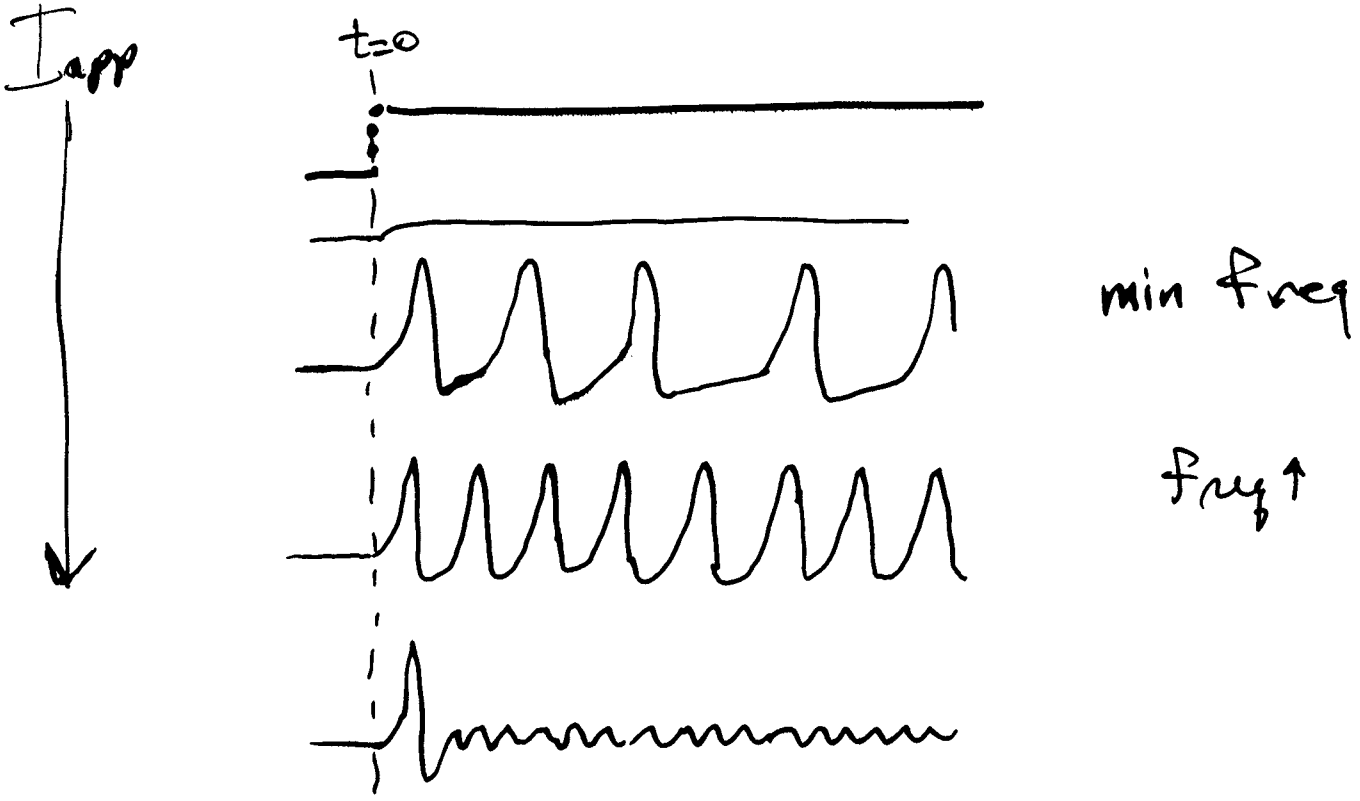
Iapp
t=0
min freq
freq ↑

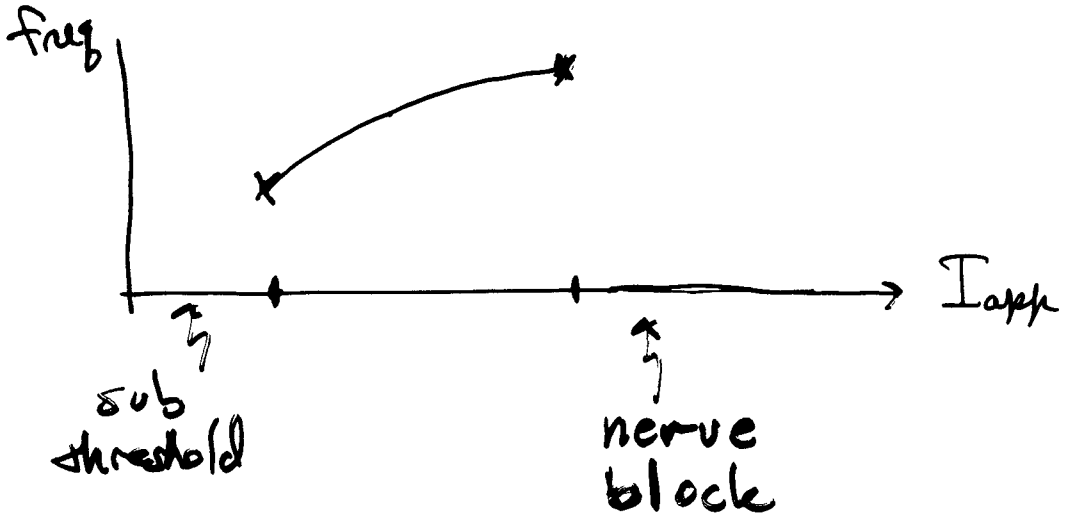
freq
Iapp
sub threshold
nerve block

Onset of oscillⁿ ~ stability of rest

J. Rinzel ('76)

Linearⁿ about rest — local analysis

$i < i_1$  damped osciⁿ

$e^{\lambda t}$, $Re\lambda < 0$

$i > i_1$  growing osciⁿ

$Re\lambda > 0$

$i \doteq i_1$  maintained osciⁿ

Hopf bifurcation

handout

Repetitive Firing, $i = \text{const}$

$\bar{v}(i)$, $\bar{w}(i)$ stability

classif^{cn} of sing. pts.

asymptotically stable if

$(v, w) = (\bar{v} + x, \bar{w} + y)$ and $x, y \to 0$ as $t \to \infty$

Linear stability

$$\frac{dx}{dt} = i - i_{ion}(\bar{v}+x, \bar{w}+y) \doteq -\frac{\partial i_{ion}}{\partial v} x - \frac{\partial i_{ion}}{\partial w} y$$

$$\frac{dy}{dt} = \phi \frac{w_\infty(\bar{v}+x) - (\bar{w}+y)}{\tau_w(\bar{v}+x)} \doteq \phi \frac{w_\infty'}{\tau_w} x - \phi \frac{1}{\tau_w} y$$

i.e. $\begin{pmatrix} \dot{x} \\ \dot{y} \end{pmatrix} = J \begin{pmatrix} x \\ y \end{pmatrix}$, $J = \begin{pmatrix} a-\lambda & b \\ c & d \end{pmatrix}$ $(\bar{v}, \bar{w})$

Sol^{ns}: $x, y \sim A e^{\lambda_1 t} + B e^{\lambda_2 t}$

$\lambda^2 - (a+d)\lambda + ad - bc = 0$ (char^{tic} eqn)

If $\mathrm{Re}(\lambda_{1,2}) < 0$, then $(\bar{v}, \bar{w})$ stable.

If $\mathrm{Re}\,\lambda_1$ or $\mathrm{Re}\,\lambda_2 > 0$, $(\bar{v}, \bar{w})$ unstable.

Classif^{cn} based on λ's.

Previous case: $\lambda_1 < \lambda_2 < 0$ stable node

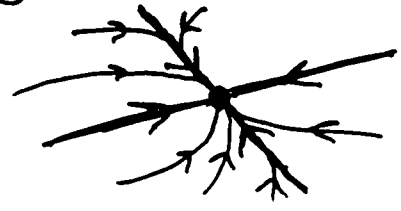

λ_2 slowest decay

loss of stability — 2 ways.

(1) $\lambda_{1,2} = 0$ i.e., $|J| = \lambda_1 \lambda_2 = 0$

(2) $\mathrm{Re}\,\lambda_1 = \mathrm{Re}\,\lambda_2 = 0$ i.e., $tr(J) = \lambda_1 + \lambda_2 = 0$

Result (1) only occurs if $\bar{v}$ at "knee" of $i_{ss}(v)$.

Proof

$$|J| = \left(-\frac{\partial i_{ion}}{\partial v}\right)\left(-\frac{\phi}{\tau}\right) - \left(-\frac{\partial i_{ion}}{\partial w}\right)\left(\phi \frac{w_\infty'}{\tau}\right)$$

$$= \frac{\phi}{\tau}\left(\frac{\partial i_{ion}}{\partial v} + \frac{\partial i_{ion}}{\partial w} w_\infty'\right)$$

$$= \frac{\phi}{\tau} \frac{d i_{ss}}{d v}, \quad i_{ss}(v) = i_{ion}(v, w_\infty(v))$$

$\therefore |J| = 0 \iff \frac{d i_{ss}}{d v} = 0$ (general)

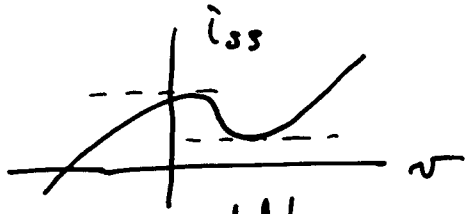

Cor.1 only occurs if $(\bar{v}, \bar{w})$ on middle branch of $\dot{v} = 0$.

Cor. 2 If $i_{ss}(v)$ is monotone then loss of stability (as $i \uparrow$) only via (2).

Mech^{m} (2): damped oscill^{n} → growing oscill^{n}

$i < i_1$	$i = i_1$	$i > i_1$
		
$\mathrm{Re}\lambda < 0$	$\mathrm{Re}\lambda = 0$	$\mathrm{Re}\lambda > 0$
stable focus	center	unstable focus

M-L and H H

Mechⁿ (2)

loss of stability $\quad i = i_1 \Rightarrow \mathrm{Re}\,\lambda = 0$

$$\mathrm{tr}\,[J] = 0 = -\frac{\partial i_{ion}}{\partial v} - \frac{\phi}{\tau_w}$$

Observe.

1. Only occurs if $\frac{\partial i_{ion}}{\partial v} < 0$ — i.e., instantaneous i–v has neg. resistᵉ.

2. Only occurs if $(\bar{v}, \bar{w})$ on middle branch of $\dot{v}$–nullcline.

(i.e., $\dot{v} = 0 \Rightarrow \quad 0 = i_{ion}(v, w) - i$

slope $= \frac{dw}{dv} = -\frac{\partial i_{ion}/\partial v}{\partial i_{ion}/\partial w} \lessgtr 0$ for outward

$\therefore \frac{\partial i_{ion}}{\partial v} < 0 \Rightarrow \frac{dw}{dv} > 0$.)

3. Only occurs if ϕ small enough.

4. destabᴵᶻᴬ if time scale of neg. resistᵉ exceeds that of recovery

Mechⁿ (2): Hopf bifurcⁿ

Thm Small amplitude periodic solⁿ emerges (bifurcates) from steady state at i_1.

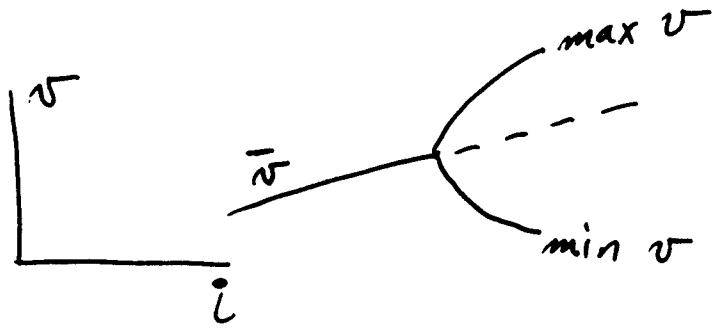

supercritical
soft
(stable periodic
$i > i_1$

or

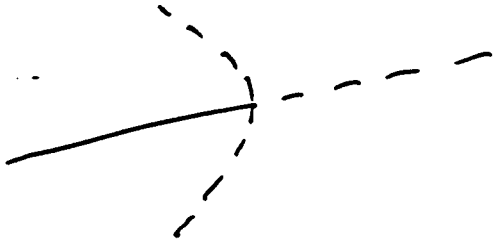

subcritical
hard
(unstable periodic
$i < i_1$)

$$|v| \sim \sqrt{|i - i_1|}$$

$$\text{freq} \sim |i - i_1| \quad , \quad \text{Im}\,\lambda_{1,2}$$

Hopf Bifurcation — normal form (e.g. Strogatz)

$$\dot{r} = \mu r - r^3$$
$$\dot{\theta} = \omega + b r^2$$

μ = control parameter

$\mu < 0$

stable spiral

$\mu > 0$

unstable spiral ⊕
stable cycle, $r \equiv \sqrt{\mu}$

---

bifurcn diagram

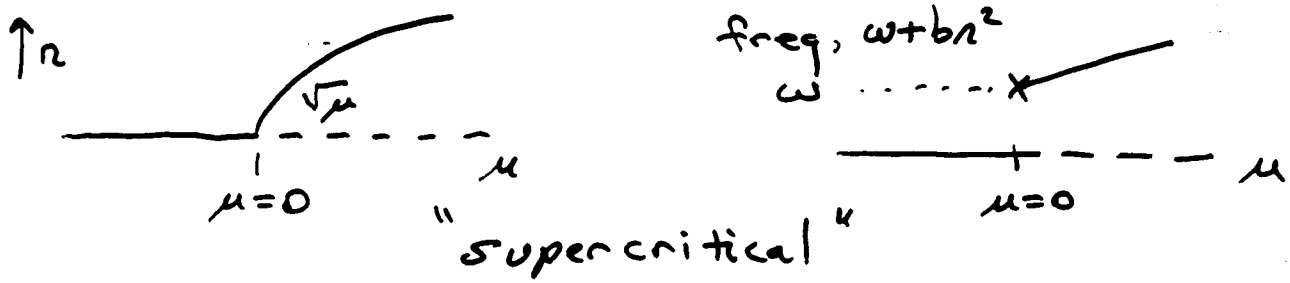

"supercritical"

LOCAL ANALYSIS

subcritical : $\dot{r} = \mu r + r^3$ $\quad \dot{\theta} = \omega + b r^2$

Generic — linear stability $\quad x = r\cos\theta \quad y = r\sin\theta$

$$\dot{x} = \mu x - \omega y + \text{cubic stuff}$$
$$\dot{y} = \omega x - \mu y + \text{cubic stuff}$$

$$J = \begin{pmatrix} \mu & -\omega \\ \omega & -\mu \end{pmatrix}$$

$$\lambda = \mu \pm i\omega$$

Transition from Excitable (stable rest) to Oscillatory — 2 types

min freq ≠ 0

Type II

Hopf bifurcn — locally:

1. iss monotone
2. subthreshold oscillns
3. excitable w/o distinct threshold
4. excitable w/ finite latency

min freq = 0

Type I

heteroclinic pair

homoclinic ($T=\infty$, $\omega=0$)

periodic

1. iss N-shaped — 3 sing pts
2. w/o subthreshold oscillns
3. excitable w/ "all-or-none" (saddle) threshold.
4. excitable w/ infinite latency

Hodgkin ('48) — 2 classes repetitive firing

Class II + I, respectively

Repetitive firing : space-clamped

I_{ss} vs V (HH eqns)

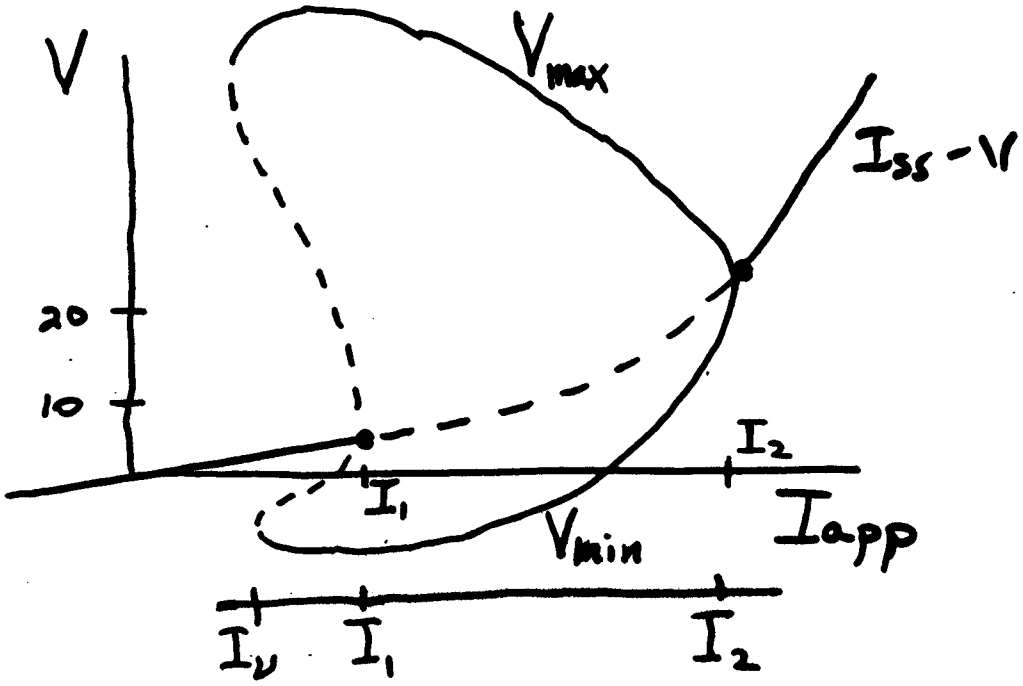

Linearized Stability: $\frac{\partial I_i}{\partial V} + \frac{C_m}{\tau_n} > 0$

w/ $n = n_\infty(V)$

Bistability for $I_v < I_{app} < I_1$

Guttman, Lewis, Rinzel ('80)

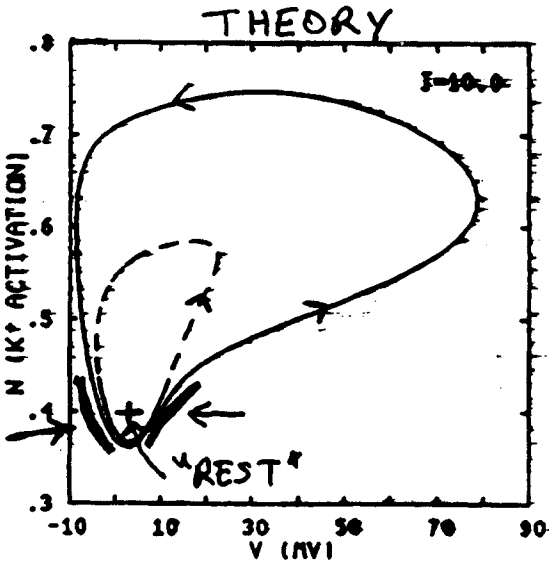

I
V

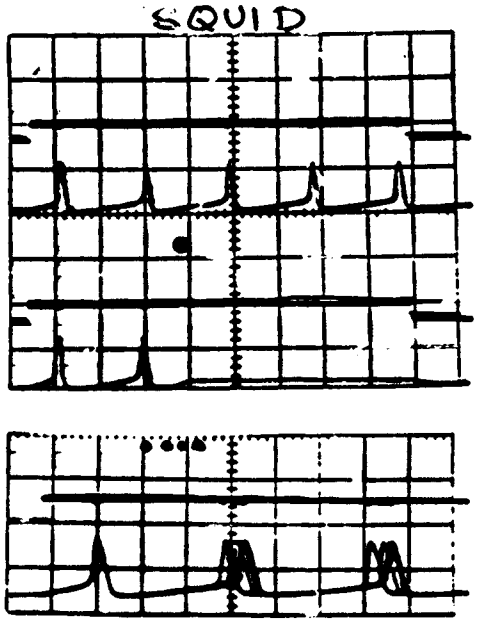

WH 91-9

F-1

Hopf Bifurcation of Periodic Solution

Local description

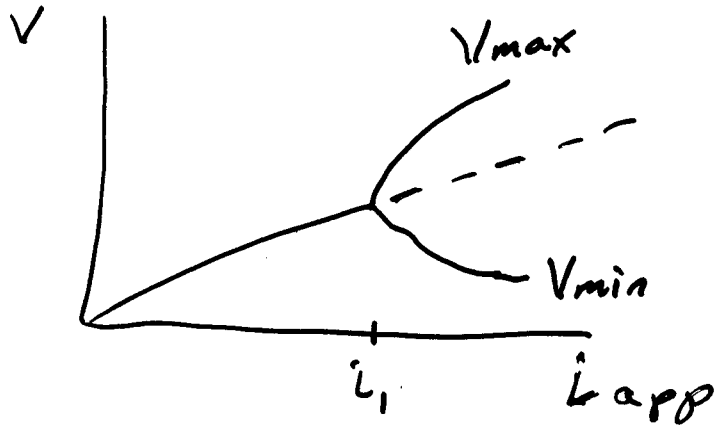

⟶ stable oscillation

(supercritical)

$|V_{max} - V_{min}| \sim \sqrt{|i - i_1|}$ freq $\sim |i - i_1|$

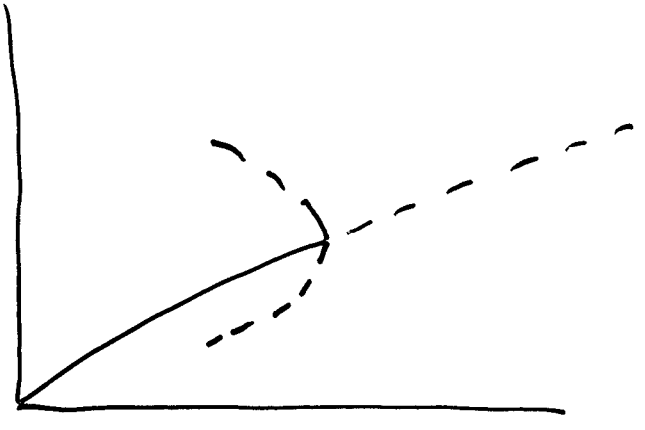

⟶ unstable oscillation

(subcritical)

Example of subcritical Hopf!

Journal of Physiology (1988), **405**, *pp.* 345–367
With 10 text-figures
Printed in Great Britain

BISTABILITY OF α-MOTONEURONES IN THE DECEREBRATE CAT AND IN THE ACUTE SPINAL CAT AFTER INTRAVENOUS 5-HYDROXYTRYPTOPHAN

BY JØRN HOUNSGAARD, HANS HULTBORN*, BO JESPERSEN AND OLE KIEHN

From the Department of Neurophysiology, The Panum Institute, University of Copenhagen, Blegdamsvej 3C, DK-2200 Copenhagen N, Denmark

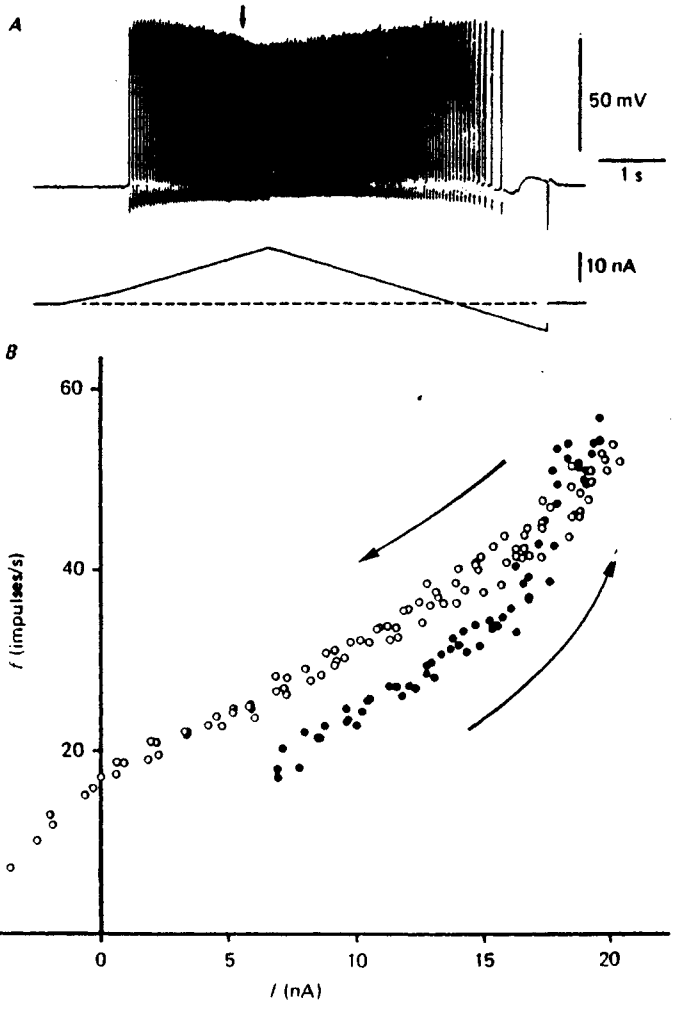

Fig. 5. Response of ~~an~~ α-motoneurone to a triangular current pulse injection. *A* illustrates an intracellular recording (IC) from a lateral gastrocnemius–soleus motoneurone (same cell as in Fig. 1) in upper trace and injected current in lower trace. The intracellular signal was passed through a 5 Hz filter for reproduction and the steady bias current was −6 nA. *B*, the instantaneous frequency *f* (impulses/s) measured in the cell in *A* is plotted against current *I* (the direction of arrows indicate the ascending (●) and descending (○) phase of the triangular waveform). The frequency–current relation shows a counter-clockwise hysteresis.

WH 91-11

Freq-Current Relations

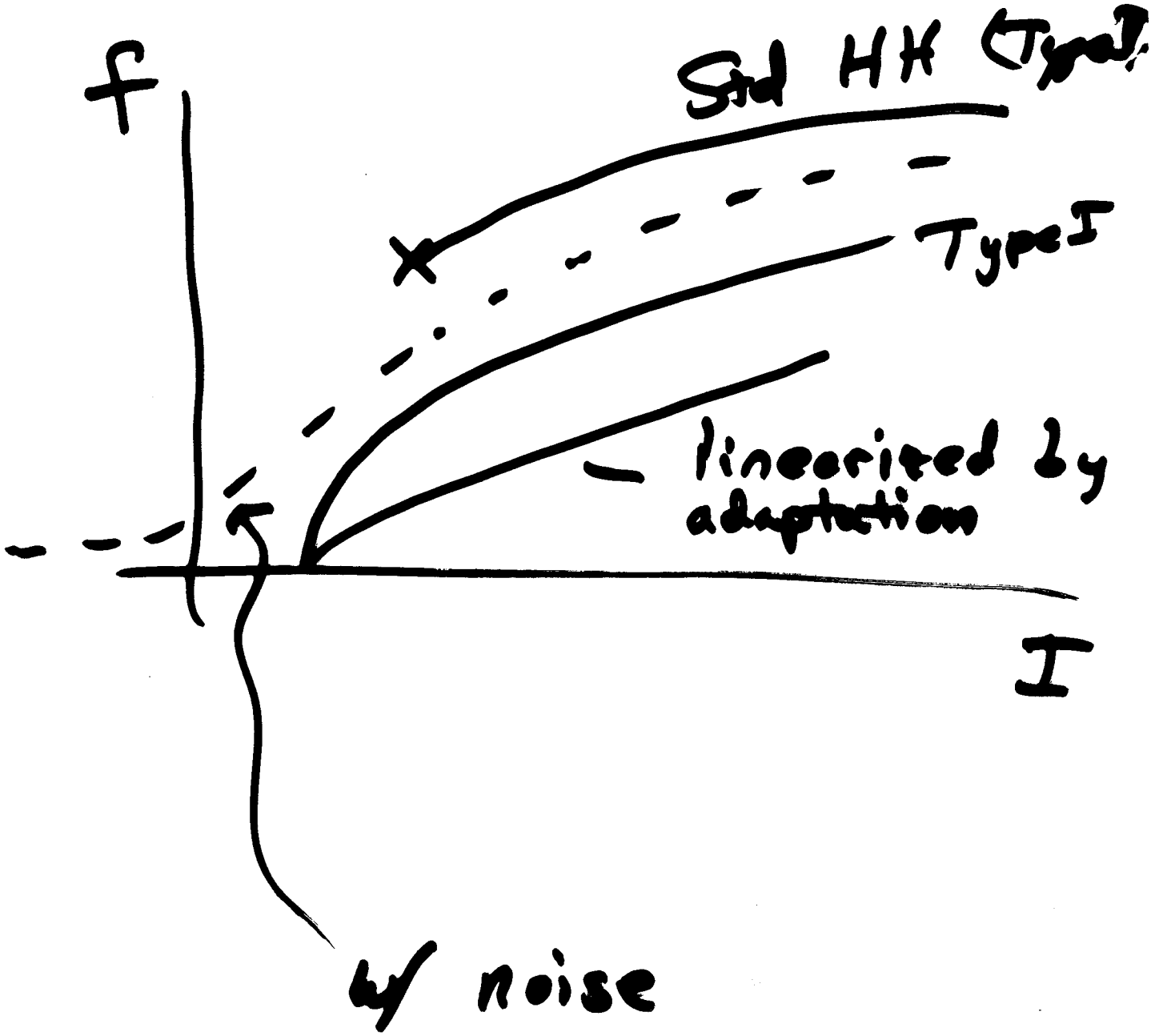

Homework

Make a model that does not fire repetitively for I_{app} = const.

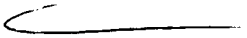

Rinzel & Hagai

& Clay JNP 1998. – squid.

Case of 3 sing. pts. — eg. adjust $w_{\infty}(v)$

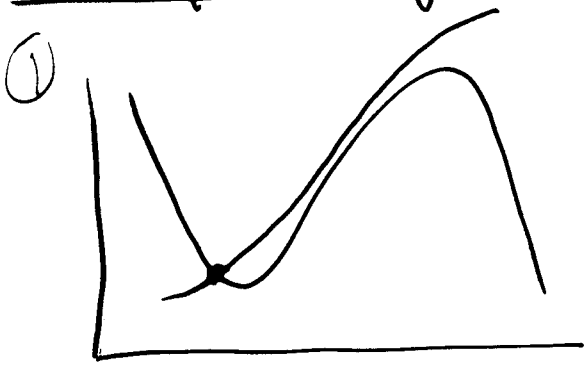

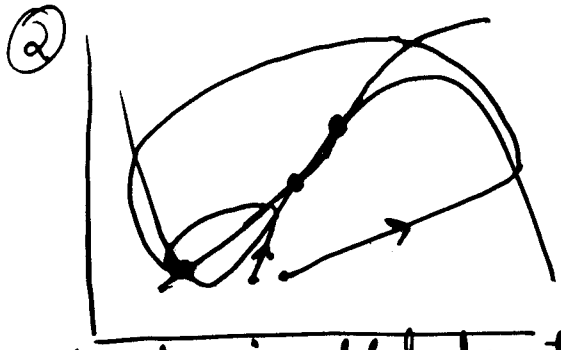

w/o changing global character of flow

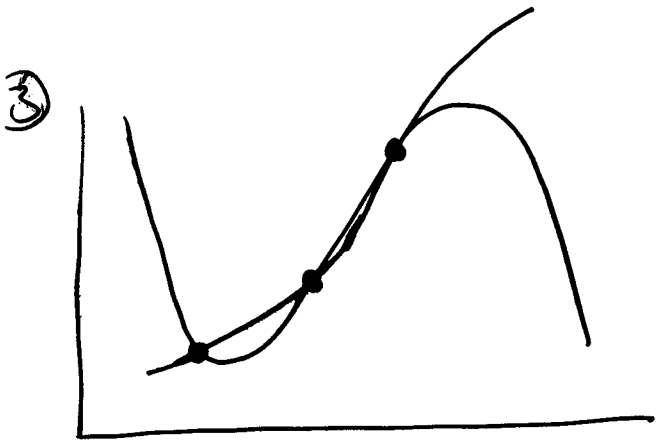

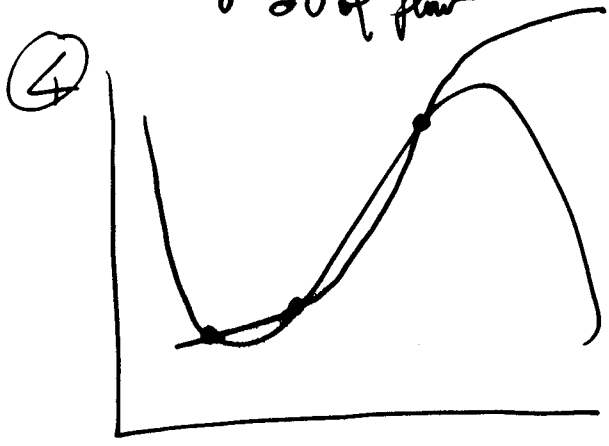

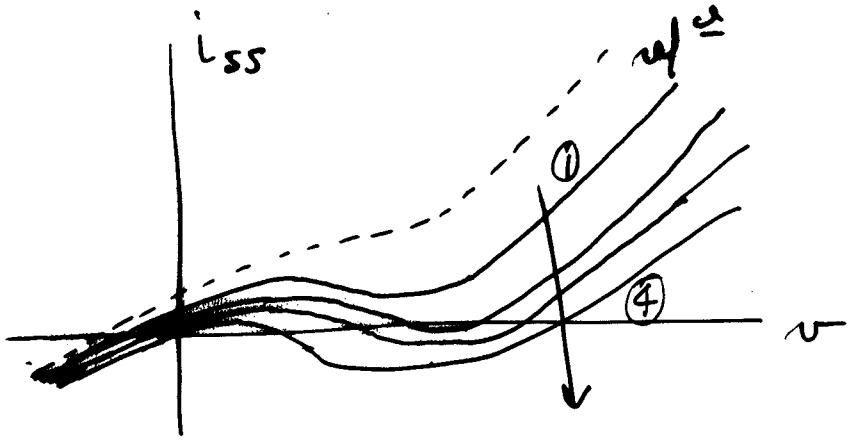

ϕ small enough then both upper state + middle state unstable

(EH 9-16-93)

Consider 3 parameter regimes with

ϕ large

small

intermediate

Control parameter is I to get

freq vs I

ampl vs I

as well as

V_{ss} vs I

Bistable

ϕ large $\Rightarrow$ 2 stable steady states

"plateauing" behavior

saddle w/ stable + unstable manifolds

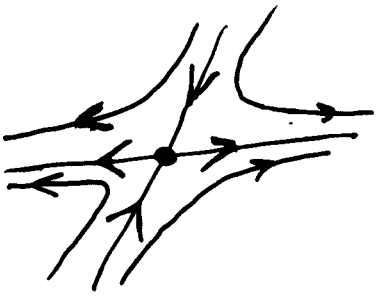

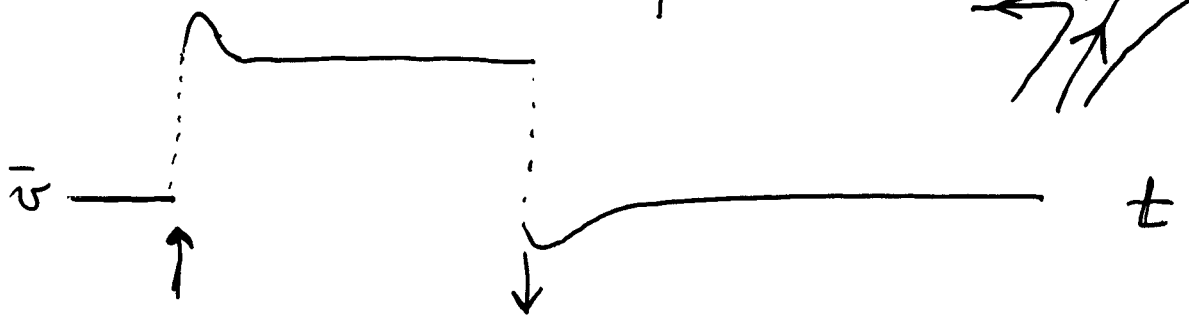

eg. HH w/ $V_K = 24\,mV$

Domain of attraction for "E" + "R"

WH 91-12 19/15

M-L model

K+E chap Figs 4-6

ϕ small

upper state — unstable node $\lambda_1 > \lambda_2 > 0$

middle state — saddle — $\lambda_1 > 0 > \lambda_2$

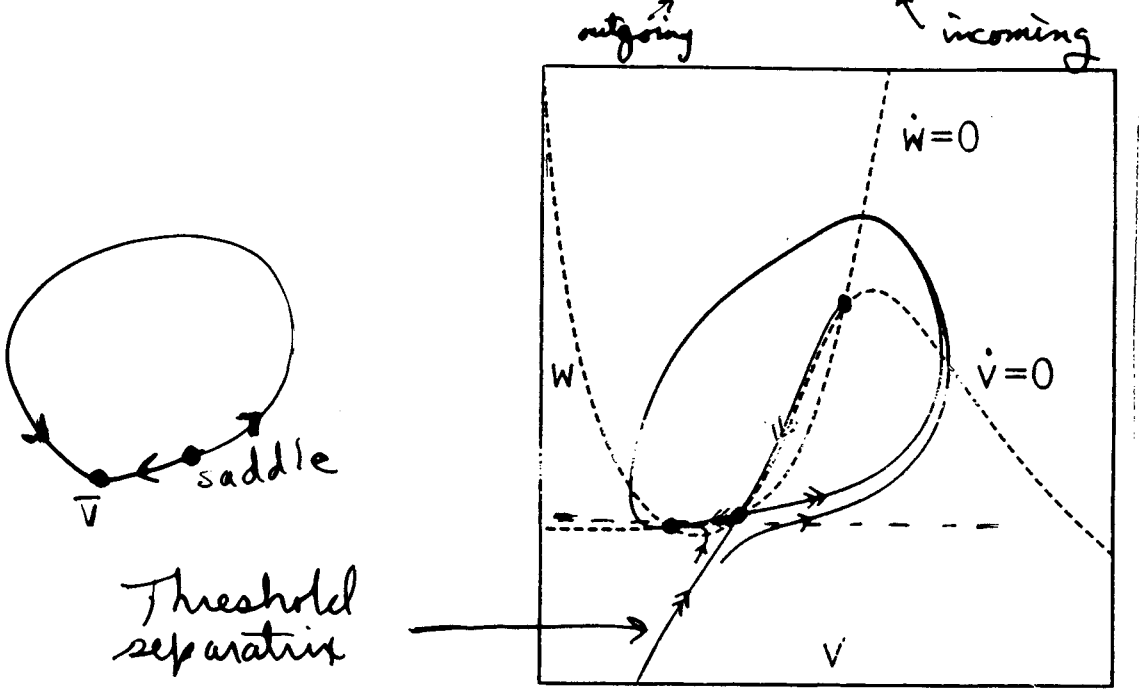

no intermediate sized response here for brief pulse.

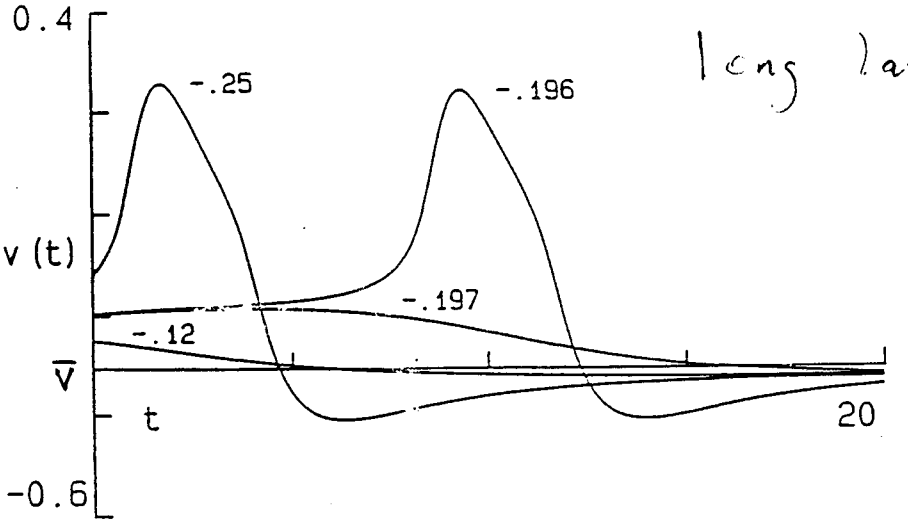

Onset of repetitive firing, i = const.

V-nullcline moves up ⇒ "rest" + saddle coalesce

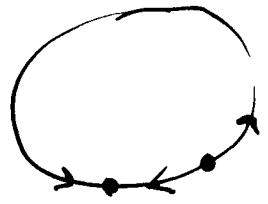

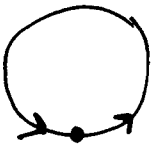

$i \approx i_1$ homoclinic

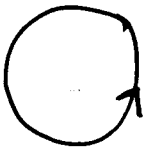

periodic — long period

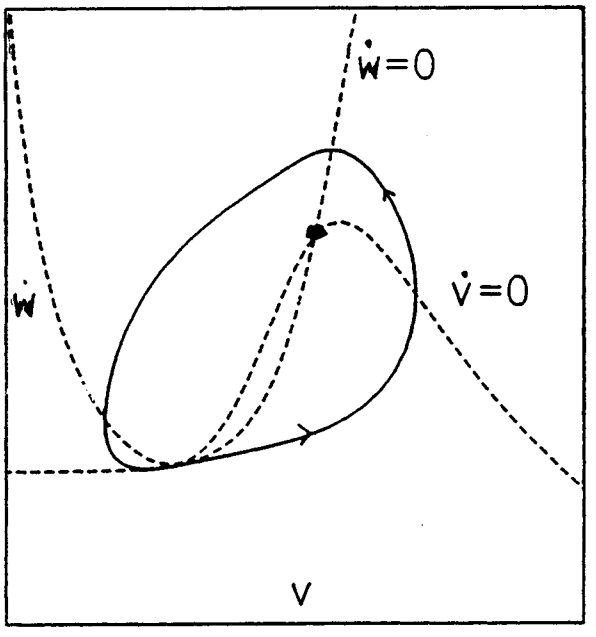

"SNIC" — saddle-node on invariant circle

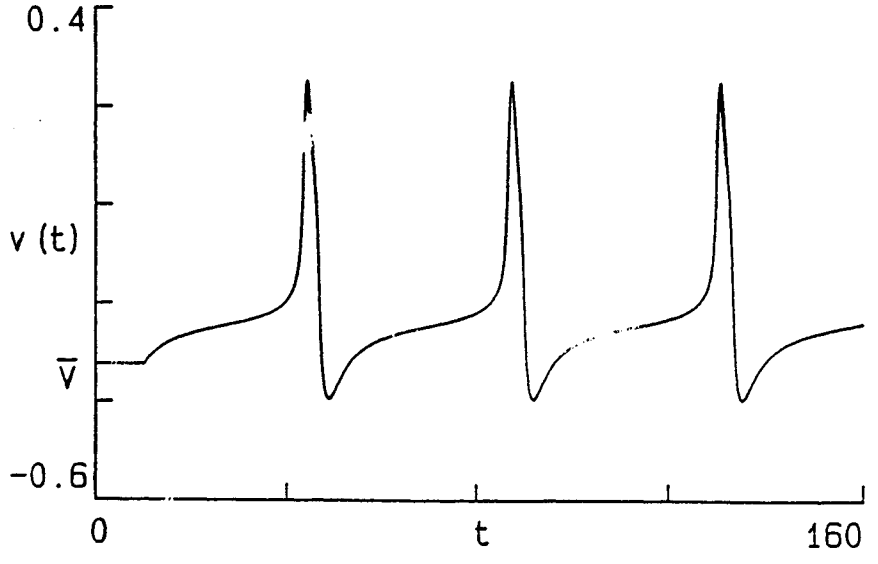

Note — not small amplitude emergence

$\omega \downarrow 0$
"linearized I-f"

Remark on I_A.

Note - no I_A.

ϕ small.

Response (or bifurc^{n}) diagram w/ i as para.

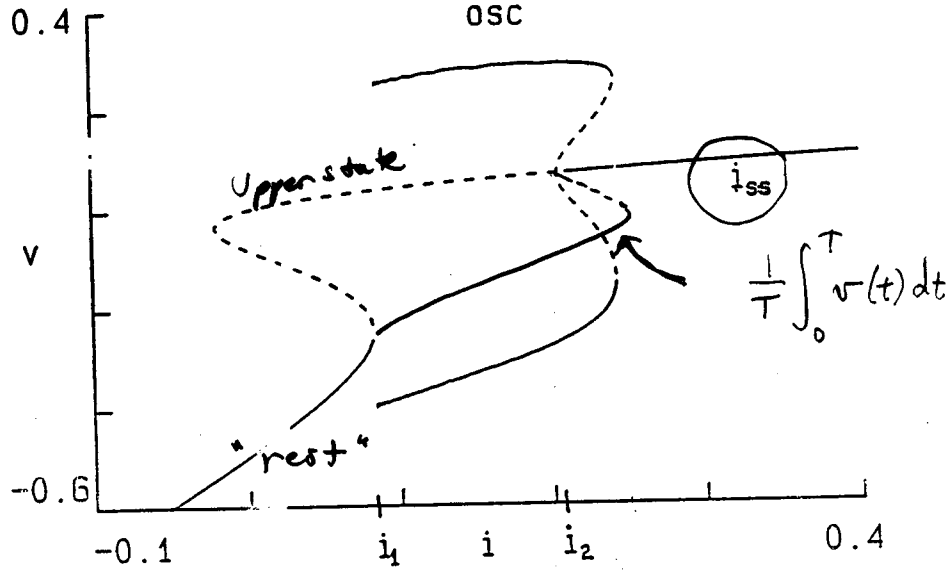

monostable or $i < i_2$

firing freq starts at 0 yet no cond^{tce} is very slow

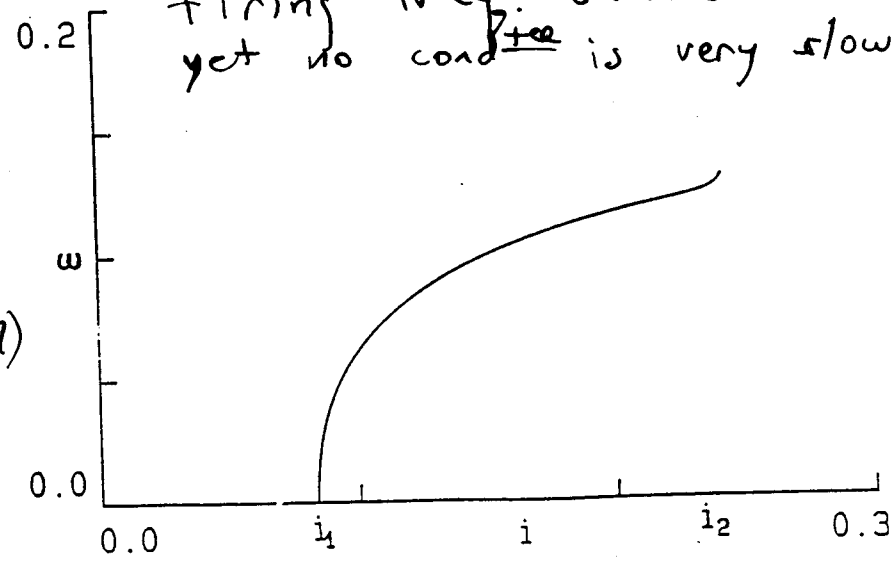

$\omega \sim \sqrt{i - i_1}$

saddle-node on invariant circle (77)

WH 92-6

18

Transition from Excitable (stable rest) to Oscillatory — 2 types

min freq ≠ 0

Type II

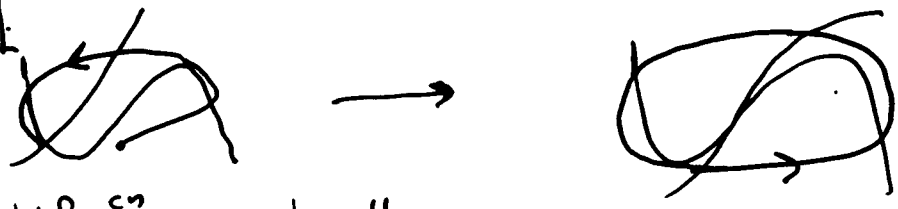

Hopf bifurcn — locally: 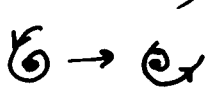

1. iss monotone
2. subthreshold oscillns
3. excitable w/o distinct threshold
4. excitable w/ finite latency

min freq = 0 **Type I**

heteroclinic pair

homoclinic ($T=\infty$, $\omega=0$)

periodic

1. iss N-shaped — 3 sing pts
2. w/o subthreshold oscillns
3. excitable w/ "all-or-none" (saddle) threshold.
4. excitable w/ infinite latency

Hodgkin ('48) — 2 classes repetitive firing
Class II + I, respectively

Intermediate ϕ. M-L

Upper state unstable — surrounded by stable periodic — Hopf bifur^{cn}

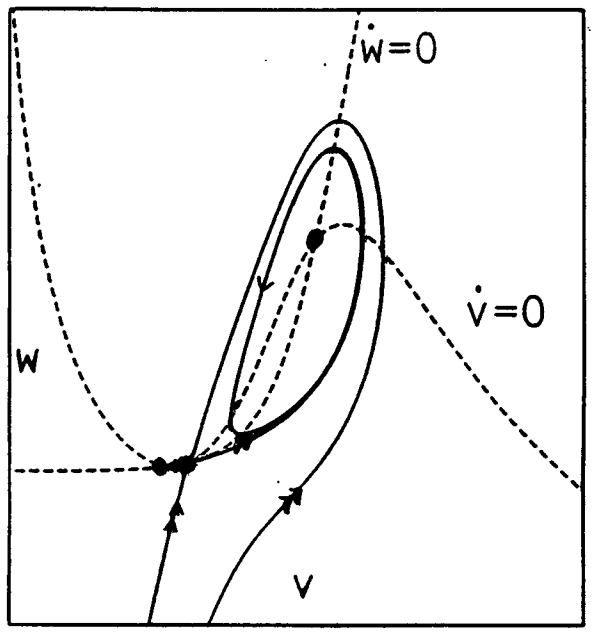

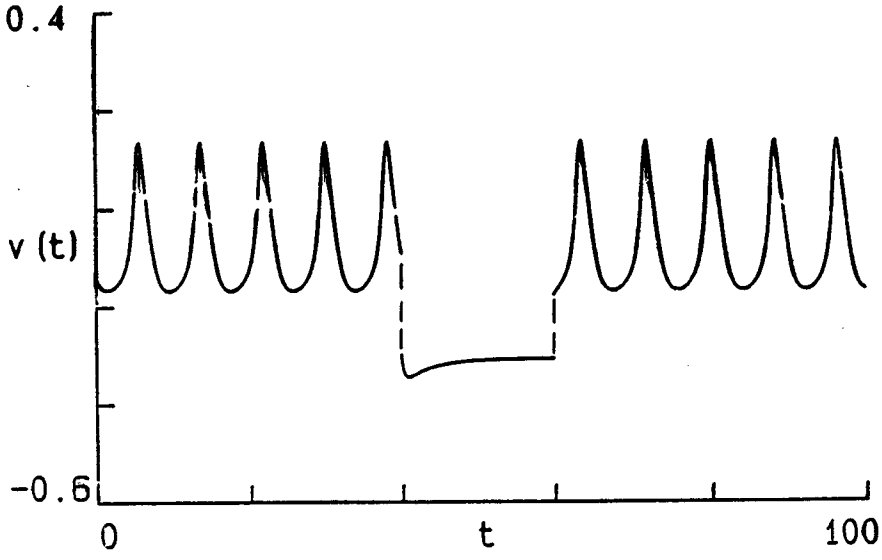

$i \downarrow \Rightarrow$
"rest" + saddle move apart.
saddle + stable periodic make contact $\Rightarrow$
$T = \infty$ for periodic

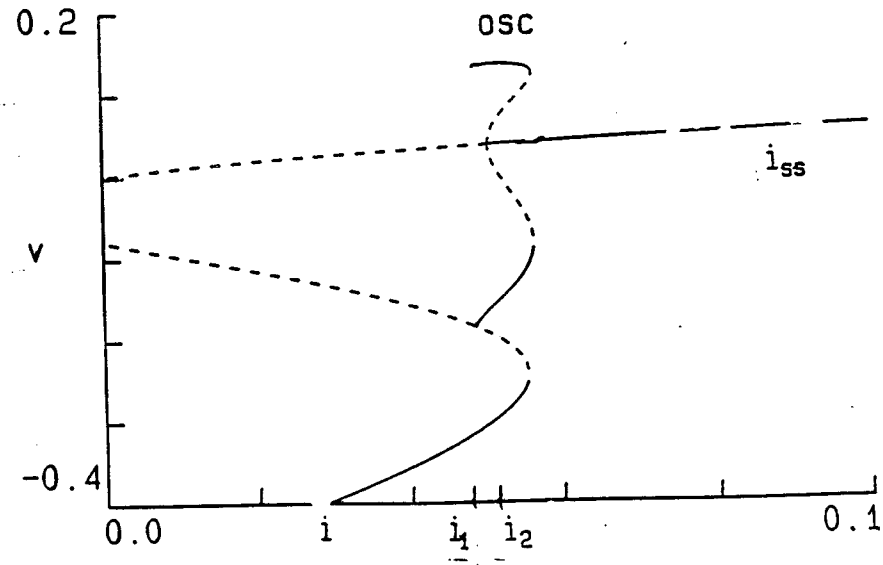

$T \sim -\ln(i - i_1)$

Saddle-loop bifur^{cn}

(MH 91-18)

20

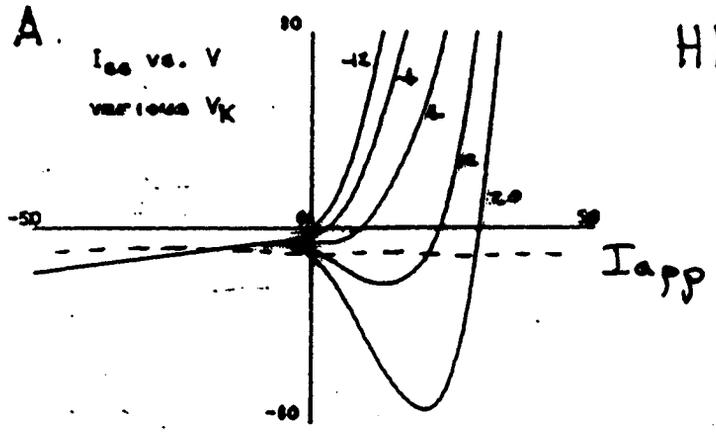

HH sq
18.5°C

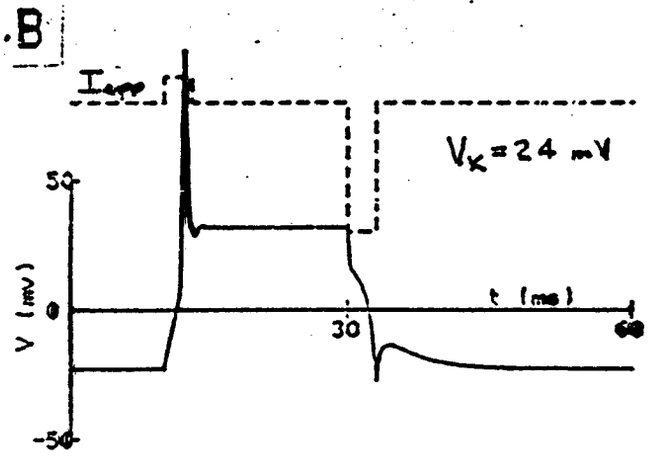

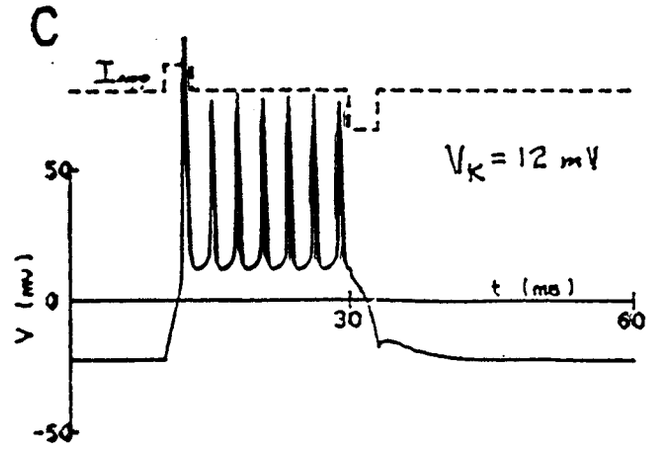

WH
91-18

2M

We have seen that Type I excitability gives f-I relⁿ that begins at zero frequency:

$$f(I_{ramp}) = 0 .$$

The two-variable M-L model is Type I in some param. regimes, and involves 2 "[illegible]" "standard" V-dependent currents.

A classic paper by Connor + Stevens (J Physiol 1971; 214: 31-53) addressed low firing rate neurons and associated the feature with a particular type of potassium current: I_A, a K^+-current with both activ^n and inactiv^n.

Later (1977) Connor et al developed an H-H model of low firing that added I_A to I_{Na} and I_K of H-H. It became "widely accepted" that "low firing rate" meant your membrane spike generator likely had an I_A present.

The simple M-L model of Type I is a counter-example. Further analysis of such models can be found in:

Rush ME, Rinzel J: The potassium A-current, low firing rates, and rebound excitation in Hodgkin-Huxley models. Bull Math Biol; 57:899-929, 1995.

Connor, Walter, McKown 1977, BiophysJ 18 81-102.)

$C\dot{V} = -I_{Na} - I_K - I_A - I_L$

$I_A = g_A a^3 b (V - V_K)$

fast $\sim \tau_m$

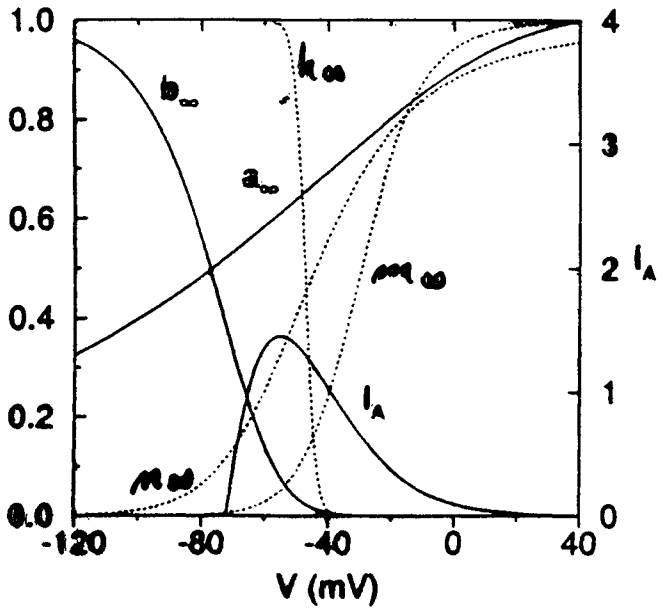

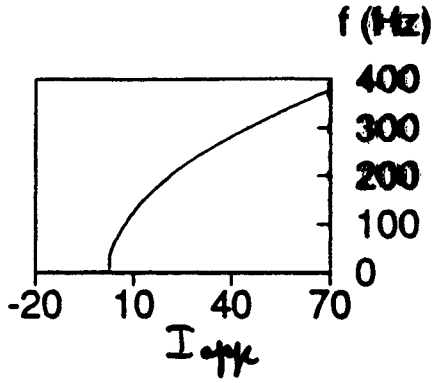

$I_{app} = 10$ — fixed.

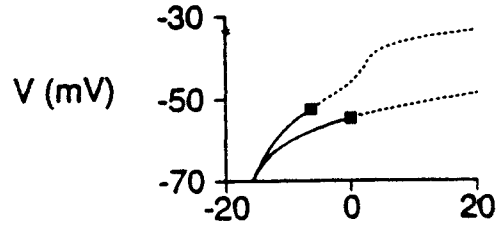

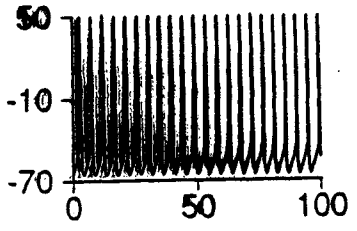

$g_A = 0$

N-shaped $I_{ss}(V)$ develops

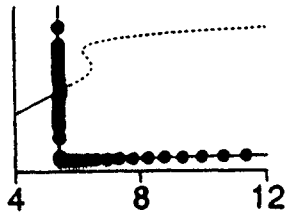

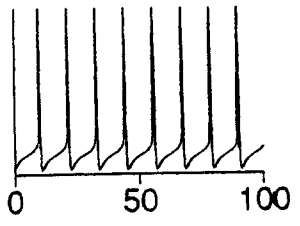

$g_A = 43$

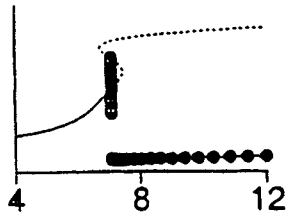

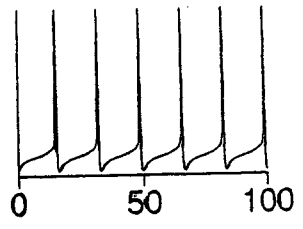

$g_A = 50$

SNIC develops

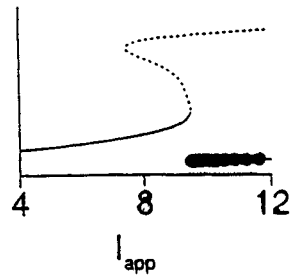

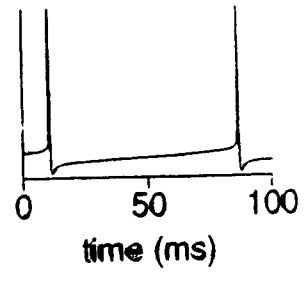

$g_A = 60$

Rush + Rinzel (1998)

Reduced HH @ I_A of CWM w/ $a = a_\infty(V)$

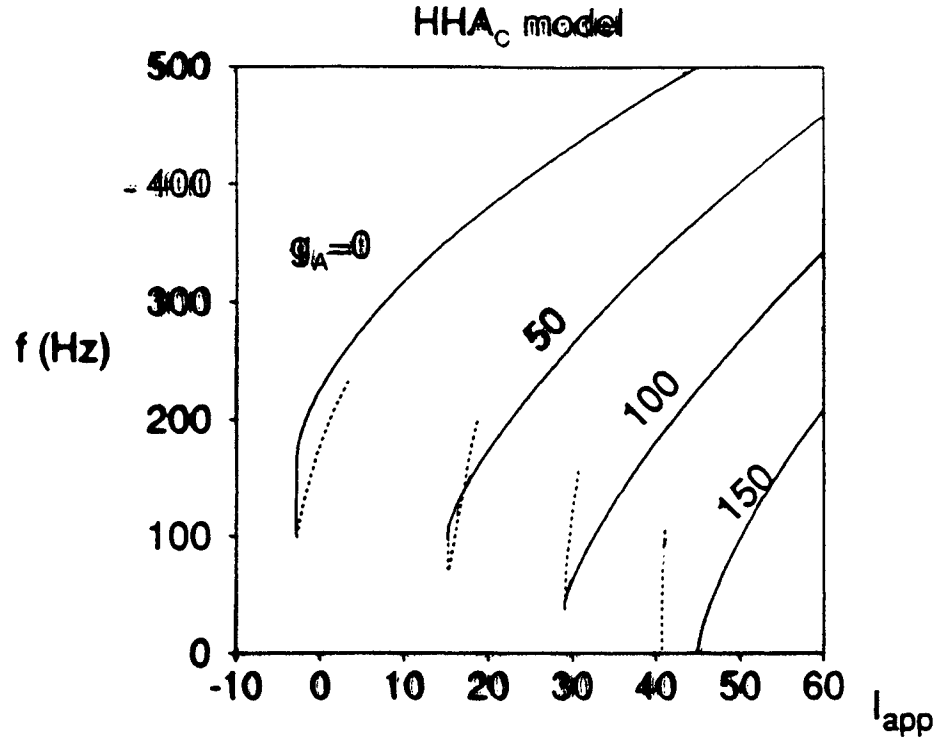

oscill^{ns} branches, not to scale

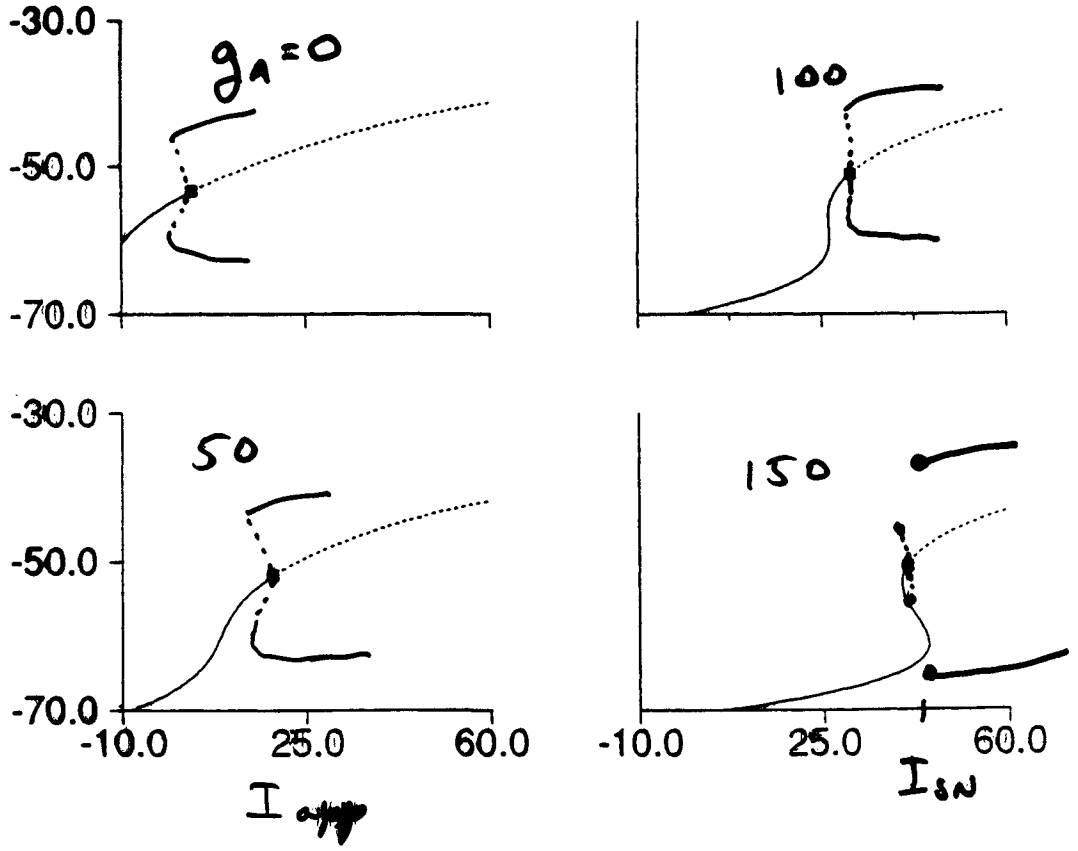

Spatial Effects —

1. Model for motoneuron bistable firing patterns
(Rush & Rinzel, 93)

2. Hippocampal CA3 model — reduced Traub
(Pinsky & Rinzel, 94)

Using 2 compartment idealizations for cable properties.

Journal of Physiology (1988), 405, pp. 345–367
With 10 text-figures
Printed in Great Britain

BISTABILITY OF α-MOTONEURONES IN THE DECEREBRATE CAT AND IN THE ACUTE SPINAL CAT AFTER INTRAVENOUS 5-HYDROXYTRYPTOPHAN

BY JØRN HOUNSGAARD, HANS HULTBORN*, BO JESPERSEN AND OLE KIEHN

From the Department of Neurophysiology, The Panum Institute, University of Copenhagen, Blegdamsvej 3C, DK-2200 Copenhagen N, Denmark

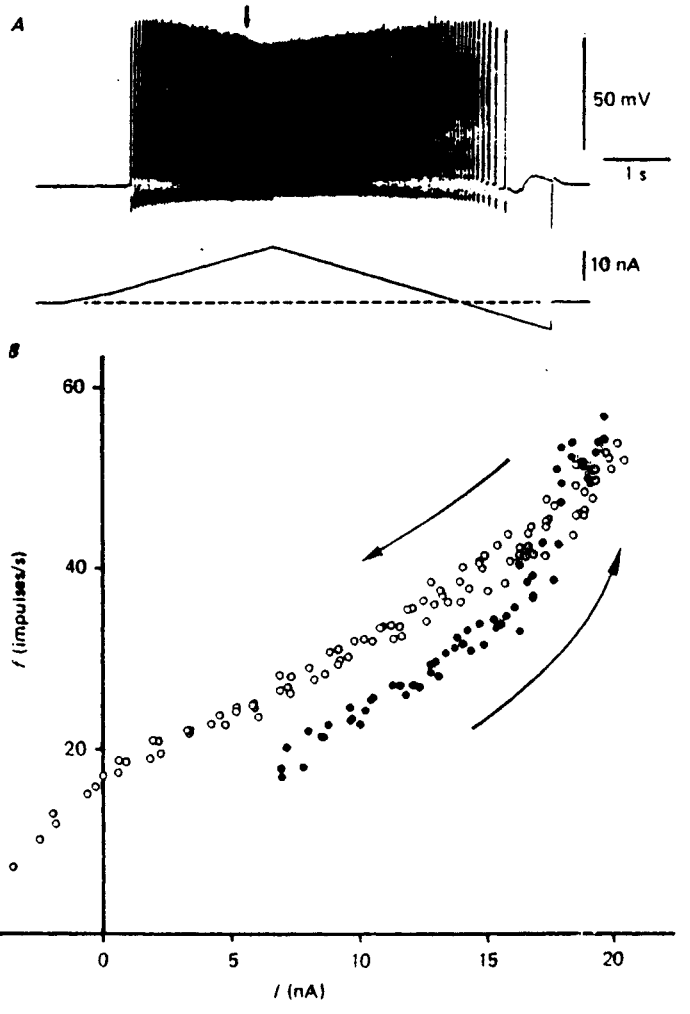

Fig. 5. Response of an α-motoneurone to a triangular current pulse injection. *A* illustrates an intracellular recording (IC) from a lateral gastrocnemius–soleus motoneurone (same cell as in Fig. 1) in upper trace and injected current in lower trace. The intracellular signal was passed through a 5 Hz filter for reproduction and the steady bias current was −6 nA. *B*, the instantaneous frequency *f* (impulses/s) measured in the cell in *A* is plotted against current *I* (the direction of arrows indicate the ascending (●) and descending (○) phase of the triangular waveform). The frequency–current relation shows a counter-clockwise hysteresis.

Idealized model of MN

Cable ⟶ 2 compartments

V_s – soma + proximal dendrites

V_d – distal dendrites

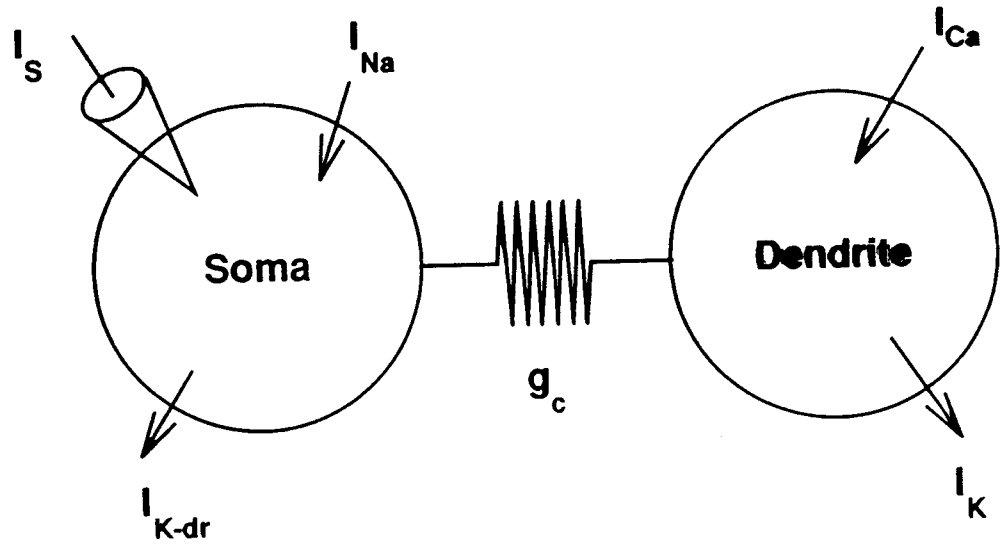

"electrotonic" parameters

g_c – coupling conductance between V_s + V_d

$$p = \frac{A_S}{A_{TOT}}$$

Isolated Soma - Response to I_{app}

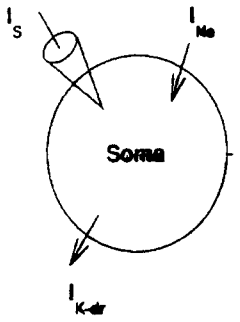

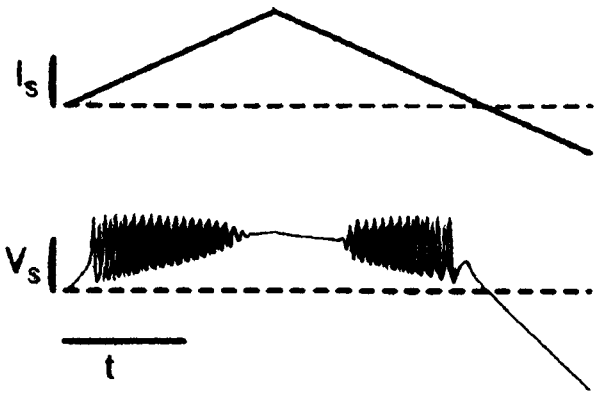

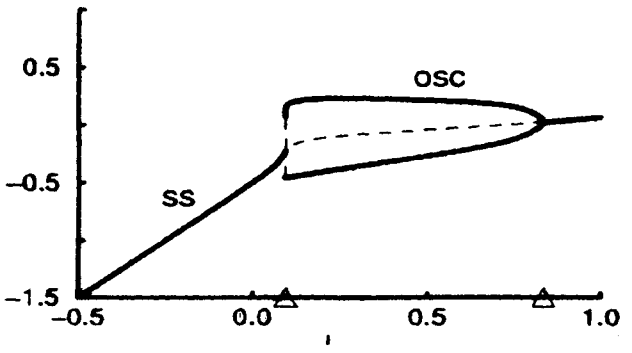

Isolated Dendrite - Response to I_{app}

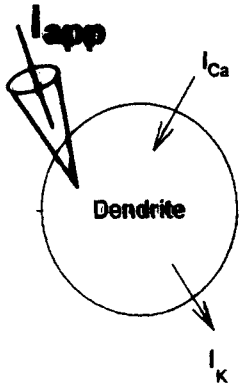

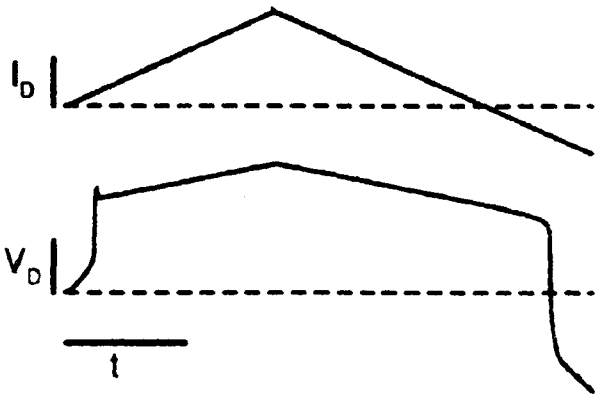

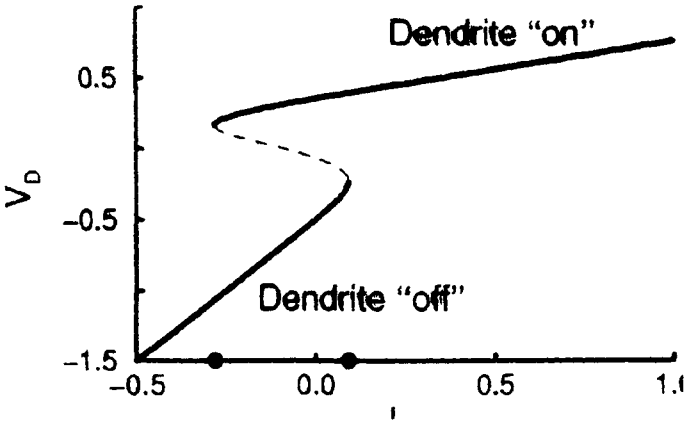

Minimal model
Bistable Motoneuron

w/ V. Booth (1994)

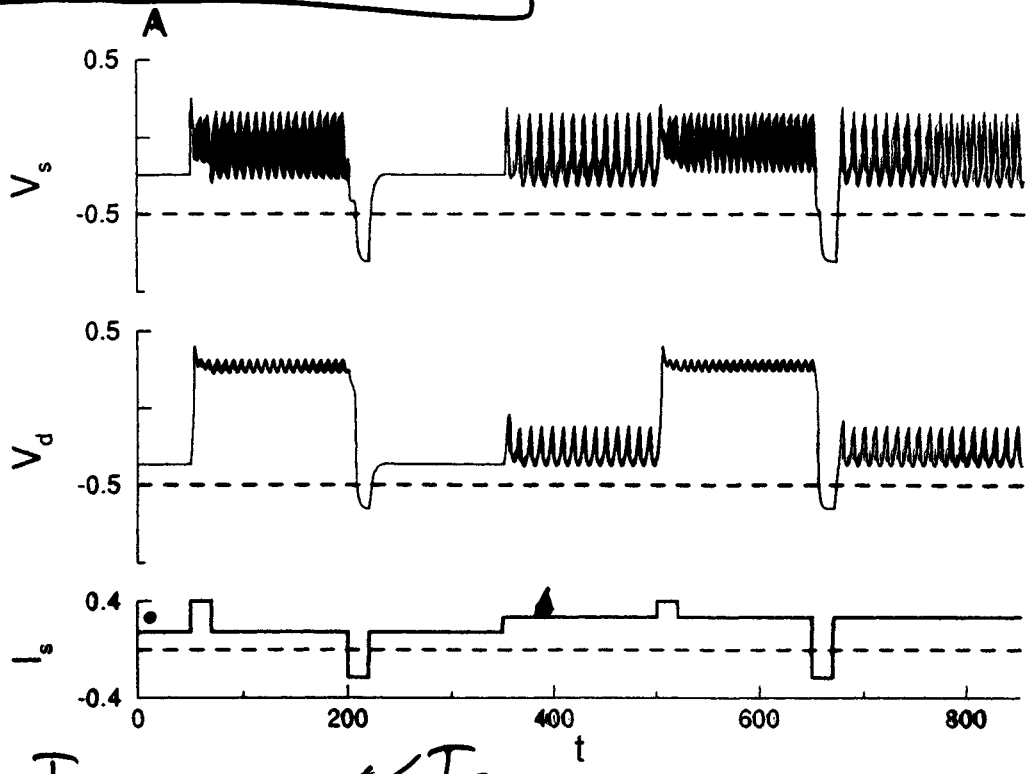

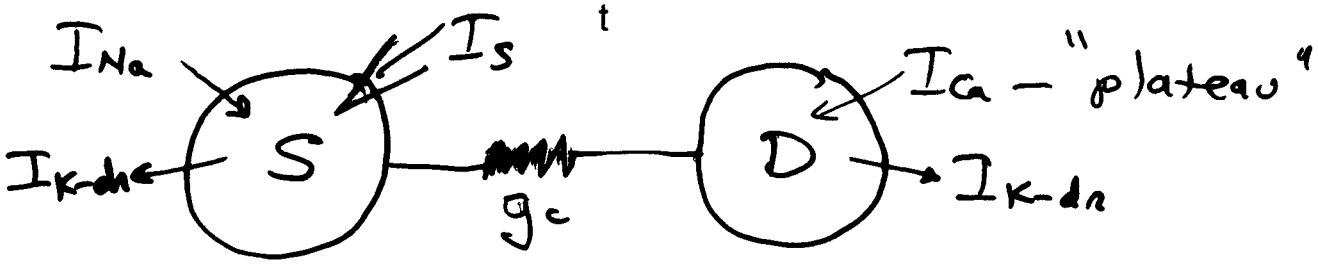

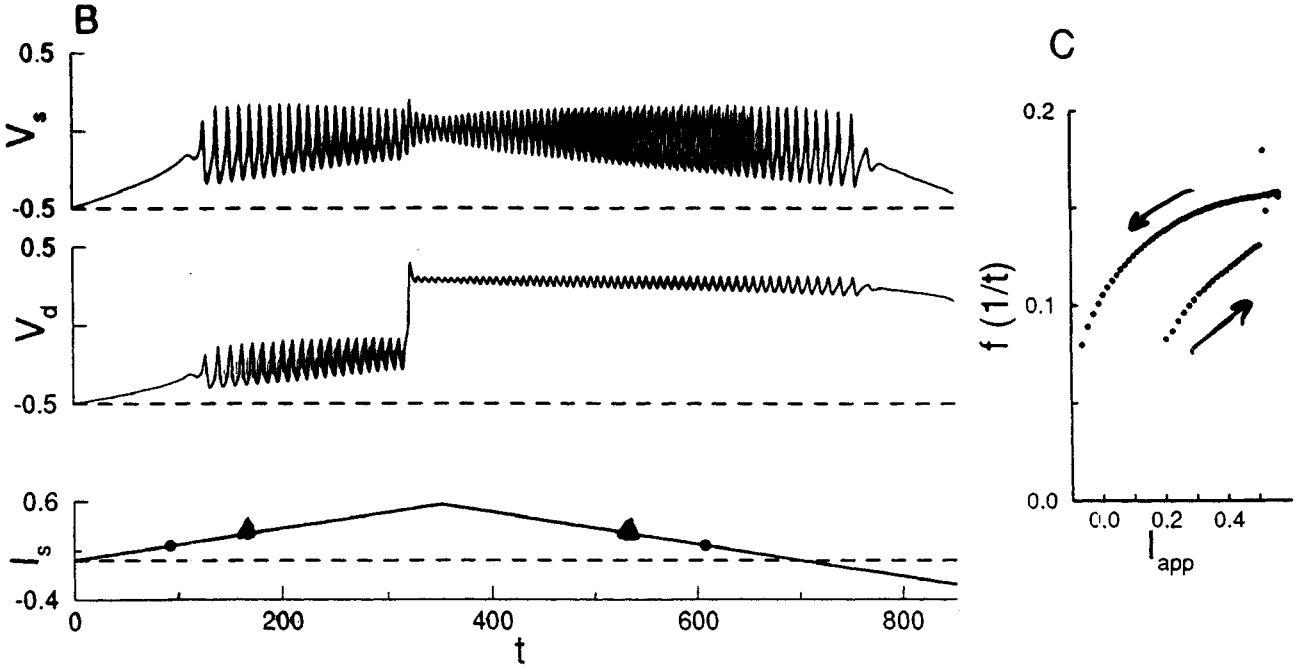

MBL
summer

FAST/SLOW Analysis of Bursting Oscillations

$\dot{X} = F(X, Y)$ — fast

$\dot{Y} = \varepsilon G(X, Y)$ — slow

Treat Y as parameter:

$$0 = F(X_{ss}, Y), \quad X_{ss} = X_{ss}(Y)$$

$$\dot{X}_{osc} = F(X_{osc}, Y), \quad X_{osc}(t) = X_{osc}(t+T), \quad T = T(Y)$$

Then superpose slow dynamics.

Square Wave Bursting

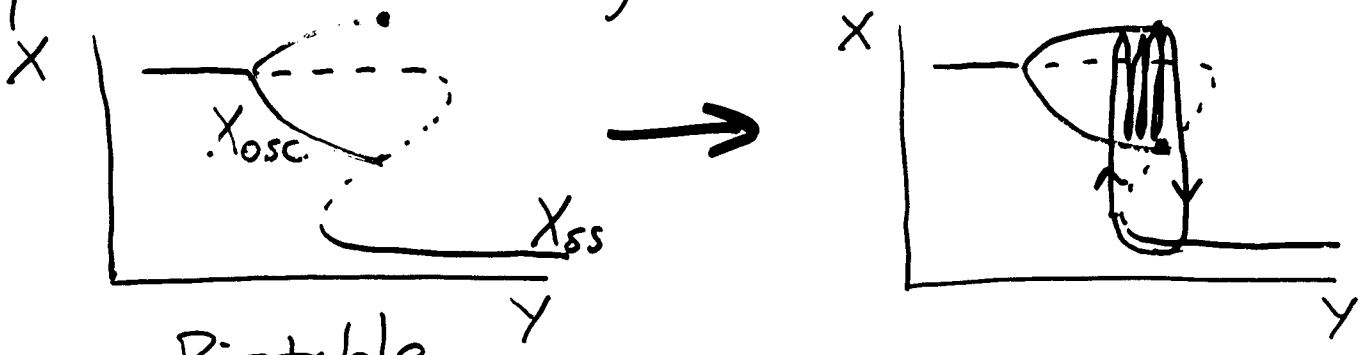

Bistable

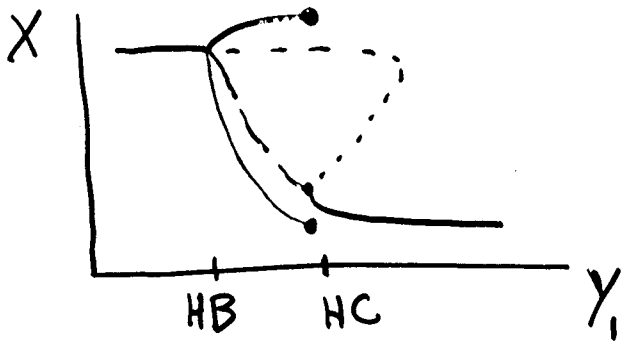

Monostable

Parabolic Bursting

$Y = (Y_1, Y_2)$

W+L

Summary

Wang + Rinzel, 1994

Hopf

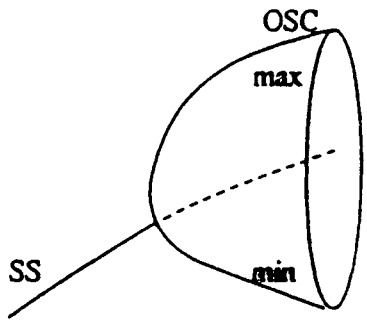

(supercritical)

Homoclinic

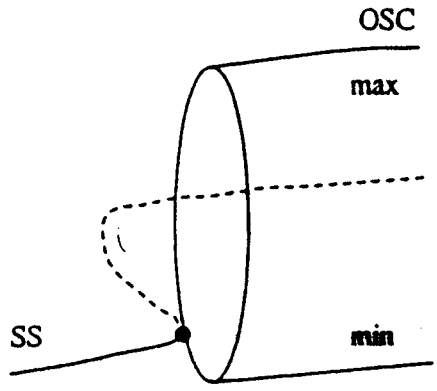

(at saddle-node)

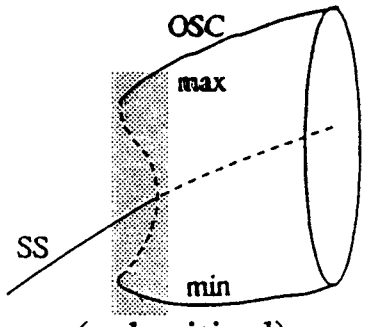

(subcritical)

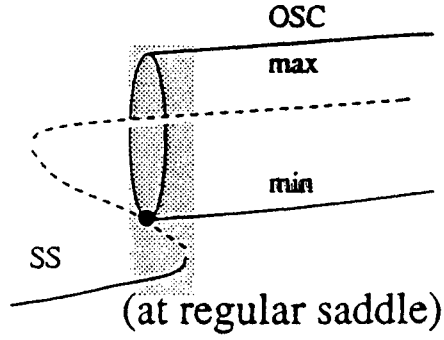

(at regular saddle)

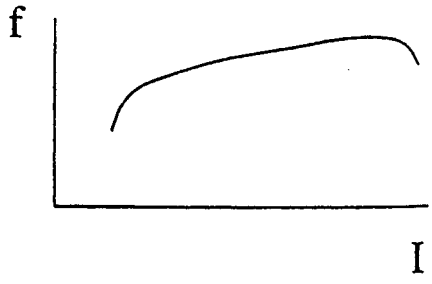

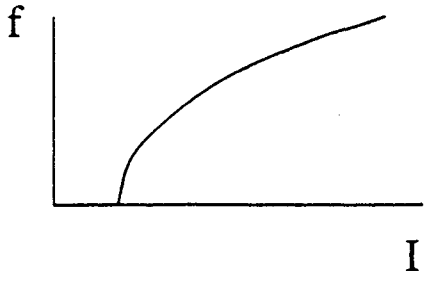

Wang & Rinzel, '94

A. B-cell

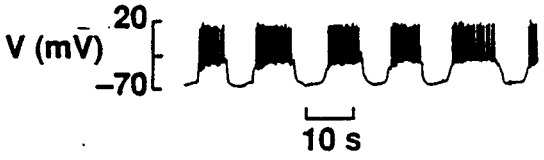

B. dopamine-neuron

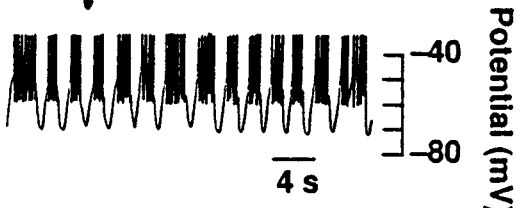

C. thalamic relay cell

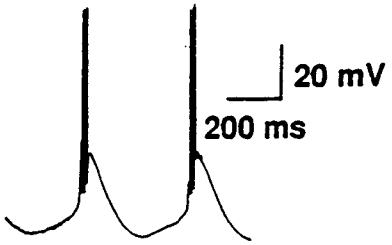

D. inferior olive cell

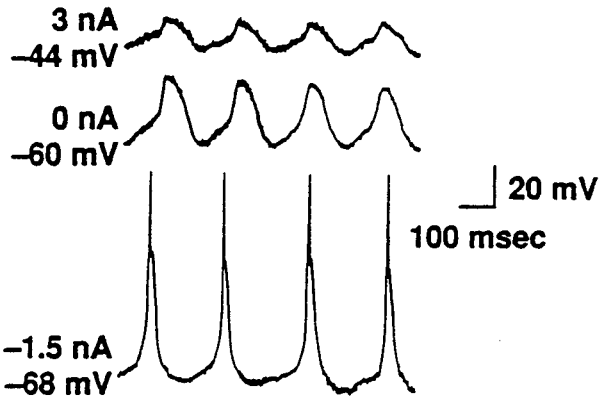

E. Aplysia R-15

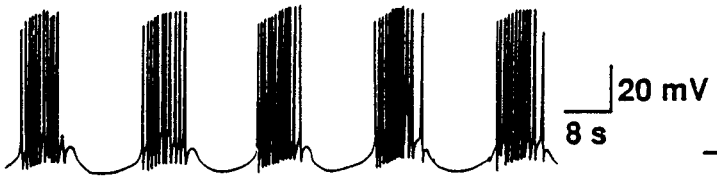

F. thalamic RE cell - cat

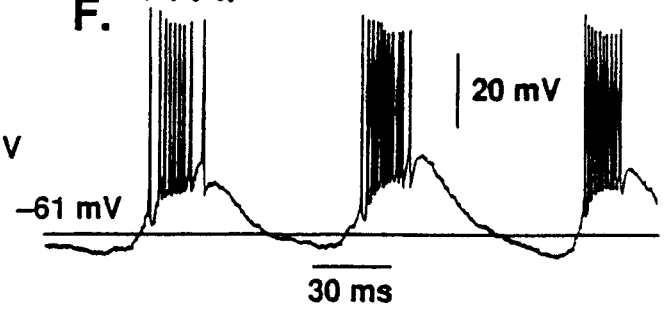

G. Sepia giant axon

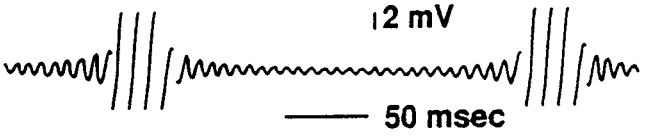

H. thalamic RE cell - rat

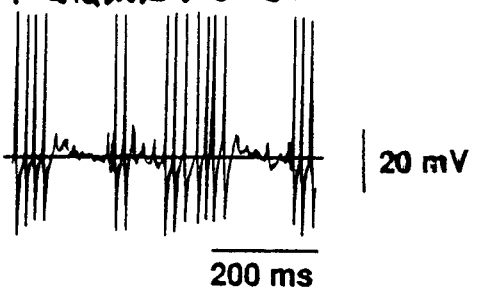

I. neocortical pyramidal

J. pituitary gonadotroph

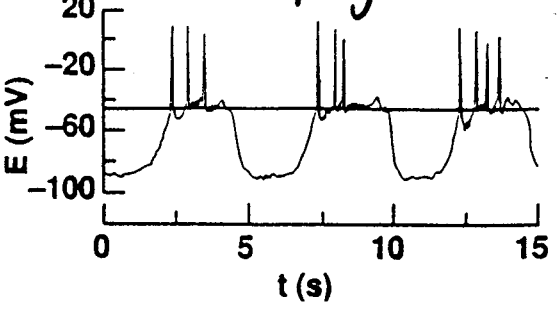

Wang + Rinzel, '94

$$\frac{dX}{dt} = F(X,Y)$$

$$\frac{dY}{dt} = \varepsilon\, G(X,Y)$$

X – fast, spike generating

Y – very slow

isopotential cell models

square wave

triangular

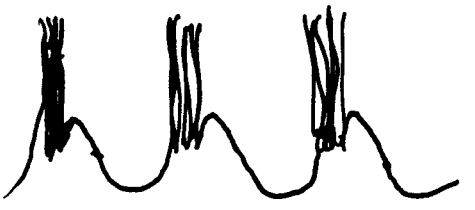

A.

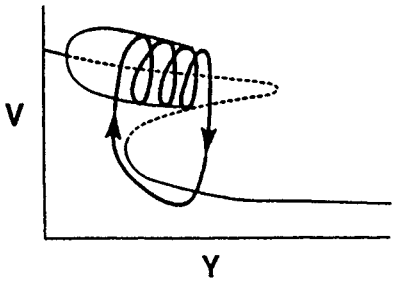

B.

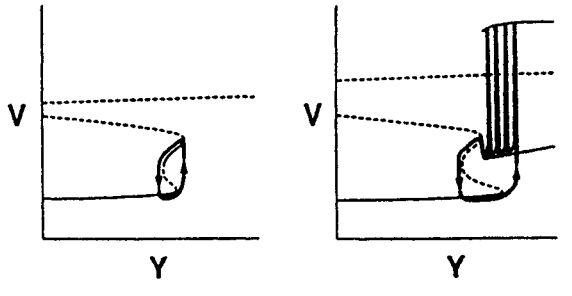

C. parabolic

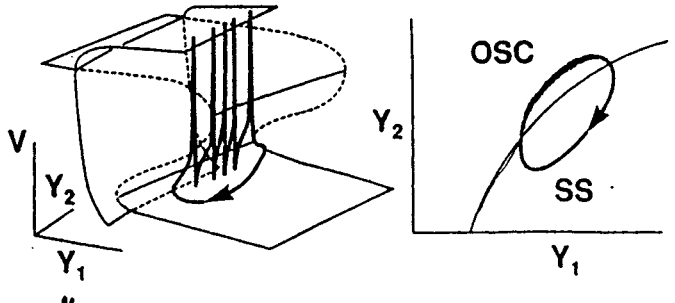

D. elliptic

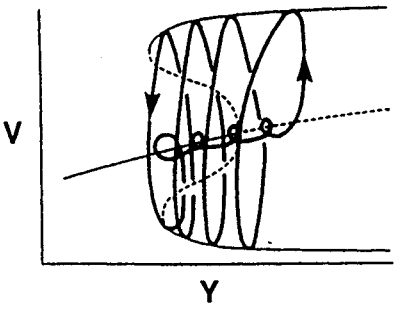

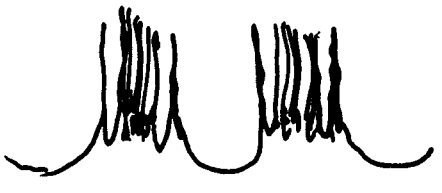

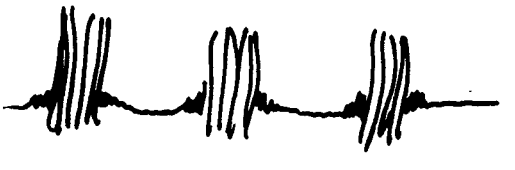

MBL

Slow adaptation can linearize f-I relation

(Ermentrout, '98)

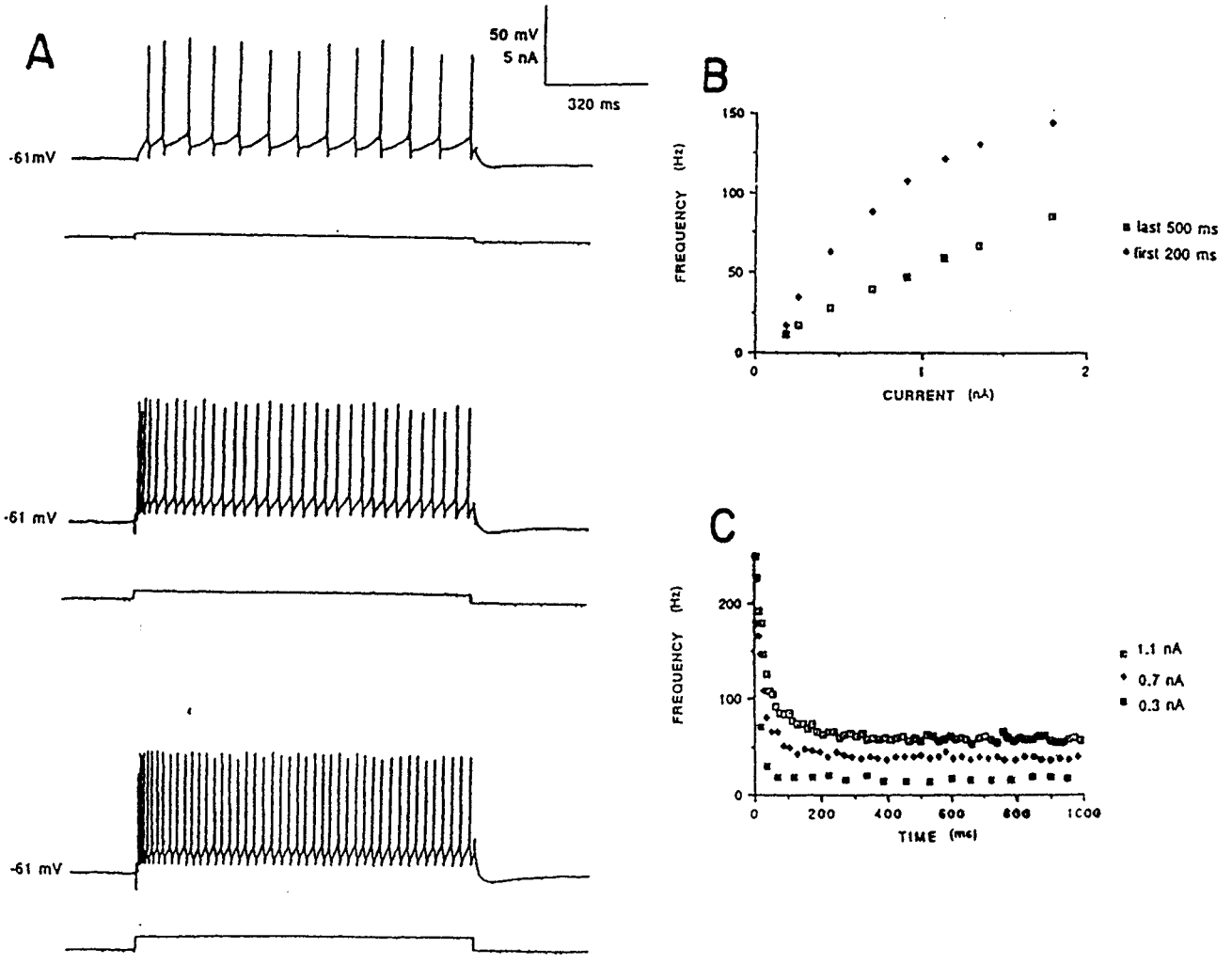

FIG. 1. Repetitive firing behavior of human neocortical neurons. *A*: repetitive firing was evoked by different stimulus intensities (0.2, 0.6, and 1.1 nA) at resting potential (RP = −61 mV). An increase in injected current resulted in a faster rate of firing. Spike amplitudes were attenuated by digitization. *B*: plot of the average firing frequency vs. injected current (f-*I*) at steady state (last 500 ms) and during the 1st 200 ms of a 1-s repetitive firing episode. *C*: plot of instantaneous firing frequency [1/interspike interval (ISI)] vs. time during the 1 s of firing (f-t) with different intensity stimuli (0.3 nA, 19 spikes; 0.7 nA, 45 spikes; 1.1 nA, 66 spikes) at RP. Note the decrease in firing frequency with time (spike frequency adaptation). *A–C* are taken from the same cell.

JOURNAL OF NEUROPHYSIOLOGY
Vol. 67, No. 2, February 1992. *Printed in U.S.A.*

Relationship Between Repetitive Firing and Afterhyperpolarizations in Human Neocortical Neurons

N. M. LORENZON AND R. C. FOEHRING
Department of Anatomy and Neurobiology, The University of Tennessee, Memphis, Tennessee 38103-4901

Idealized treatment.

$$C\dot{V} = -I_{HH} + I - \beta z$$

$$\dot{m} = \quad -$$

$$\vdots$$

βz — slow negative feedback current, strength β

eg. $\dot{z} = \varepsilon (z_\infty(V) - z)$

Suppose for $\beta = 0$:

$$f = A\sqrt{I - I_{SN}} \qquad (SNIC)$$

Since z is slow, it "averages" V-spikes and $\dot{V}$ feels only this average.

$z \doteq \eta f$ $\qquad$ η = "unitary" current / spike

f = spike freq.

$\Rightarrow$ (approx^{n})

$$C\dot{V} = -I_{HH} + I - \underbrace{\beta \eta f}$$

an f-dependent decrease of input.

(good for low f)

Thus, steady state firing

$$f = A\sqrt{I_{eff} - I_{SN}} = A\sqrt{I - \beta\eta f - I_{SN}}.$$

Slope $\frac{df}{dI}$?

$$\frac{df}{dI} = \frac{A}{2} \frac{1}{\sqrt{I-I_{SN}}} \left(1 - \beta\eta \frac{df}{dI}\right)$$

$$\Rightarrow \left.\frac{df}{dI}\right|_{I \sim I_{SN}} = \frac{1}{\beta\eta}$$ sth. st. f-I is linear

$\beta \sim$ "gain".

$\beta \downarrow 0 \Rightarrow \frac{df}{dI} \uparrow \infty$

$\beta \uparrow \Rightarrow \frac{df}{dI} \downarrow$

(high gain ⟶ "larger dynamic range" — in neuro's def^{n})

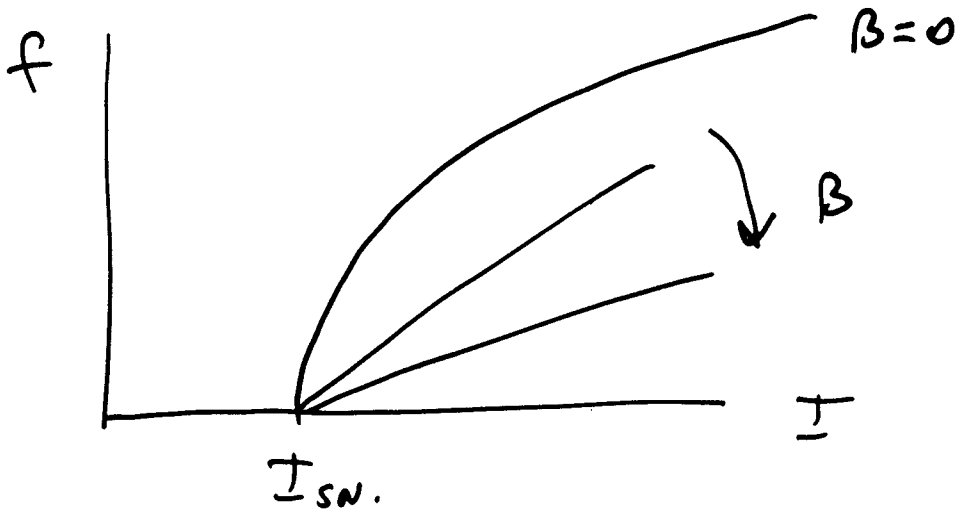

Time Course of Adaptation

eg. $C\dot{V} = -I_{HH} + I - \beta z (V - \bar{V})$

slow cond^{tc} ↑ say, V_K

$\vdots$

$\dot{z} = \varepsilon [z_\infty(V) - z]$

Let $s \doteq \langle z \rangle = \frac{1}{T} \int_0^T z(s)\,ds$

$\frac{ds}{dt} = \varepsilon [s_\infty(s, I) - s]$ "averaging" — replace z by s

$s_\infty = \frac{1}{T} \int_0^T z_\infty (V(t; s, I))\,dt$

not $z_\infty(\langle V \rangle)$.

Approx^n

what is $s_\infty(s, I)$? ... compute numerically

$s_\infty(s, I) \doteq f\,\eta$

low f

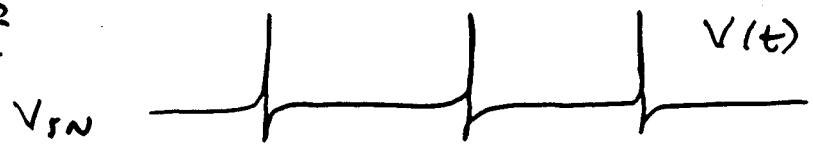

① $V \sim V_{SN}$ most of time

② $z_\infty(V(t)) \sim$ "δ-fn"

$\Rightarrow \quad \frac{ds}{dt} = \varepsilon [f\eta - s]$

$C\dot{V} = -I_{HH} + I - \beta s (V_{SN} - \bar{V})$

$= -I_{HH} + I - \beta' s$ $\qquad \beta' = \beta (V_{SN} - \bar{V})$

Now, slow J $\Rightarrow$ (SNIC)

$$f = f(I, J) = A\sqrt{I - \beta' J - I_{SN}}$$

$\therefore$

$$\frac{dJ}{dt} = \varepsilon\left[\eta A\sqrt{I - \beta' J - I_{SN}} - J\right]$$

If β' small (Ermentrout — empirical)

$$\sqrt{I - I_{SN} - \beta' J} \sim \sqrt{I - I_{SN}} - \frac{1}{2}\frac{\beta'}{\sqrt{I - I_{SN}}} J$$

$$\frac{dJ}{dt} = \varepsilon\left[\eta A\sqrt{I - I_{SN}} - \left(\frac{\eta A}{2}\frac{\beta'}{\sqrt{I - I_{SN}}} + 1\right) J\right]$$

$$\Rightarrow \quad \frac{1}{\tau_{adapt}} = \varepsilon\left(1 + \frac{\eta A}{2}\frac{\beta'}{\sqrt{I - I_{SN}}}\right) > \varepsilon$$

adaptation proceeds faster than rate ε, especially for $I \sim I_{SN}$

e.g. see Ermentrout ('98) Fig 2- w/ Traub's model

Also see Wang ('98) for $I_{K\text{-}Ca}$ example.

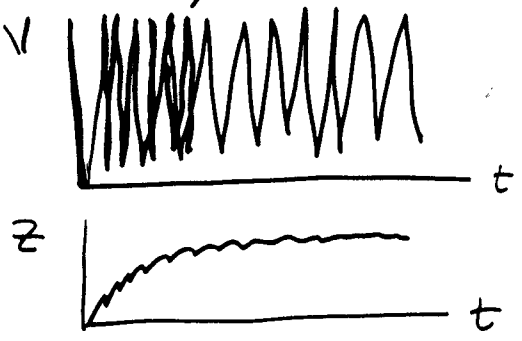

Example of

$f \sim \sqrt{I - I_{SN}}$

neocortical Layer V

Fatstrom, etal.

J Neurophys. 52 (1984) 264-277.

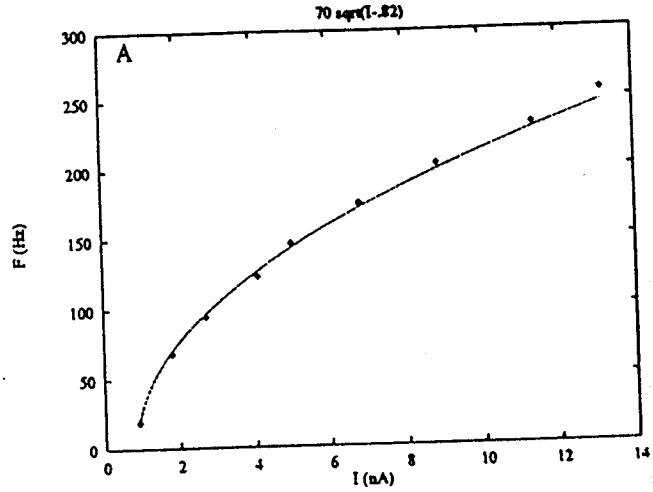

Slow adaptation shown by model of Traub for hippocampal neuron

(Traub + Miles, 1991, Neuronal Networks of the Hippocampus. Cambridge Univ. Press)

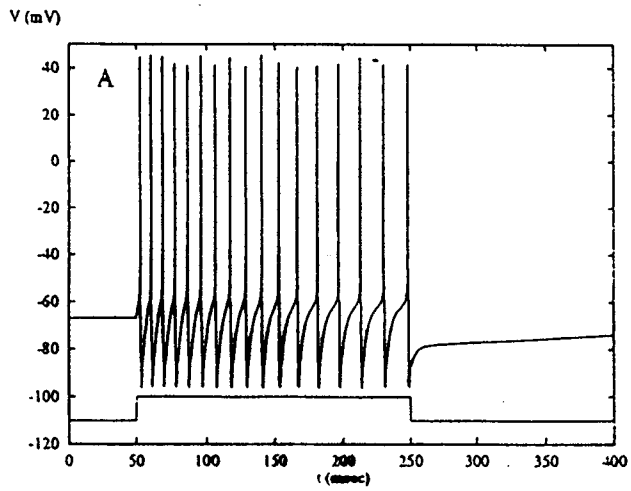

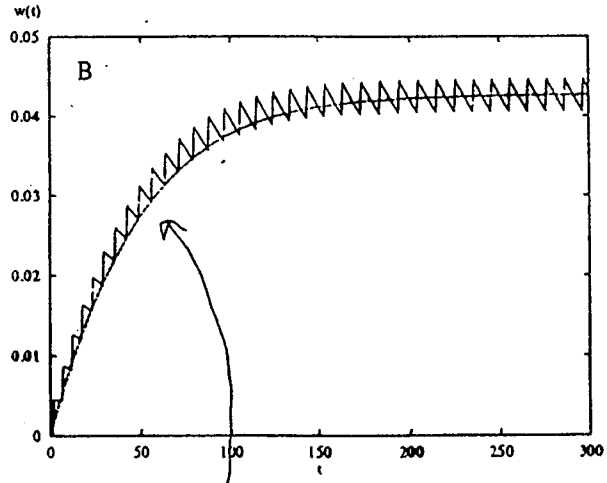

Smooth curve — approximate theory based on "averaging" adapt^{n} gating variable

Calcium Coding and Adaptive Temporal Computation in Cortical Pyramidal Neurons

XIAO-JING WANG

Center for Complex Systems and Department of Physics, Brandeis University, Waltham, Massachusetts 02254

Wang, Xiao-Jing. Calcium coding and adaptive temporal computation in cortical pyramidal neurons. *J. Neurophysiol.* 79: 1549–1566, 1998. In this work, we present a quantitative theory of temporal spike-frequency adaptation in cortical pyramidal cells. Our model pyramidal neuron has two-compartments (a "soma" and a "dendrite") with a voltage-gated Ca^{2+} conductance (g_{Ca}) and a Ca^{2+}-dependent K^+ conductance (g_{AHP}) located at the dendrite or at both compartments. Its frequency-current relations are comparable with data from cortical pyramidal cells, and the properties of spike-evoked intracellular [Ca^{2+}] transients are matched with recent dendritic [Ca^{2+}] imaging measurements. Spike-frequency adaptation in response to a current pulse is characterized by an adaptation time constant τ_{adap} and percentage adaptation of spike frequency F_{adap} [% (peak − steady state)/peak]. We show how τ_{adap} and F_{adap} can be derived in terms of the biophysical parameters of the neural membrane and [Ca^{2+}] dynamics. Two simple, experimentally testable, relations between τ_{adap} and F_{adap} are predicted. The dependence of τ_{adap} and F_{adap} on current pulse intensity, electrotonic coupling between the two compartments, g_{AHP} as well the [Ca^{2+}] decay time constant τ_{Ca}, is assessed quantitatively. In addition, we demonstrate that the intracellular [Ca^{2+}] signal can encode the instantaneous neuronal firing rate and that the conductance-based model can be reduced to a simple calcium-model of neuronal activity that faithfully predicts the neuronal firing output even when the input varies relatively rapidly in time (tens to hundreds of milliseconds). Extensive simulations have been carried out for the model neuron with random excitatory synaptic inputs mimicked by a Poisson process. Our findings include *1*) the instantaneous firing frequency (averaged over trials) shows strong adaptation similar to the case with current pulses; *2*) when the g_{AHP} is blocked, the dendritic g_{Ca} could produce a hysteresis phenomenon where the neuron is driven to switch randomly between a quiescent state and a repetitive firing state. The firing pattern is very irregular with a large *coefficient of variation* of the interspike intervals (ISI CV > 1). The ISI distribution shows a long tail but is not bimodal. *3*) By contrast, in an intrinsically bursting regime (with different parameter values), the model neuron displays a random temporal mixture of single action potentials and brief bursts of spikes. Its ISI distribution is often bimodal and its power spectrum has a peak. *4*) The spike-adapting current I_{AHP}, as delayed inhibition through intracellular Ca^{2+} accumulation, generates a "forward masking" effect, where a masking input dramatically reduces or completely suppresses the neuronal response to a subsequent test input. When two inputs are presented repetitively in time, this mechanism greatly enhances the ratio of the responses to the stronger and weaker inputs, fulfilling a cellular form of lateral inhibition in time. *5*) The [Ca^{2+}]-dependent I_{AHP} provides a mechanism by which the neuron unceasingly adapts to the stochastic synaptic inputs, even in the stationary state following the input onset. This creates strong negative correlations between output ISIs in a frequency-dependent manner, while the Poisson input is totally uncorrelated in time. Possible functional implications of these results are discussed.

INTRODUCTION

Cortical neurons display a large repertoire of voltage- and calcium-gated potassium ion channels with kinetic time constants ranging from milliseconds to seconds (Llinás 1988; Rudy 1988; Storm 1990). The diversity and richness of K^+ conductances indicate that they likely contribute to neuronal input-output computation in ways more complex than sculpturing the waveform of action potentials or regulating the overall membrane excitability. For example, slow K^+ currents, in interplay with Ca^{2+} and/or Na^+ currents, can generate rhythmic firing patterns intrinsic to single neurons (Llinás 1988; Wang and Rinzel 1995). Or a slowly inactivating K^+ current can integrate synaptic inputs in a temporal-history–dependent manner (Storm 1988; Turrigiano et al. 1996; Wang 1993). Moreover, K^+ channels at dendritic sites are capable of modifying cable properties and may regulate synaptic transmission (Hoffman et al. 1997) and prevent input saturation (Bernander et al. 1994; Wilson 1995).

Spike-frequency adaptation that depends on a Ca^{2+}-gated K^+ conductance is a conspicuous neuronal firing characteristic exhibited by a majority of ("regular spiking") pyramidal neurons in neocortex and hippocampus (Avoli et al. 1994; Connors et al. 1982; Foehring et al. 1991; Gustafsson and Wigström 1981; Lanthorn et al. 1984; Lorenzon and Foehring 1992; Mason and Larkman 1990; McCormick et al. 1985). In response to a constant current pulse, the firing frequency of an adapting neuron is initially high then decreases to a lower steady-state plateau level within hundreds of milliseconds. This phenomenon has been studied intensively in in vitro slice experiments (as is the case for all afore-cited references). Recently, Ahmed et al. (1993; B. Ahmed, C. Anderson, R. J. Douglas; K.A.C. Martin, unpublished results) observed and quantified spike-frequency adaptation of in vivo cortical neurons with intracellular recordings from the primary visual cortex of the anesthetized cat. They found that when subjected to a injected current pulse, the adaptation time course of cortical cells can be fitted empirically by an exponential time course (Ahmed et al. 1993; unpublished results), i.e., the instantaneous firing rate $f(t) = f_{ss} + (f_0 - f_{ss}) \exp(-t/\tau_{adap})$, where f_0 is the initial firing rate, f_{ss} is the steady-state firing rate, and τ_{adap} is an *adaptation time constant*. Thus this time course is characterized by two quantities: τ_{adap} and the percentage adaptation of firing frequency $F_{adap} = (f_0 - f_{ss})/f_0$. Ahmed

0022-3077/98 $5.00

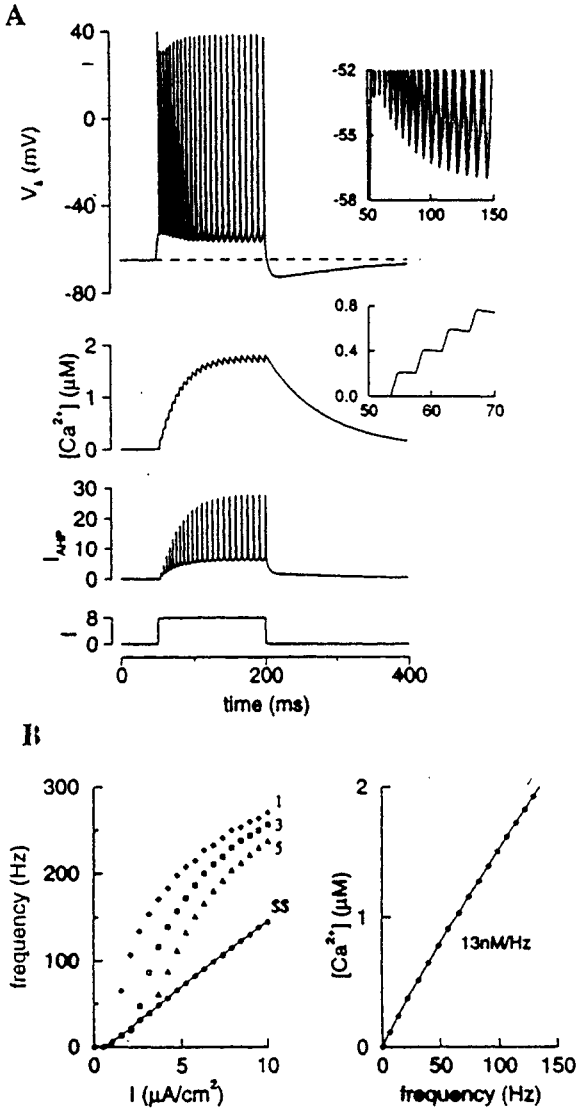

FIG. 1. Spike-frequency adaptation characteristics. *A*: an example of spike-frequency adaptation in response to a current pulse. Adaptation is accompanied by a gradual increase of the fast spike afterhyperpolarization (AHP; *top, inset*). Each action potential generates a $[Ca^{2+}]$ influx of ~200 nM (*bottom, inset*), and the adaptation time course follows that of $[Ca^{2+}]$ (hence I_{AHP}) accumulation. Slow AHP after the spike firing mirrors the $[Ca^{2+}]$ decay process. *B*: 1st, 3rd, and 5th instantaneous firing rates and the steady-state firing rate vs. the applied current intensity (*left*). Initial *f-I* curves are nonlinear, but the steady-state *f-I* relation is essentially linear. Plateau $[Ca^{2+}]$ level is a linear function of the steady-state firing rate, with a slope of ~13 nM/Hz (*right*).

subroutine Spctrm.c from Numerical Recipes (Press et al. 1989), modified by Yinghui Liu.

RESULTS

Time course of spike-frequency adaptation

In response to a depolarizing current pulse, the model neuron initially fires at a high frequency, then adapts to a lower steady-state frequency (Fig. 1*A*). Spike-frequency adaptation is accompanied by a gradual increase of the fast spike AHP (from −53 to −57 mV, see Fig. 1*A*, *inset*). This

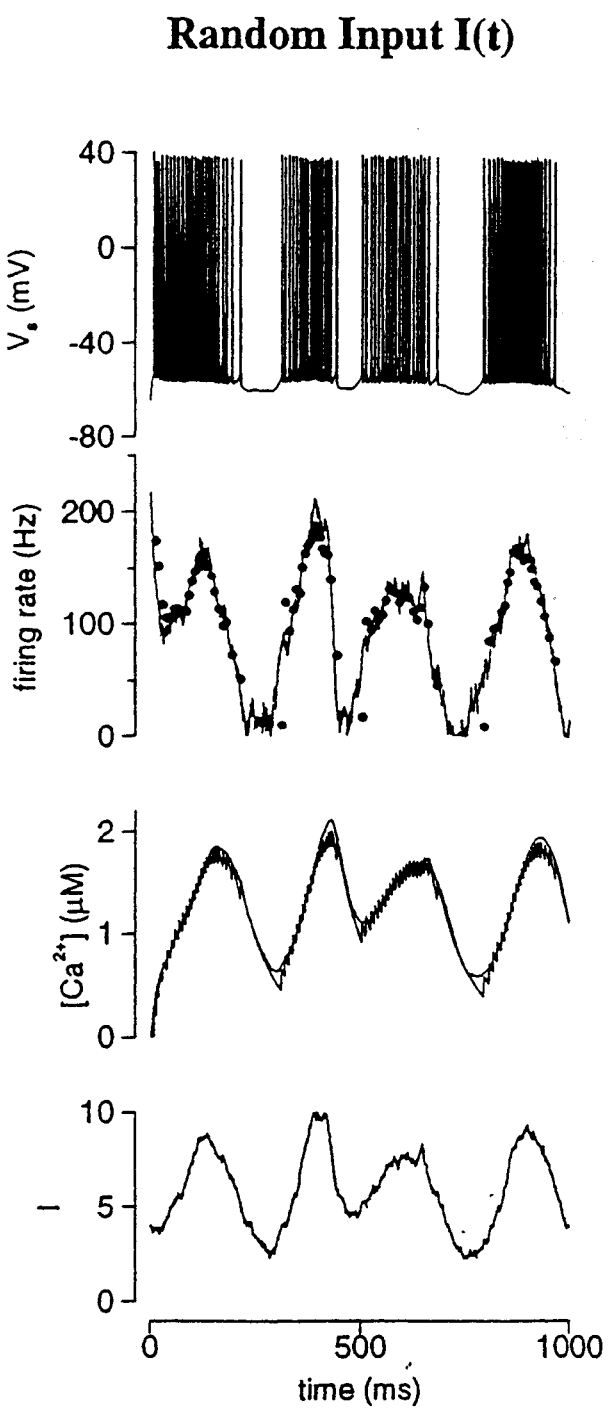

FIG. 4. Calcium coding of neuronal electrical activity. In response to a temporally varying input $I(t)$ (*bottom*), the cell's firing (*blue dots, middle top*) and $[Ca^{2+}]$ time course (*blue curve, middle bottom*) are well predicted by the reduced calcium model *Eqs. 14* and *15* (*red curves*).

Relations between τ_{adap} and F_{adap}

In addition to the neuronal electrotonic structure, spike-frequency adaptation depends also on the channel conductances g_{Ca} and g_{AHP}, as well as the $[Ca^{2+}]$ kinetic parameters α and τ_{Ca}. These dependences were explored within the framework of our calcium-model. First, the initial firing rate

Square Wave Bursting.

2 examples

- pancreatic β-cell (whole islet) in response to glucose
- pacemaker cells in mammalian respiratory CPG.

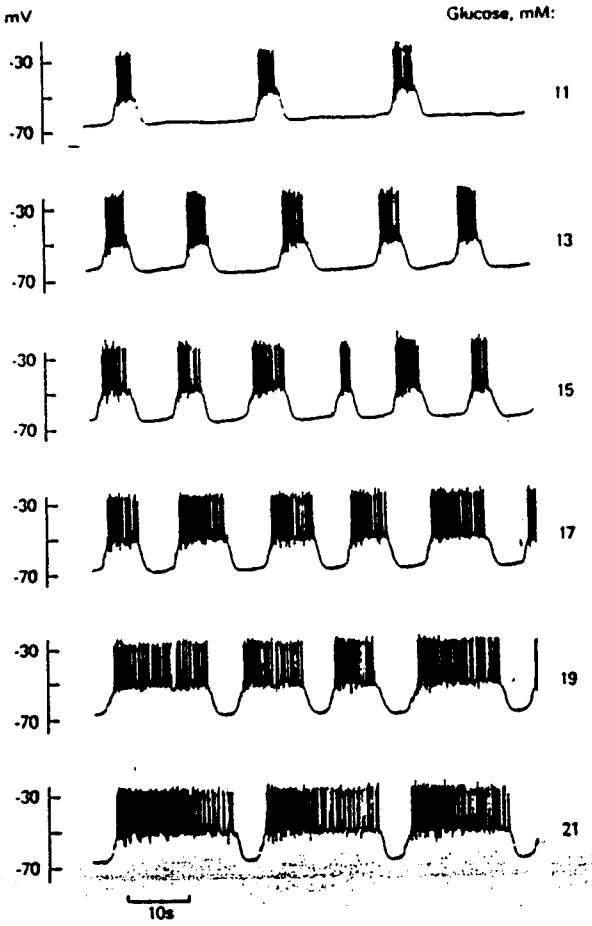

Fig. 5–14. Effect of graded increments of glucose concentration on membrane electrical activity. The figure shows steady state portions of a continuous record obtained at each glucose concentration from a single B-cell. Membrane potential during active phase (and during silent phase) is constant as glucose increases from 11 to 21 mM. The time spent in the active phase increases with glucose concentration. Note that the burst frequency first increases, then decreases as glucose concentration increases. (From Santos RM, unpublished data.)

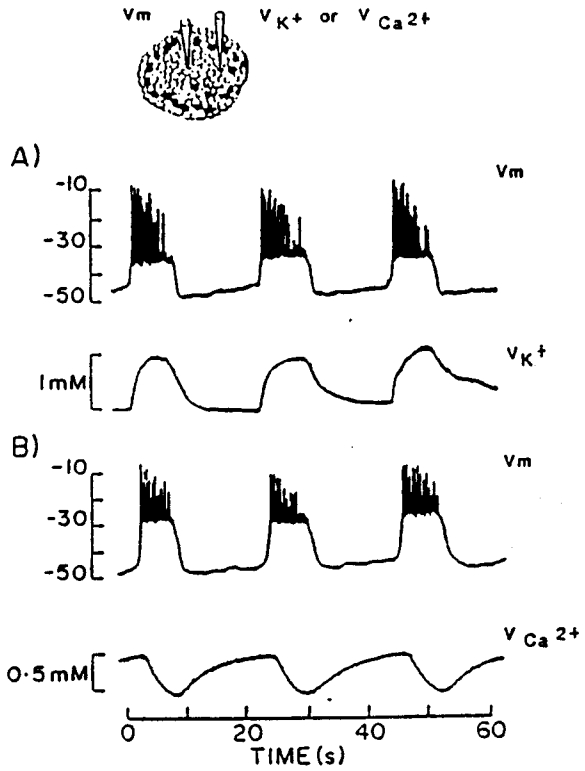

Fig. 5–30. Simultaneous measurements of glucose-evoked membrane potential fluctuations and cation-sensitive microelectrode potential. **A:** shows the membrane potential record from a cell about 20 μm from the surface of the islet. V_{K^+} represents the $[K^+]$-sensitive microelectrode potential record made with the tip at a depth of about 65 μm. The microelectrode tips were separated by about 110 μm. Islet perifused with Krebs solution plus 11 mM glucose at 37°C. **B:** represents the membrane potential record from a B-cell in another islet. V_{Ca}^{2+} represents the Ca^{2+}-sensitive electrode responses at approximately the center of islet. Islet in the presence of 11 mM glucose at 37°C. (Redrawn from Perez-Armendariz and Atwater, In *Biophysics of the Pancreatic B-cell*, 1986.)

Carroll Li
from Atwater et al 1989 — review ~~for Brenner~~
in Insulin Secretion v.I.
eds B. Pratin, S. Melmed, D. LeRoith
1989

First HH-like model for β-cell:

Chay & Keizer '84, Biophys J

Fast dynamics:

$m = m_\infty(V)$

$$C\dot{V} = -I_{Ca} - I_{K\text{-}dr} - I_{K\text{-}Ca} - I_L$$

$$\dot{n} = \phi \frac{n_\infty(V) - n}{\tau_n(V)} \quad \leftarrow \text{for } I_{K\text{-}dr}$$

$I_{K\text{-}Ca}$ — slow negative feedback

(next page)

Square Wave Bursting

- minimal
- 1 slow variable (neg. feedback)

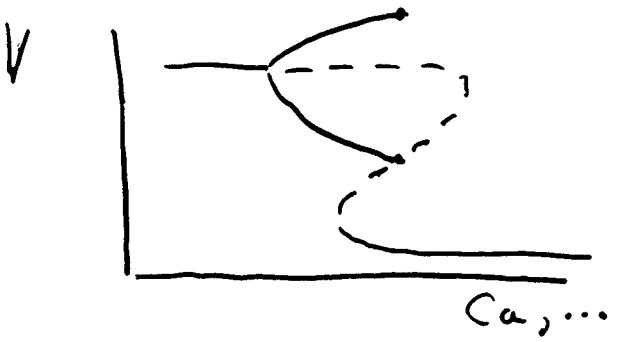

eg. $I_{K\text{-}Ca}$ – Ca-slow

I_{Ca} w/ Ca-inactiv^n
Ca-slow

I_{Ca} w/ slow V-inactiv^n

$$\dot{Ca} = f\left[-\alpha I_{Ca} - k\,Ca\right]$$

buffering, $f = \dfrac{[Ca^{2+}_{free}]}{[Ca_{TOT}]}$ ← how small?

removal rate

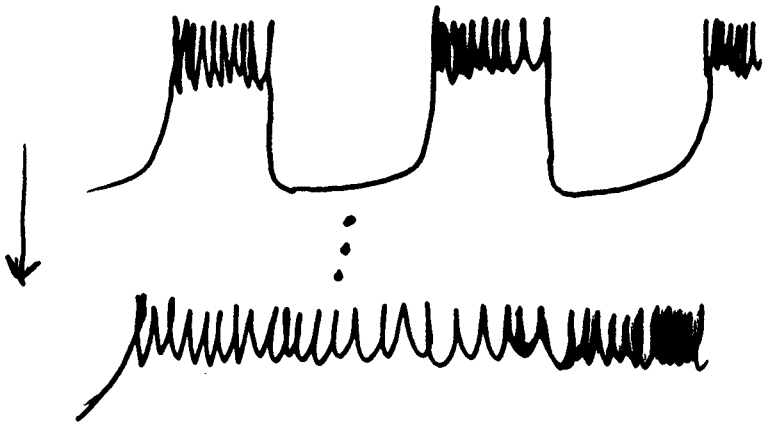

• "burst trajectory" indep. of k

• T_{Burst}

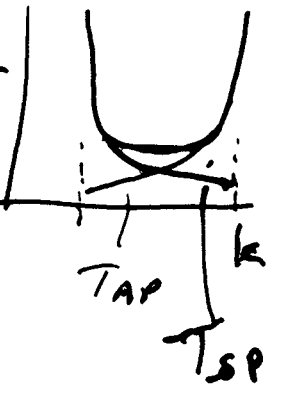

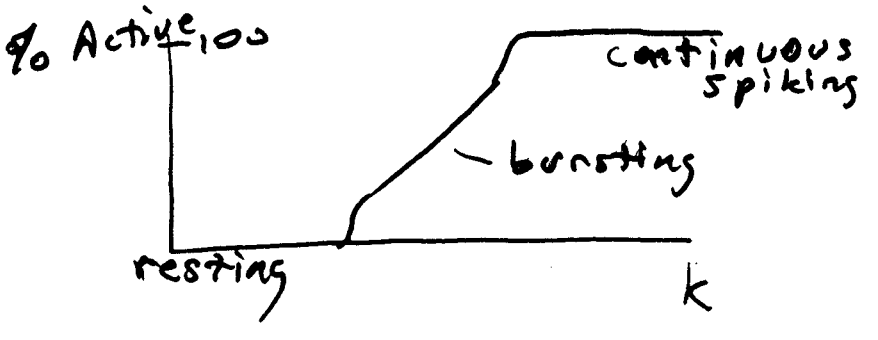

- resetting for brief I_{app}
- bistability crucial

$I_{K\text{-}Ca}$ — Ca-activated K^+-current

$$= \bar{g}_{K\text{-}Ca} \frac{Ca^q}{K^q + Ca^q} (V - V_K)$$

↑ dissociation const.

$I_{Ca\text{-}Ca}$ — inactiv^n of I_{Ca} by slow Ca

$$= \bar{g}_{Ca\text{-}Ca} m^p \left(\frac{1}{K + Ca}\right)^n (V - V_K)$$

↗ fast or slow

inactiv^n.

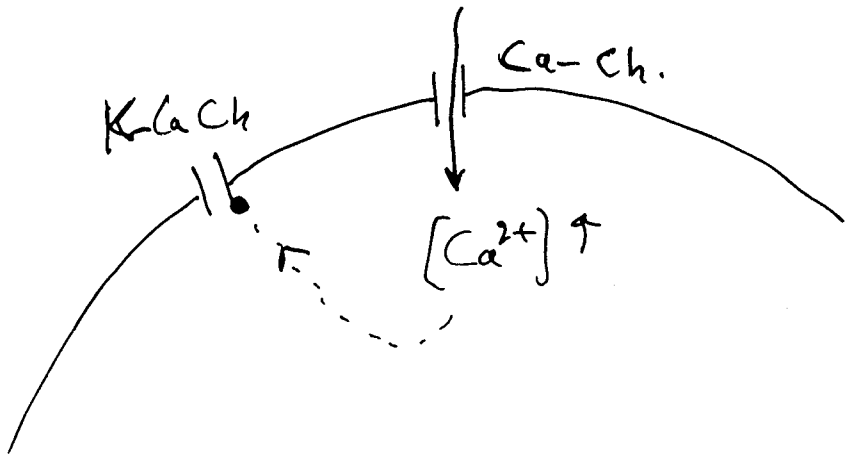

Fig 9 of Chapter, Rinzel + Ermentrout ('98)

Sq. Wave Bursting

$$z = \frac{Ca^6}{1 + Ca^6}$$

Ca, scaled $[Ca^{2+}]$

$$= \frac{[Ca^{2+}]}{K_D}$$

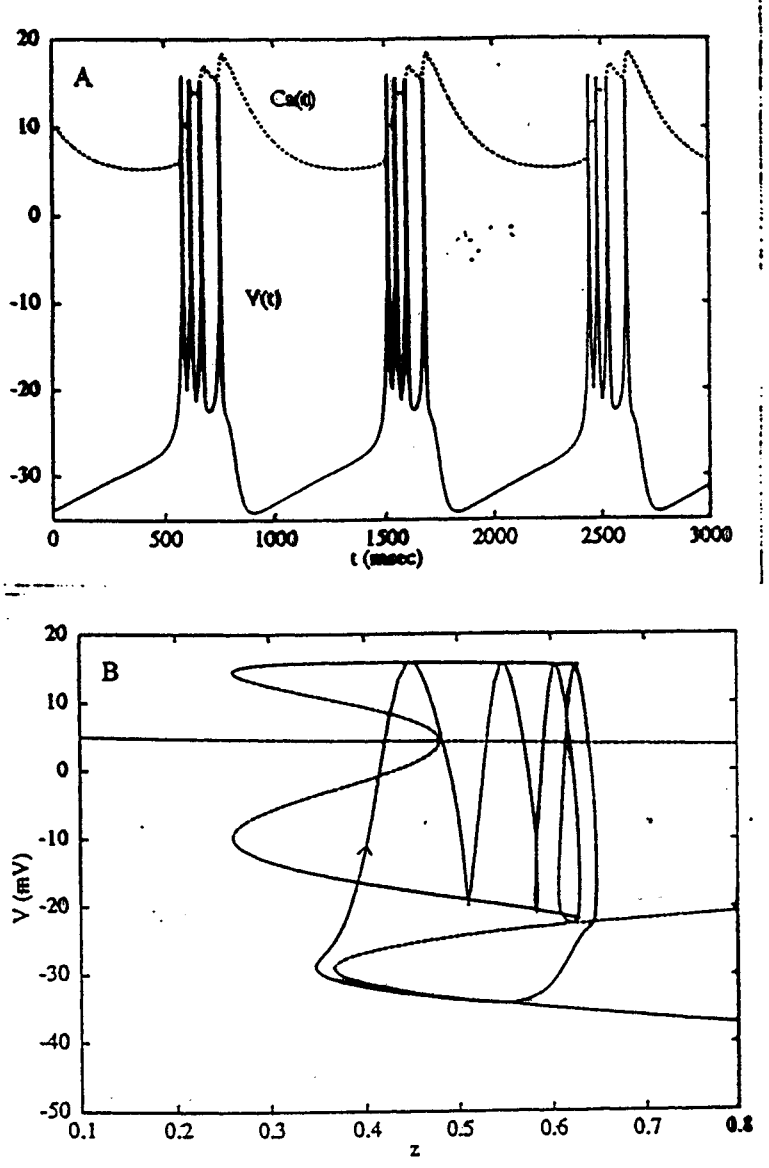

SUBMITTED VERSION
J Neurophys (in press)

Models of Respiratory Rhythm Generation in the pre-Bötzinger Complex: I. Bursting Pacemaker Neurons

Robert J. Butera, Jr.[1,2], John Rinzel[1,2,3], and Jeffrey C. Smith[2]

[1]Mathematical Research Branch, NIDDK
National Institutes of Health, Bethesda, MD USA

[2]Laboratory of Neural Control, NINDS
National Institutes of Health, Bethesda, MD USA

[3]Center for Neural Science and Courant Institute of Mathematical Sciences
New York University, New York, NY USA

To be submitted to *Journal of Neurophysiology*
September 21, 1998

Running Title: Respiratory Pacemaker Neurons

Abstract Word Count: 227
Manuscript Pages: 21
Figures: 11

Address correspondence to: Robert J. Butera, Jr.
Mathematical Research Branch, NIDDK, NIH
9190 Rockville Pike, Suite 350
Bethesda, MD 20814-3800 USA

Phone: (301) 496-9644
FAX: (301) 402-0535
email: butera@helix.nih.gov

Respiratory CPG pacemaker neurons

$\doteq$ HH

$$C\dot{V} = -I_{Na} - I_K - I_L - I_{Na,P} + I_{app} - I_{syn,tonic}$$

"persistent" Na-current w/ very slow inactivation

$$I_{Na,P} = \bar{g}_{Na,P}\, m_{P,\infty}(V)\, h_P\, (V - V_{Na})$$

ζ

slow negative feedback

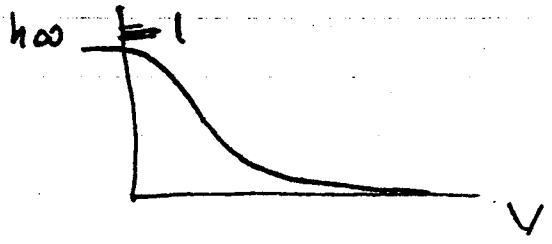

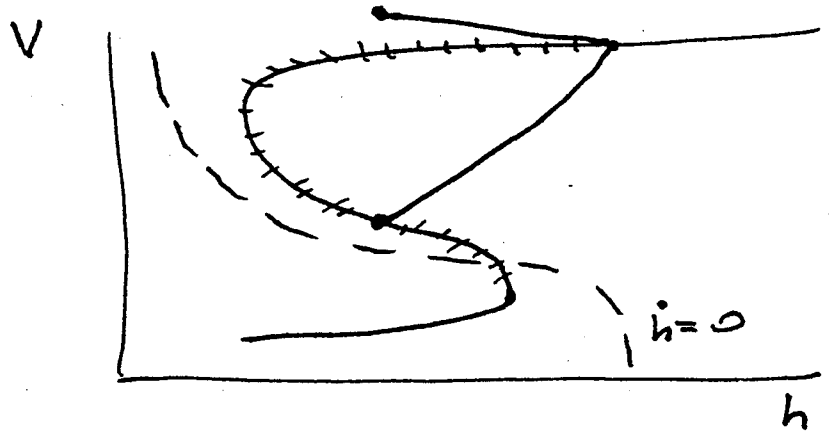

Fast subsystem

Lower branch & knee very sensitive to I_{app} and $I_{syn,tonic}$ – since no V-dependent conductances in low-V regime.

↑ treat as parameter

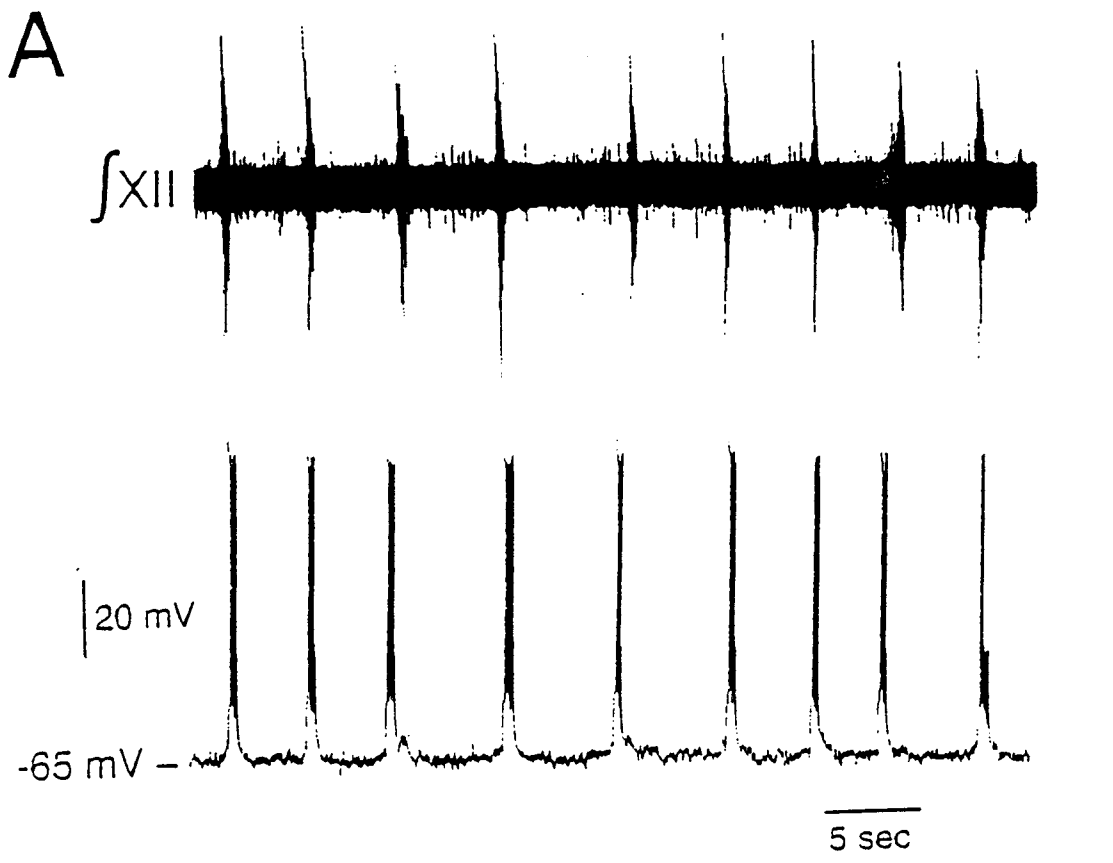
A
∫XII
20 mV
-65 mV
5 sec

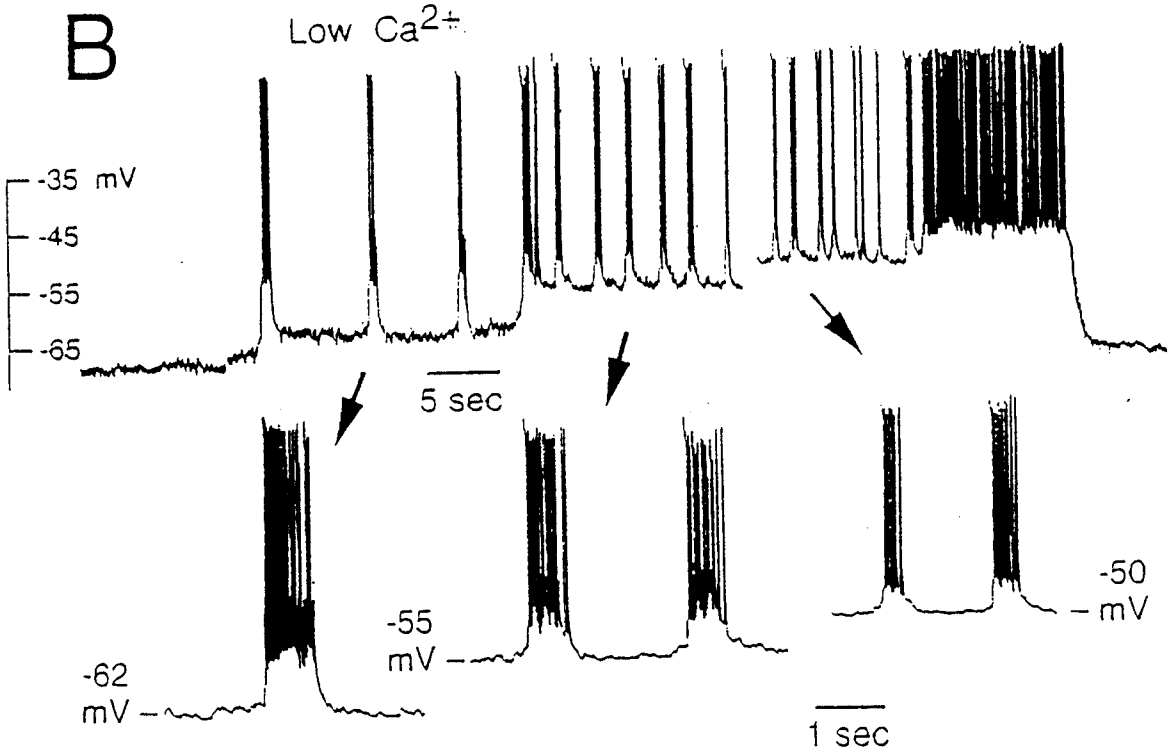
B
Low Ca2+
-35 mV
-45
-55
-65
5 sec
-62 mV
-55 mV
-50 mV
1 sec

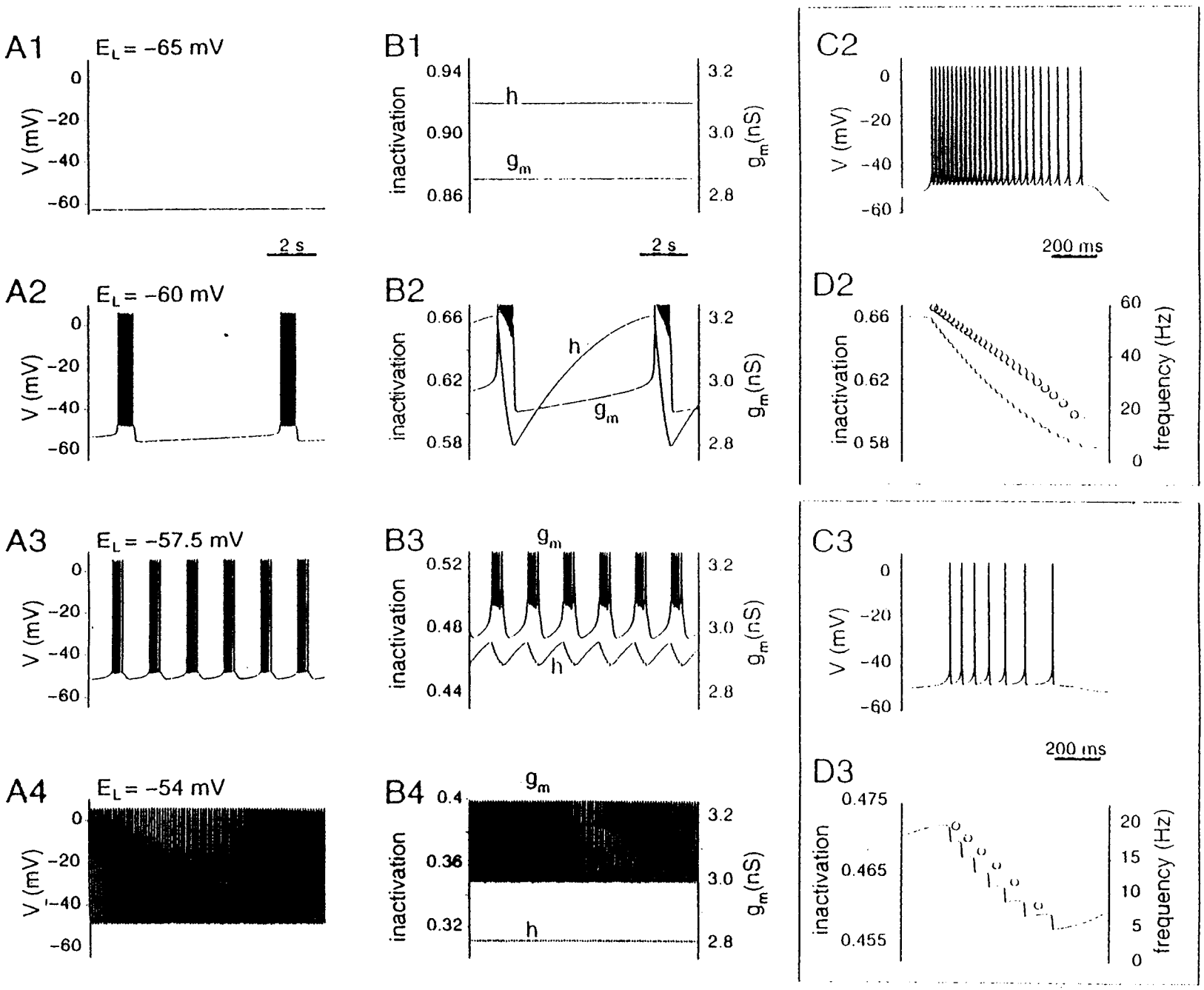
A1
E_L = −65 mV
V (mV)
0
−20
−40
−60
2 s
B1
inactivation
0.94
0.90
0.86
h
g_m
3.2
3.0
2.8
g_m(nS)
2 s
C2
V (mV)
200 ms
A2
E_L = −60 mV
B2
D2
inactivation
frequency (Hz)
60
40
20
0
0.66
0.62
0.58
A3
E_L = −57.5 mV
B3
0.52
0.48
0.44
C3
D3
200 ms
0.475
0.465
0.455
15
10
5
A4
E_L = −54 mV
B4
0.4
0.36
0.32

Elliptic Bursting

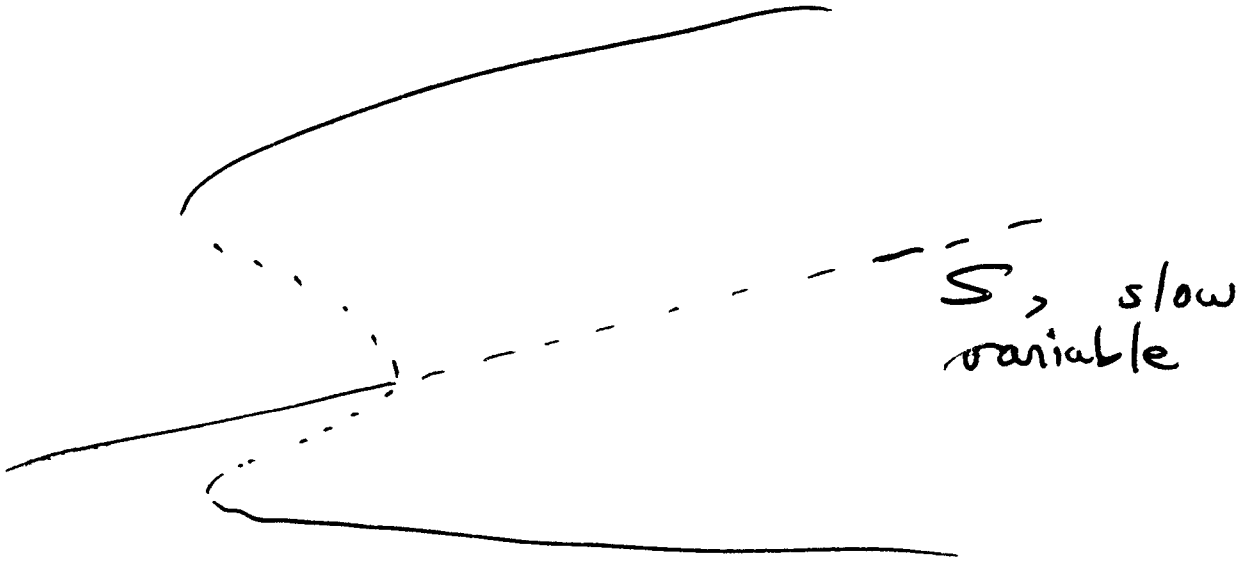

bistable — subcritical Hopf.

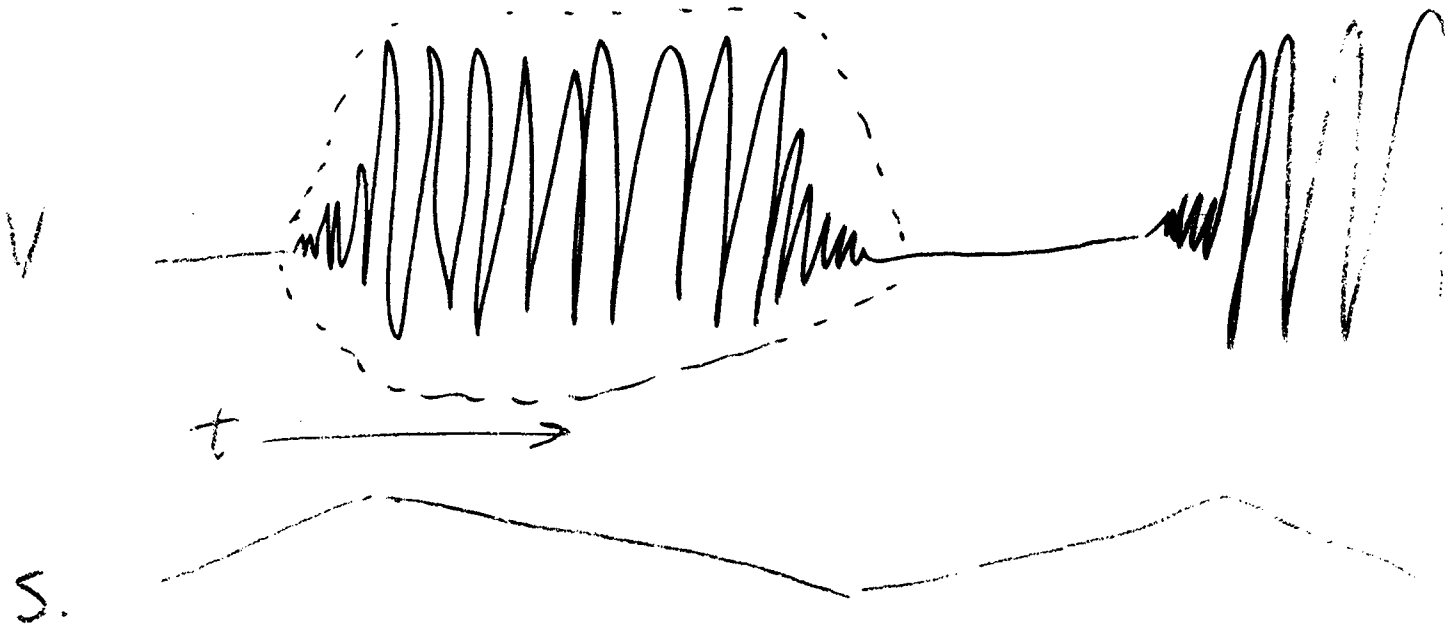

Example of "Elliptic Bursting"

from Chapt., Rinzel + Ermentrout ('98)

Fig. 10

w/ $I_{K\text{-}Ca}$ ⊕ Type II

$z = \frac{Ca^P}{1+Ca^P}$

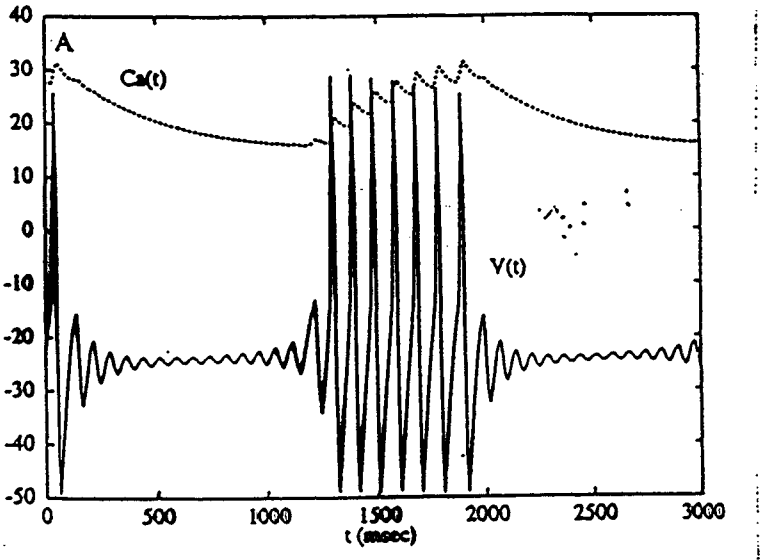

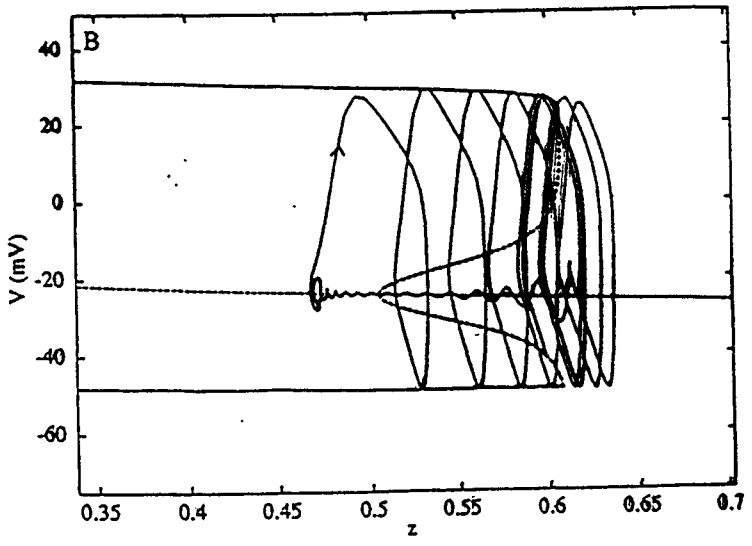

"elliptic" bursting mediated by I_A w/ slow inactiv?

$I_A = g_A a_\infty^3 b (V - V_K)$

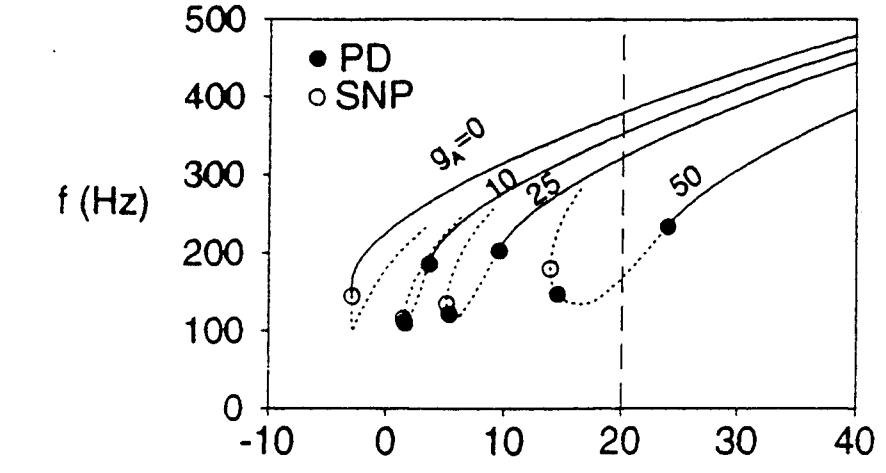

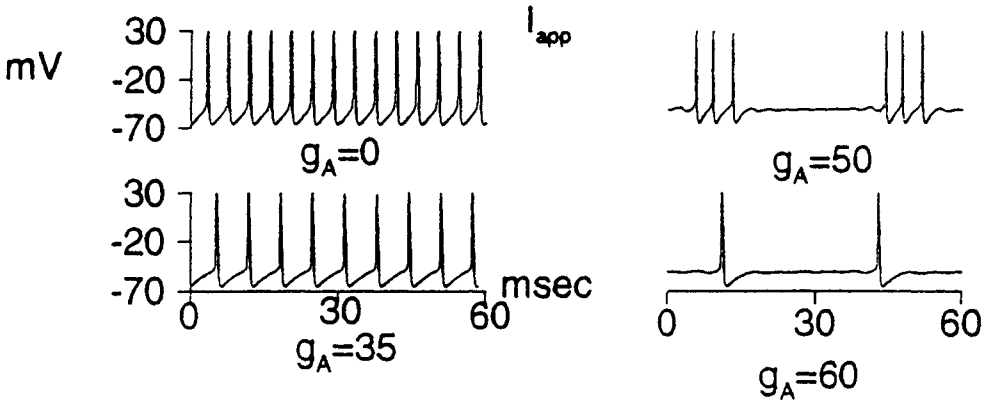

$\tau_b = 10ms$

P's undershoot b recovery of b

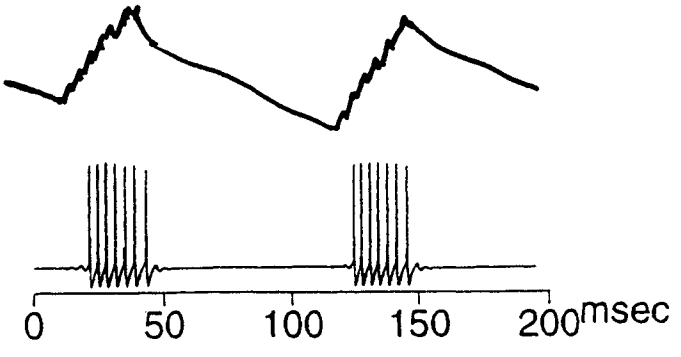

$\tau_b = 30ms$

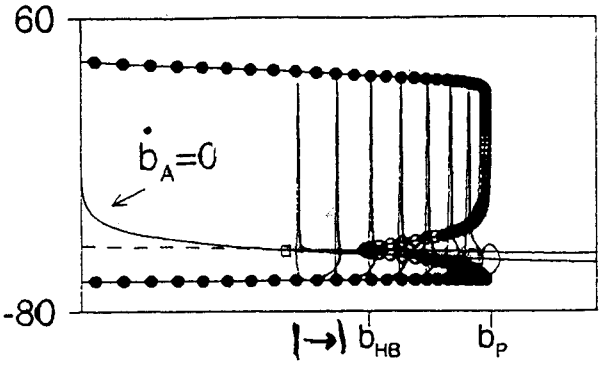

Rush + Rinzel (1995)

NeuroReport 5, 221–224 (1993)

Ionic basis for intrinsic 40 Hz neuronal oscillations

Xiao-Jing Wang

Department of Mathematics and the James Franck Institute, University of Chicago
5734 S. University Ave.
Chicago, Illinois 60637, USA

We present a biophysical model of a slowly inactivating potassium ion current I_{Ks} based on recent voltage-clamp data from layer V pyramidal neurons in the cat sensorimotor cortex and show that the interplay between a persistent sodium current I_{Nap} and I_{Ks} is able to produce intrinsic membrane potential oscillations in the 10- to 50-frequency range. A most notable characteristic of such rhythmicity is what may be termed *mixed-mode bursting*, where clusters of action potentials alternate in time with epochs of small subthreshold oscillations.

Key words: 40 Hz brain rhythm; Biophysical model; Hodgkin–Huxley formalism; Persistent sodium channel; Slowly inactivating potassium channel; Subthreshold oscillation; Clustering of Na^+ spikes; Mixed-mode bursting

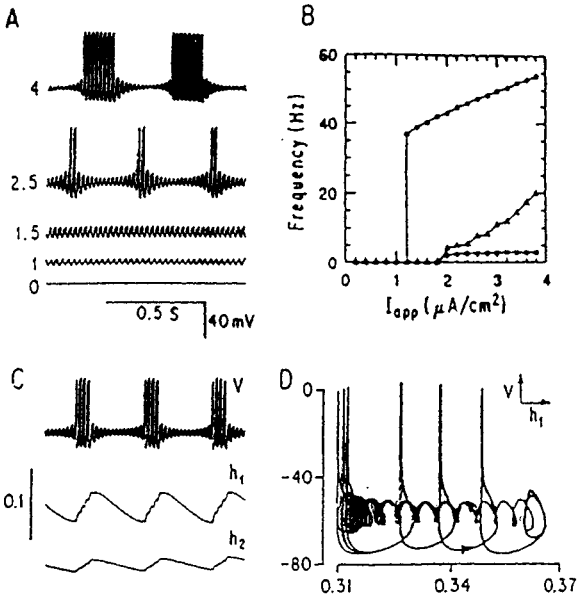

FIG. 2. (A) Membrane potential time courses at various I_{app} values (in μA cm^{-2}), showing transitions from the resting state, to subthreshold oscillation, then to bursting with Na^+ spike clusters interspersed with subthreshold oscillatory epochs. (B) The oscillation frequency (circle) is in a narrow range (35–55 Hz for $I_{app} < 4$). The bursting frequency (square) remains remarkably constant (~ 3 Hz), while the spike firing rate (triangle) (equal to the bursting frequency times the number of spikes per burst) increases gradually. The subthreshold oscillatory phase (respectively the burst) is associated with the gradual decrease (resp. increase) of h_1 and h_2 hence of I_{Ks}, as can be seen in the time traces (C) and the V-versus-h_1 plot (D) (with $I_{app} = 3$). ($\tau_m = 6$ ms, $\sigma = 0$ mV).

Evidence for a Novel Bursting Mechanism in Rodent Trigeminal Neurons

Christopher A. Del Negro,* Chie-Fang Hsiao,* Scott H. Chandler,* and Alan Garfinkel*#
*Department of Physiological Science and #Department of Medicine (Cardiology), University of California at Los Angeles, Los Angeles, California 90095-1568 USA

ABSTRACT We investigated bursting behavior in rodent trigeminal neurons. The essential mechanisms operating in the biological systems were determined based on testable predictions of mathematical models. Bursting activity in trigeminal motoneurons is consistent with a traditional mechanism employing a region of negative slope resistance in the steady-state current-voltage relationship (Smith, T. G. 1975. *Nature.* 253:450–452). However, the bursting dynamics of trigeminal interneurons is inconsistent with the traditional mechanisms, and is far more effectively explained by a new model of bursting that exploits the unique stability properties associated with spike threshold (Baer, S. M., T. Erneux, and J. Rinzel. 1989. *SIAM J. Appl. Math.* 49:55–71).

INTRODUCTION

Neuronal bursting is produced as slow membrane processes dynamically modulate the activity of faster membrane processes responsible for action potentials. Specific mechanisms for bursting have been studied mathematically and can be differentiated based on mechanism and phenomenology (Bertram et al., 1995).

Traditional bursting systems require inactivation-resistant inward currents that create a region of negative slope resistance (NSR) in the steady-state (or quasi-steady-state) current-voltage (*I-V*) relationship (Canavier et al., 1991; Li et al., 1996; Schwindt and Crill, 1980; Smith, 1975). The N-shaped *I-V* relationship provides the potential for two stable voltage states, one on each side of spike threshold (one state is quiescent and the other oscillatory). The cell then alternates between the two states during bursting (although it need not be bistable). The regenerative region of inward current separating the stable states predicts phenomenological features that can be used to identify traditional bursting in the laboratory, where membrane potential is frequently the only measurable variable: 1) cells can be locked into quiescent or active states by sufficient current bias; 2) bursts initiate rapidly, in contrast to the slow trajectory of the quiescent phase, with a marked upswing in membrane potential; 3) spikes in the active phase emerge at full amplitude from the steady-state membrane potential of the quiescent phase; and 4) burst termination is accompanied by a decline in spike frequency. Traditional bursting has been observed in many experimental preparations. Canonical examples include the pancreatic β cell (Ashcroft and Rorsman, 1989; Atwater et al., 1980) for bistable (or type 1; Bertram et al., 1995) bursting and *Aplysia*'s R15 neuron for parabolic (or type 2; Bertram et al., 1995) bursting (Benson and Adams, 1989; Canavier et al., 1991; Rinzel and Lee, 1987).

Another mechanism for bursting has been proposed theoretically (Av-Ron et al., 1993; Bertram et al., 1995; Honerkamp et al., 1985; Rinzel, 1987, Fig. 4; Wang, 1993b) but has not yet been identified experimentally. This novel mechanism, which we will call type 3 bursting, based on Bertram's classification scheme (Bertram et al., 1995), does not require a region of NSR in the steady-state *I-V* relationship, but rather exploits unique stability properties near spike threshold. The mechanistic framework also predicts phenomenology that can be used empirically to identify type 3 bursting: 1) bursting evolves from intermittent discharge as cells are depolarized by current bias, 2) bursts initiate with a slow linear voltage trajectory (as opposed to a rapid voltage upswing in traditional bursting), 3) full-amplitude spikes emerge from subthreshold oscillations (as opposed to a steady-state potential as in traditional bursting), and 4) spike frequency may not decline at burst termination.

Bursting mechanisms in rodent trigeminal neurons controlling jaw movements can be assigned based on the theoretical predictions above. Using experimental data, we identify, for the first time, type 3 bursting dynamics in a biological system: the neonatal rat trigeminal interneuron (TI). We contrast this new mechanism with the traditional bursting that occurs in trigeminal motoneurons (TMNs) (Hsiao et al., 1998).

MATERIALS AND METHODS

Electrophysiological experiments were performed on TIs obtained from 300-μm-thick transverse slices of neonatal rat brain stem (0–7 days). Slices were perfused (4 ml/min) at room temperature by oxygenated solution containing (in mM) 124 NaCl, 3 KCl, 1.25 NaH_2PO_4, 26 $NaHCO_3$, 10 D-glucose, 2 $CaCl_2$, and 2 $MgCl_2$. Whole-cell patch-clamp recordings were made with an Axopatch-1D amplifier (Axon Instruments, Burlingame, CA). Patch electrodes (3–7 MΩ) were filled with the following solution (in mM): 9 NaCl, 140 KCl, 1 $MgCl_2$, 10 HEPES buffer, 0.2 EGTA, 10 phosphocreatine, 0.1 leupeptin, 5 K_2-ATP, and 1 Na_3-GTP (pH $\cong$ 7.25).

Received for publication 20 February 1998 and in final form 15 April 1998.

Address reprint requests to Dr. S. H. Chandler, Department of Physiological Science, 2851 Slichter Hall, Los Angeles, CA 90095-1568. Tel.: 310-206-6636; Fax: 310-825-6616; E-mail: schandler@physci.ucla.edu.

0006-3495/98/07/174/09 $2.00

Therefore, during the active phase when SLOW moves the oscillatory solution back through the Hopf point (z is increasing beyond -0.5; Fig. 1 *C*), the system continues in its (Hsiao et al., 1998) (Fig. 2 *A*). Conversely, TIs never exhibited a region of NSR, regardless of protocols used to generate the *I-V* relationship (Fig. 2 *B*). The *I-V* curve of a

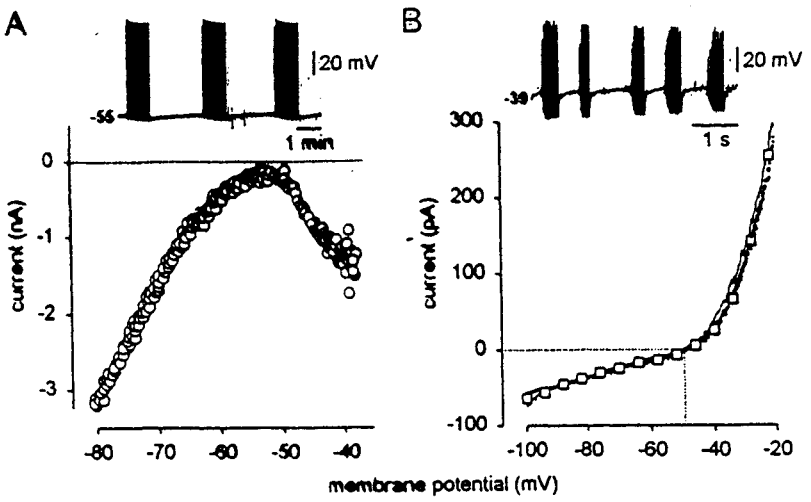

FIGURE 2 The steady-state current-voltage relationship of trigeminal neurons. (*A*) the steady-state *I-V* curve of a TMN in the presence of 10 μM serotonin obtained by a slow voltage ramp protocol (7.5 mV/s). Regenerative inward currents underlying the region of NSR activate at −52 mV. The curve is obscured at potentials more positive than −40 mV due to spike oscillations in unclamped regions of the soma-dendritic membrane. More complete steady-state *I-V* curves for TMNs, obtained in the presence of 10 μM serotonin and 0.5 μM tetrodotoxin, are available (Hsiao et al., 1998). Bursts initiated autonomously in this TMN, because the region of NSR was located in the region of net inward current (*below the zero current axis, dotted line*). Bursting in this TMN is shown in the inset (+0.1 nA holding current). (*B*) Steady-state *I-V* curve in a TI in the presence of 20 μM bicuculline and 5 μM strychnine to block spontaneous inhibitory synaptic noise. Three protocols were used: long-duration voltage step commands (5 s, *open squares*), slow voltage ramps (10 mV/s, *solid line*), and fast voltage ramps (in the presence of 0.5 μM tetrodotoxin to block Na^+ spikes) (100 mV/s, *dots*). The inset shows bursting in this TI (+65 pA holding current) (same cell as in Fig. 3).

FIGURE 3 The behavior of trigeminal neurons in response to current bias and trajectories of burst initiation. (*A*) 10 μM serotonin-induced bursting in this TMN (*middle trace*, −0.2 nA holding current) could be converted to stable quiescent behavior (at −70 mV) by increasing the hyperpolarizing current injection to −0.8 nA (*lower trace*), or to tonic spiking activity by sufficient depolarizing current injection (+0.1 nA, *upper trace*). (*B*) An example of burst initiation in TMNs expanded from *A* (*box*). Note the rapid upswing in voltage trajectory. (*C*) Bursting activity in TIs emerged as the cells were progressively depolarized to potentials near and above spike threshold (−45 mV). This TI's resting potential was −65 mV (not shown). At the quiescent potentials −50 and −47 mV, the bias current was +20 and +25 pA, respectively (*lower traces*). These quiescent states were more depolarized than quiescent potentials in TMNs: −47 (*C*) versus −70 mV (*A*). Intermittent discharge occurred near threshold; bias currents were +30 and +45 pA at near-threshold potentials −45 and −43 mV, respectively (*middle traces*). Bursting occurred when TIs were biased to suprathreshold potentials (−39 mV, +65 pA holding current, *top trace*). This TI was recorded in the presence of 20 μM bicuculline and 5 μM strychnine to block spontaneous inhibitory synaptic noise. (*D*) An example of burst initiation in TIs expanded from *C* (*box*). Note the linear voltage trajectory and growing subthreshold oscillations. Voltage calibration applies to all traces. Time calibrations are separate for *A* and *C*.

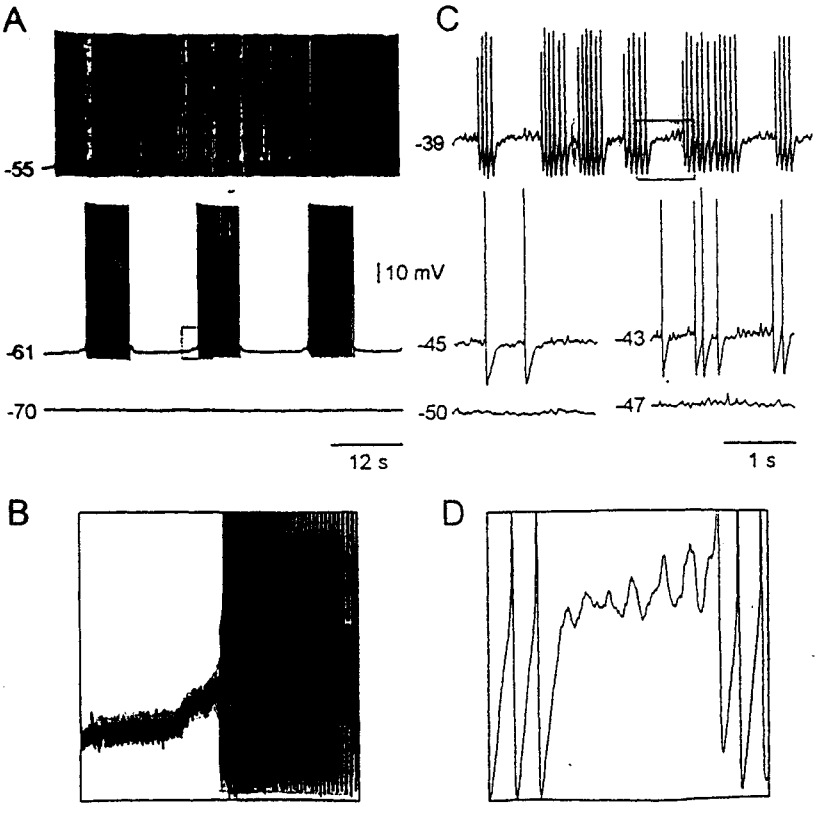

Thalamic Slow Rhythms

Destexhe, Babloyantz, Sejnowski

BiophysJ ('93)

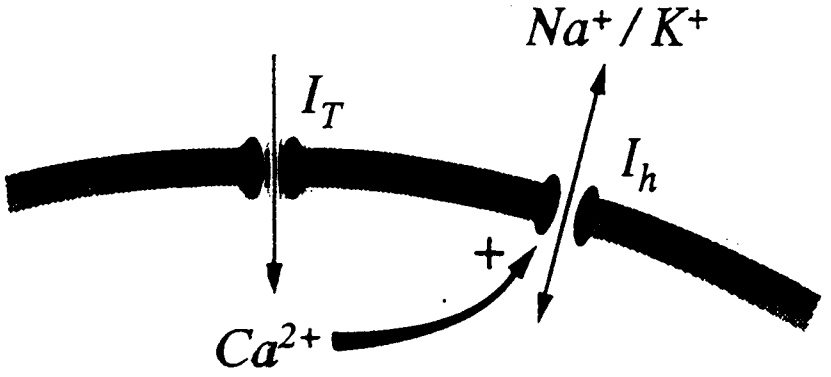

S_2

Slow activ^n gate of I_h is Ca-dependent

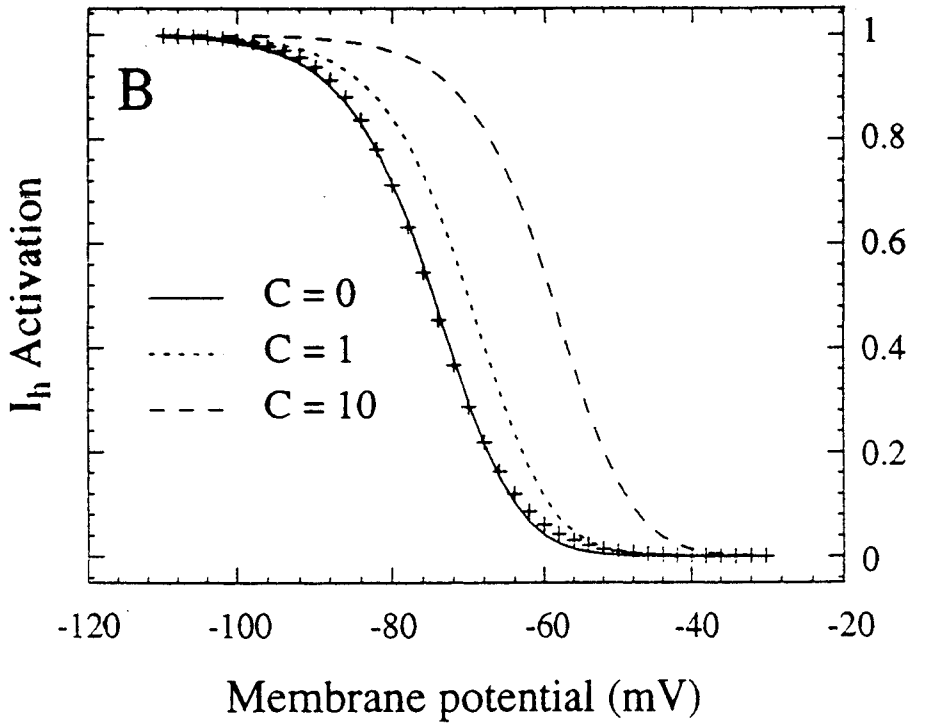

Effect of I_h — on hyperpol^n V-h gate starts at steady state then h_∞ slowly ↑ ⇒ h of I_T reduces needs slowly increase

FIG. 1.

Ca^{2+}-induced shift of the activation function of I_h. A. Schematic diagram illustrating the currents in the model. The low-threshold Ca^{2+} current (I_T) lets Ca^{2+} ions enter the cell; these ions bind to the mixed Na^+/K^+ channel I_h and modify its voltage-dependent properties. B. Direct binding of intracellular Ca^{2+} to I_h channels shifts the voltage-dependence of the current towards positive membrane potentials. $H_\infty(V,[Ca_i])$ is represented as a function of the membrane potential V for different values of $[Ca]_i$. The activation function at resting level of $[Ca]_i$ (solid line - C=0) was estimated from voltage-clamp experiments [31] on TC cells (+ symbols). For increasing concentrations of intracellular Ca^{2+}, the activation function shows progressively larger shifts towards positive membrane potential (dashed lines, C = 1 and C = 10). $C = ([Ca]_i/Ca_c)^2$.

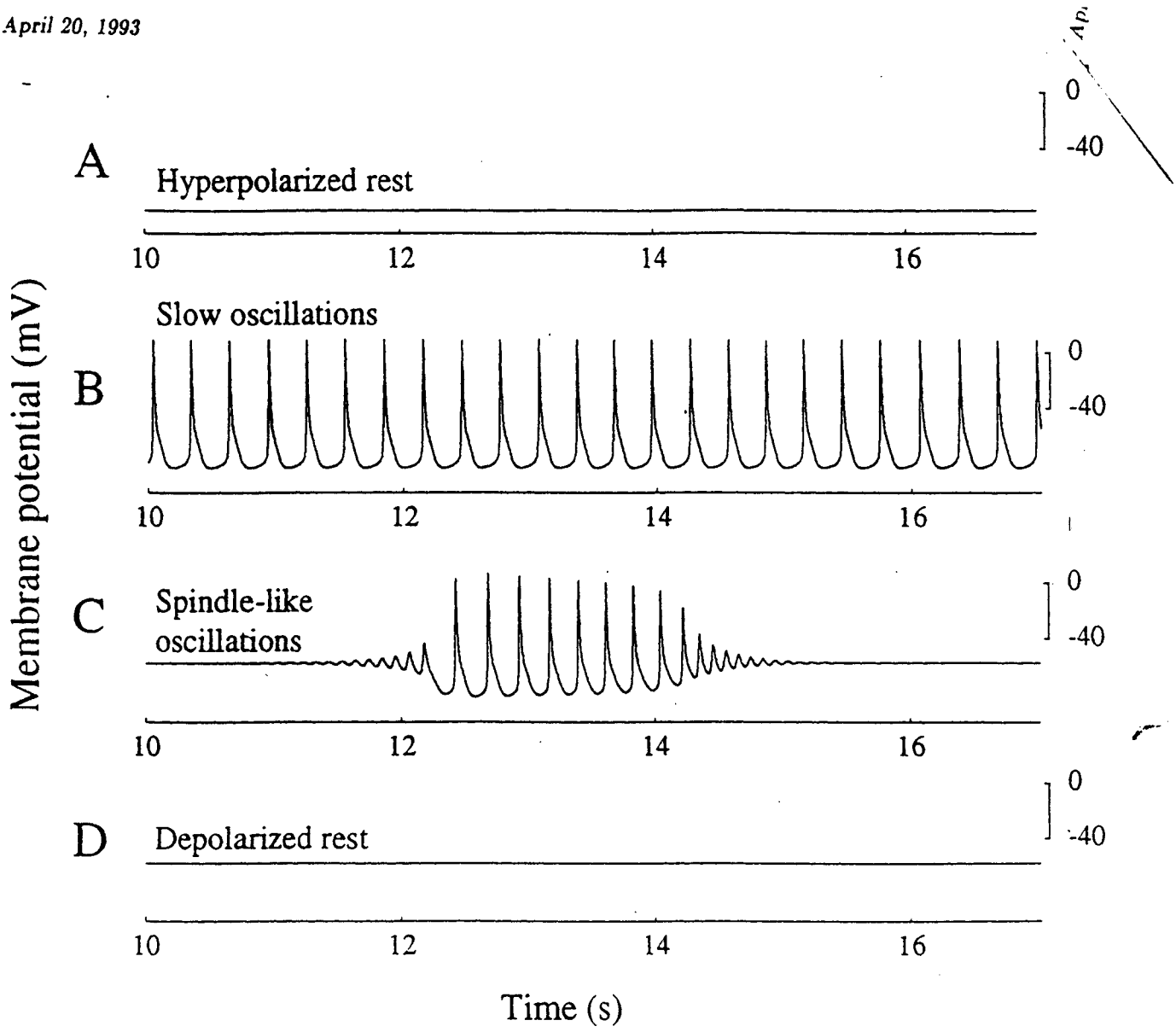

FIG. 3.

Resting states and slow oscillations in the presence of I_T and Ca^{2+}-dependent I_h obtained at four values of the maximal conductance of I_h. A. Hyperpolarized resting state close to -84 mV for $\bar{g}_h$=0. B. Slow oscillations of about 3.5 Hz for $\bar{g}_h$=0.01 mS/cm^2. C. Spindle-like oscillations of about 4-8 Hz for $\bar{g}_h$=0.04 mS/cm^2. D. Depolarized resting state around -58 mV for $\bar{g}_h$=0.11 mS/cm^2. The maximum conductance of I_T was kept fixed at $\bar{g}_{Ca}$=1.75 mS/cm^2.

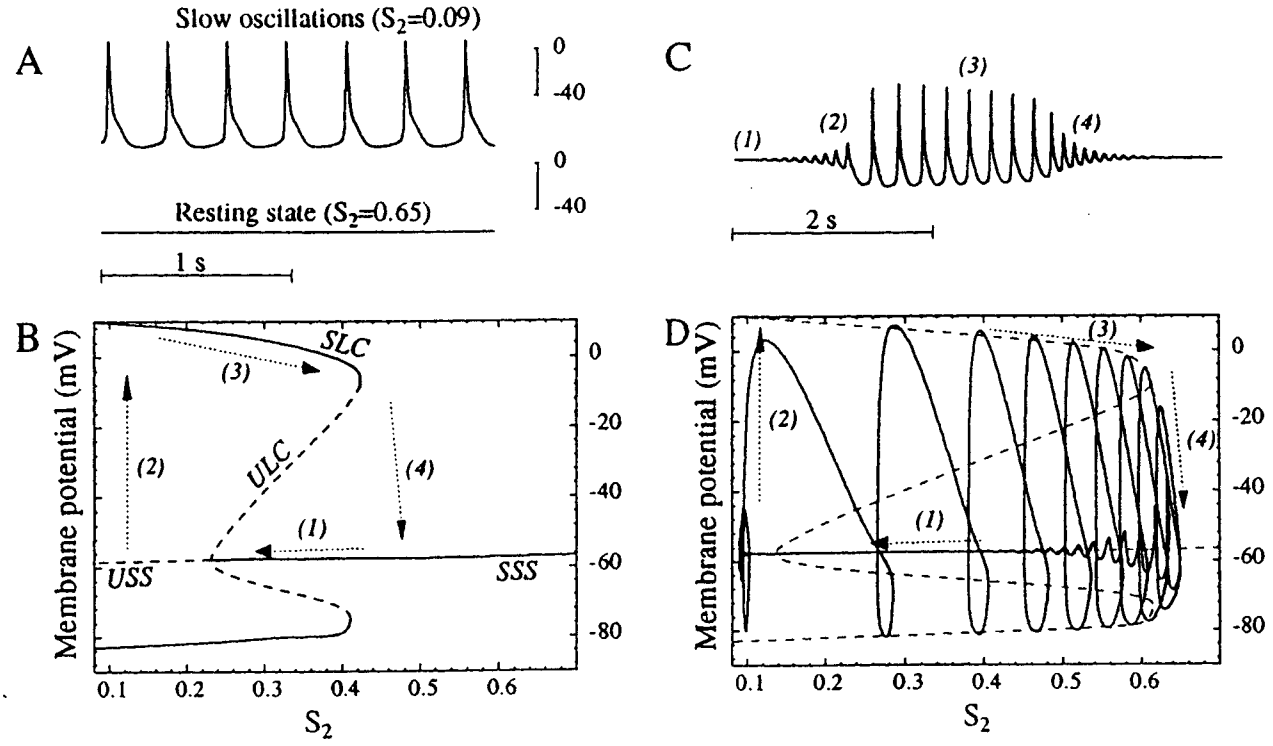

This type of instability may ⇒ resetting behavior !!

FIG. 10.

Singular approximation applied to the Ca^{2+}-dependent model of spindle-like oscillations. A. For extreme values of the slow variable S_2 treated as a parameter, the system exhibits either slow oscillations (S_2=0.09) or a stable stationary state (S_2=0.65). Other parameters are the same as in Fig. 3C. B. Bifurcation diagram of the system as a function of S_2. During the slow oscillations of S_2, the system alternates between a slow oscillatory state and a resting state, tracing a hysteresis loop as shown in the diagram. The order of events underlying the spindle-like sequence are indicated by dotted arrows. Dashed lines represent unstable states (USS: unstable stationary state, ULC: unstable limit cycle), and continuous lines represent stable states (SSS: stable stationary state, SLC: stable limit cycle). C. Corresponding sequence of events in a single cycle of the spindle-like oscillations. D. Trajectories of spindle-like oscillations in the V/S_2 diagram. Dashed lines represent the presumed position of oscillatory and stationary branches and dotted arrows depict the same sequence of events as in B.

Parabolic Bursting

Classic example : ~~Aby~~ Aplysia R-15 neuron — bursting pacemaker

Two examples of bursting oscill^{ns}

Aplysia R-15 "parabolic"

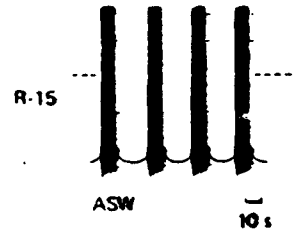

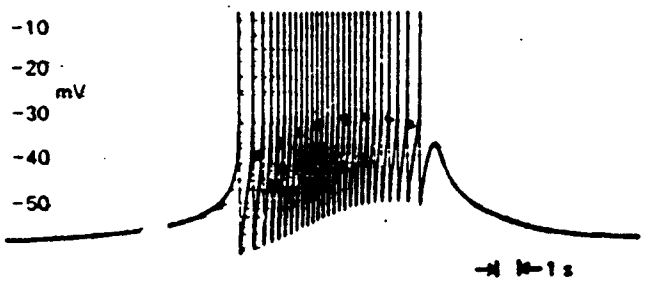

- slow wave – identifiable
  – smooth
- spikes undershoot
- ISI ↑ at start/end
- models since '76

Pancreatic β-cell (whole islet)

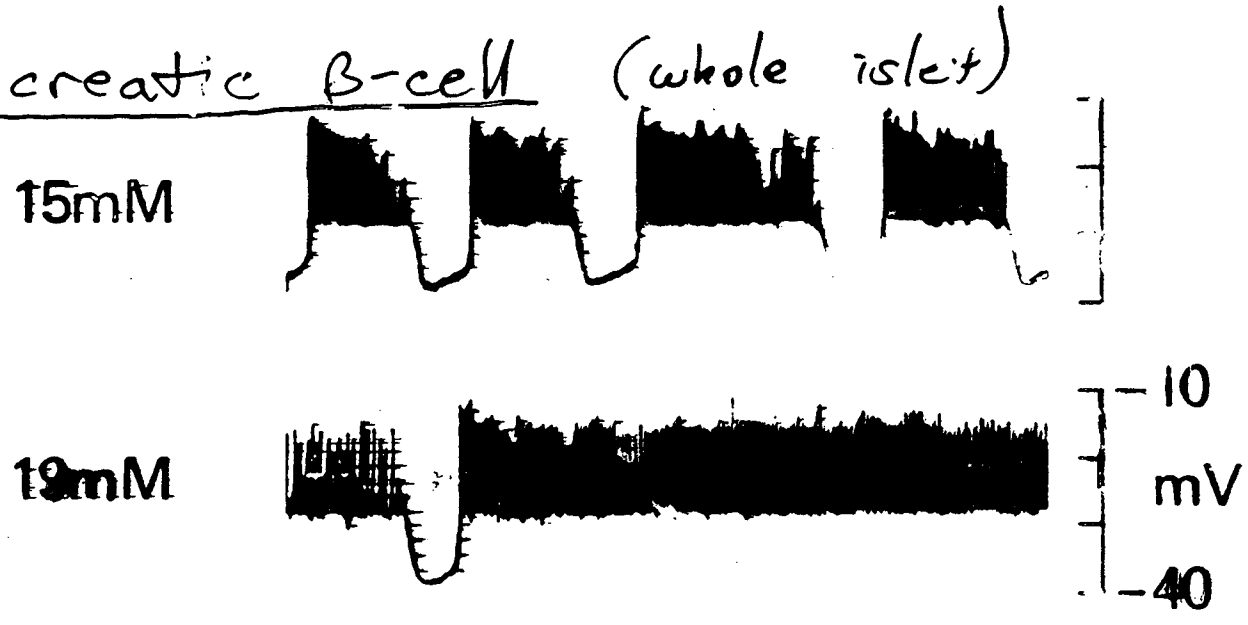

- slow wave? – not smooth
- plateau
- ISI ↑ at end.
- model since '83 – "Chay-Keizer"

Rinzel + Lee (1986)

Analysis of R-15 Parabolic Bursting

Minimal: $\underbrace{I_{Na} + I_{K\text{-}DR}}_{\text{Na- Spikes}} + \underbrace{I_{Ca\text{-}Ca}}_{\text{slow wave}}$

$= \bar{g}_{Ca}\, m_{Ca}\, \frac{1}{K_D + Ca}\,(V - V_{Ca})$

m_{Ca}, Ca slow

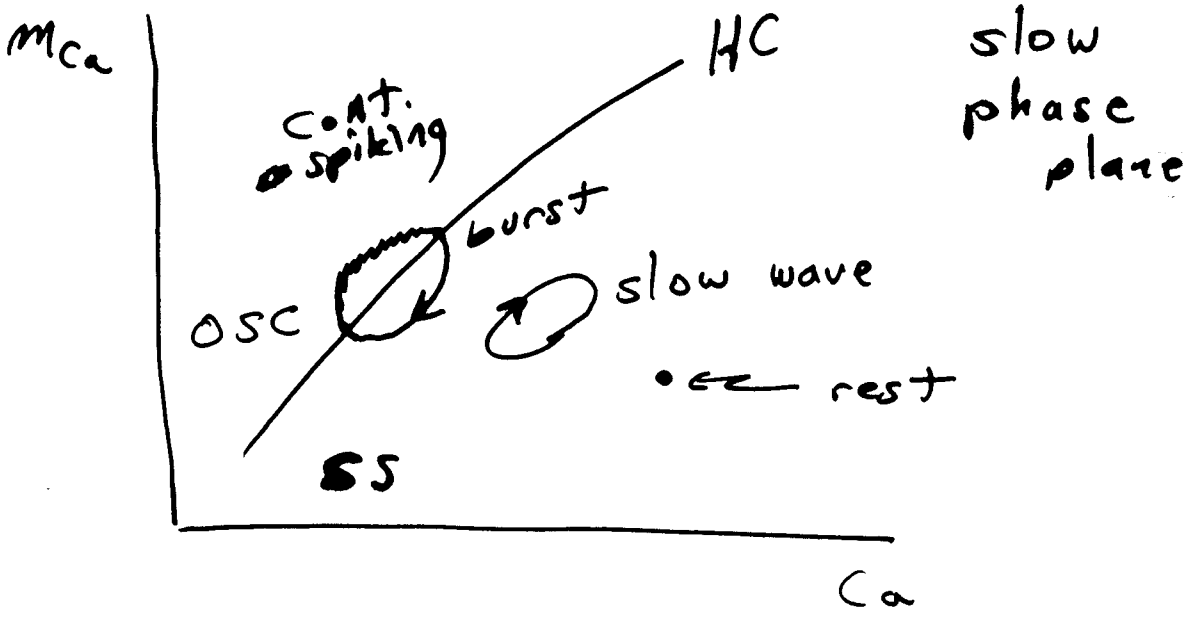

Schematic — as $I_{app}\uparrow$

Note — "resetting" — not w/ brief I_{app}.

"Reduced" - minimal: 3 variables

spiking = "ring"

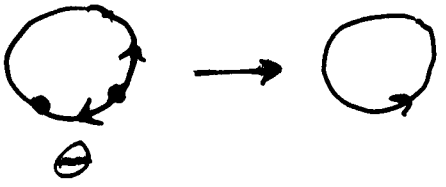

Baer, Rinzel, Carrillo (1994)

model of Aplysia R-15 Bursting Oscillations
Canavier et al J Neurophys 66 (1991) 2107

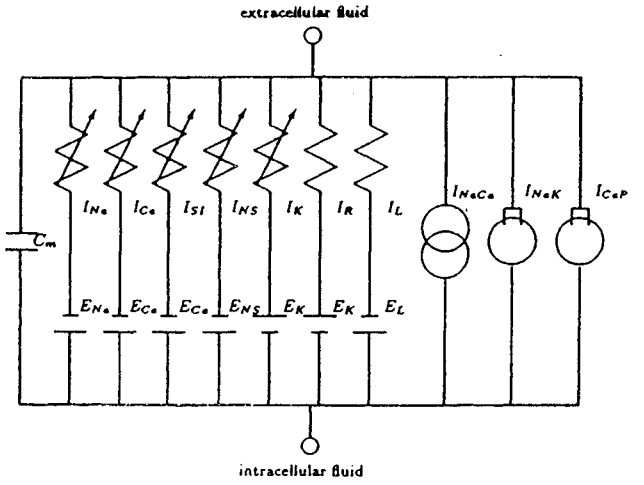

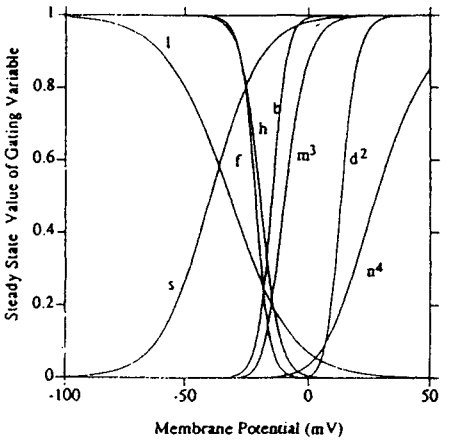

FIG. 2. Gating parameters of the model. Steady-state values of the gating variables are plotted vs. potential. The variables m^3 and h are associated with I_{Na}; n^4 and l with I_K; d^2 and f with I_{Ca}; h with I_{NS}; and s with I_{SI}.

I_{SI} — slow Ca current — Ca-inactiv^{n}.

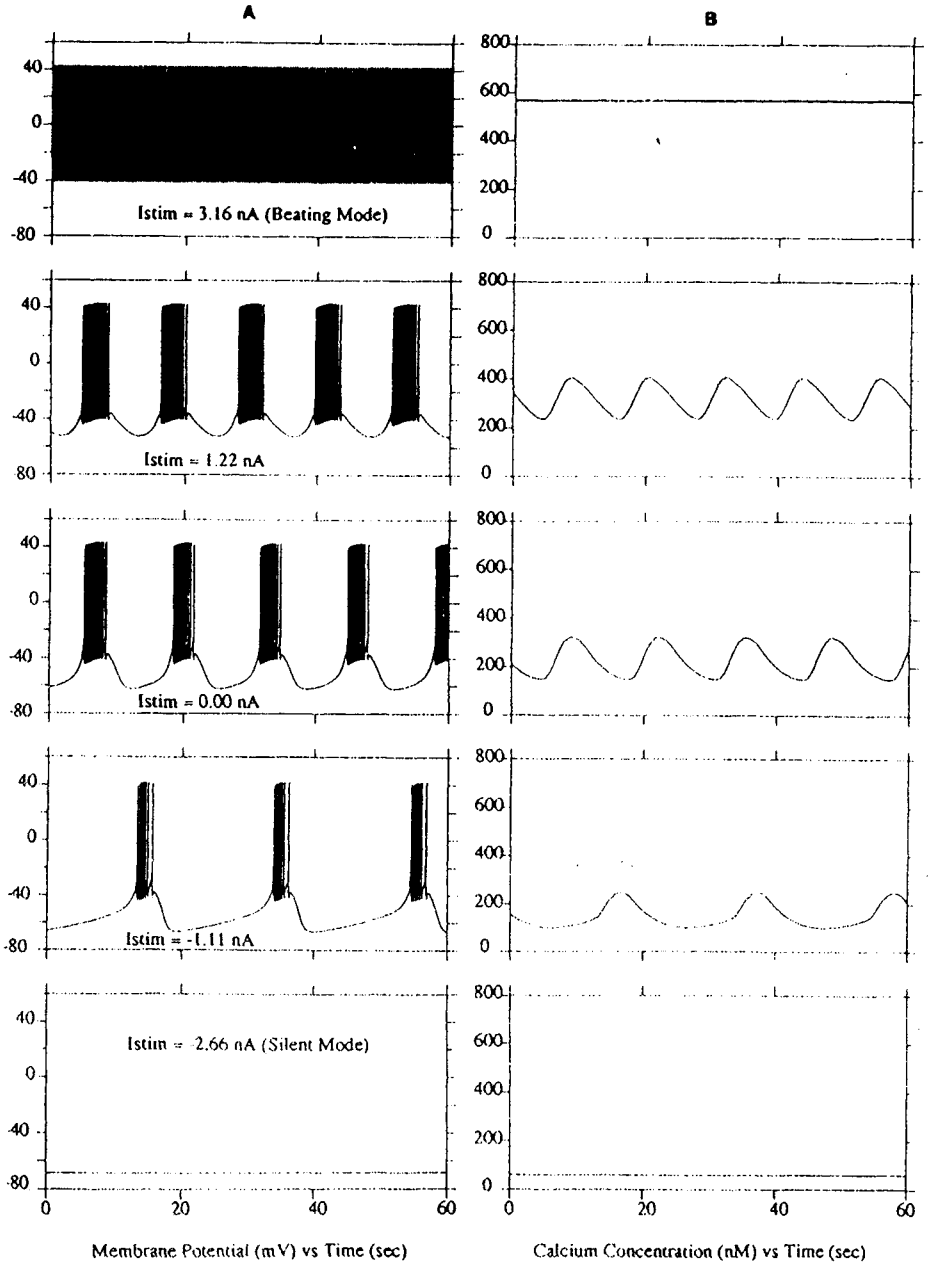

or I_{app} ↑

T_{AP} ↑ T_{SP} ↓

resting → bursting → cont. spiking

$\langle V \rangle$ ↑, V_{min} ↑

FIG. 5. Simulation of different modes of activity as a function of applied current. *A*: membrane potential. *B*: calcium concentration. With hyperpolarizing current (−2.66 nA) the cell is silent, but as the hyperpolarization is reduced, the model generates a bursting rhythm with the frequency, interburst interval, and magnitude of the interburst trough being a function of the applied current. As the depolarizing current increases (3.16 nA), the simulated activity switches from a bursting to a beating mode. Note that a stimulus current of 3.16 nA exactly cancels the current generated by the Na^+-K^+ pump (I_{NaK}).

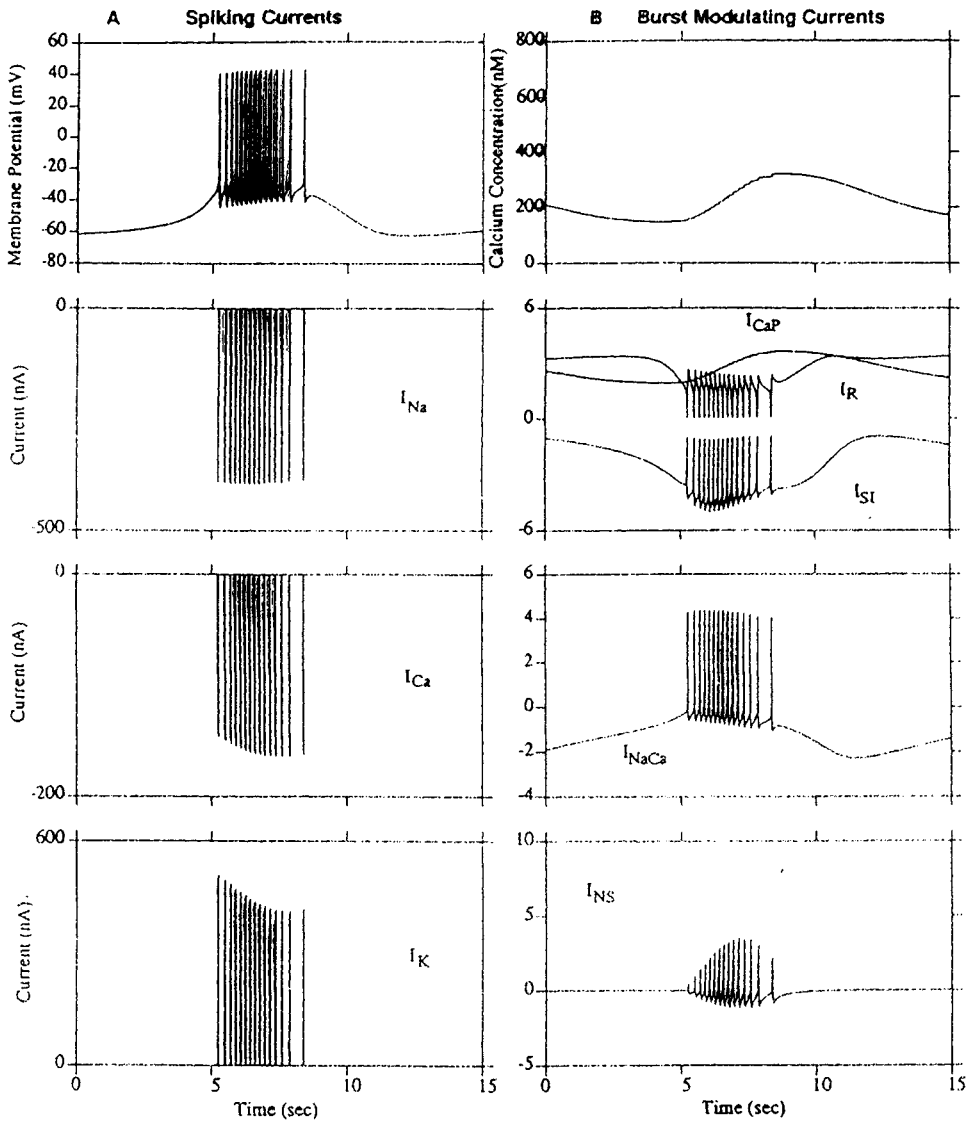

FIG. 8. Membrane currents contributing to the electrical activity. *A*: *top panel* illustrates a burst generated with the same parameters as Fig. 5 ($I_{STIM} = 0$) but shown on an expanded time scale. The large-amplitude currents contributing to the spikes during a burst are plotted below the membrane potential on the same time scale. *B*: corresponding levels of $[Ca]_i$ are shown in the *top panel*, and the low-amplitude currents contributing to the slow oscillations of potential are illustrated below.

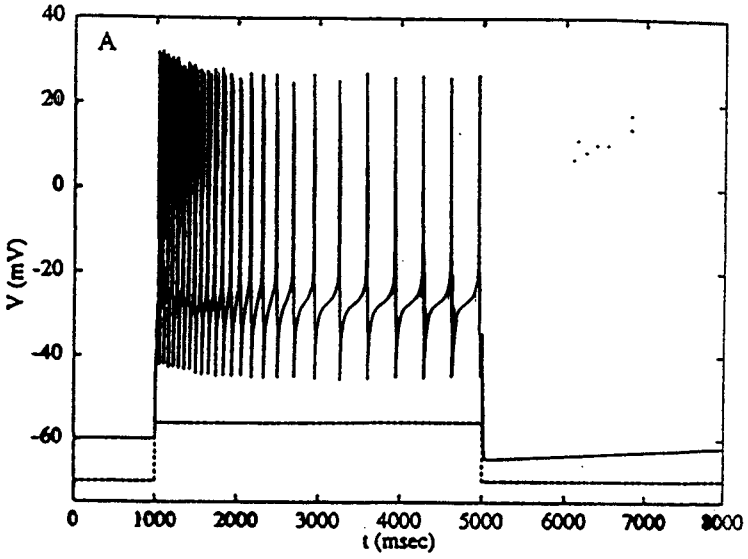

Parabolic Bursting — example in Rinzel-Ermentrout chapter

Fig 11

$$C\dot{V} = -I_{m-l} - I_{k-ca} - I_{ca,s}$$

$$I_{ca,s} = g_{ca-s}\, s\, (V - V_{ca})$$

$$\tau_s \frac{ds}{dt} = \varepsilon \left[s_\infty(V) - s \right]$$

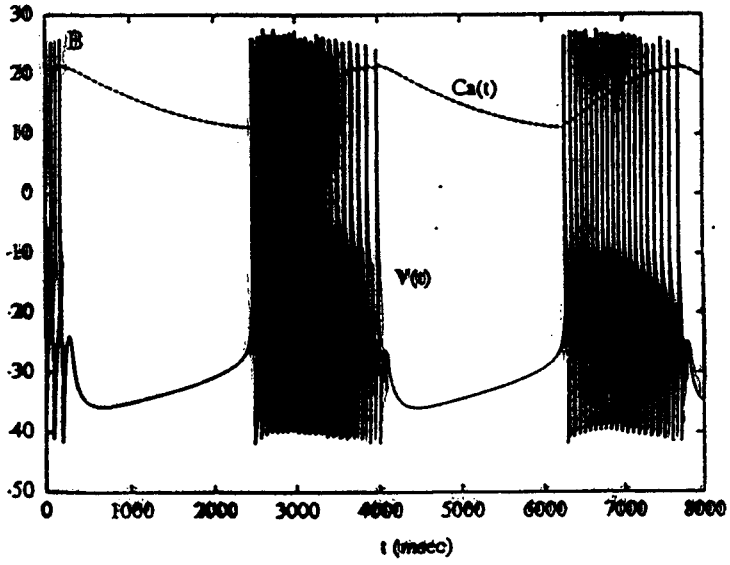

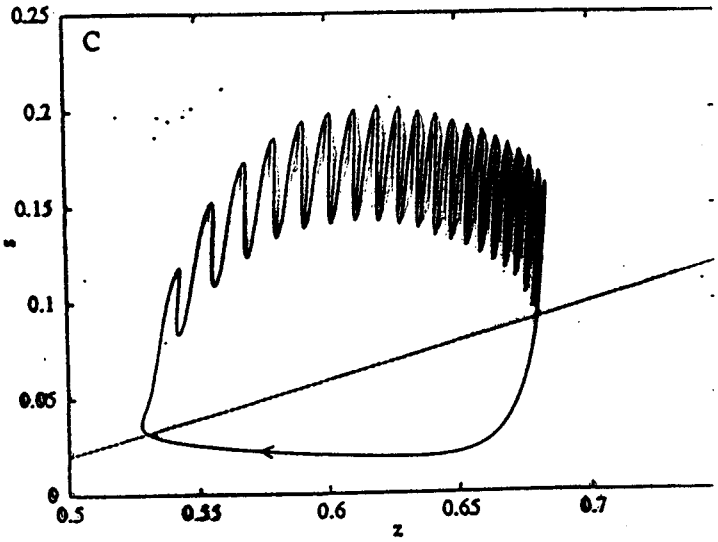

Triangular style bursting.

Example: thalamic relay neuron

(refer to lecture on ~~"Sleeping"~~ thalamic sleep rhythms)

Firing Modes of Thalamic Relay Cell

Rush & Rinzel, 1994

A

(like Jahnsen et al. 1986)

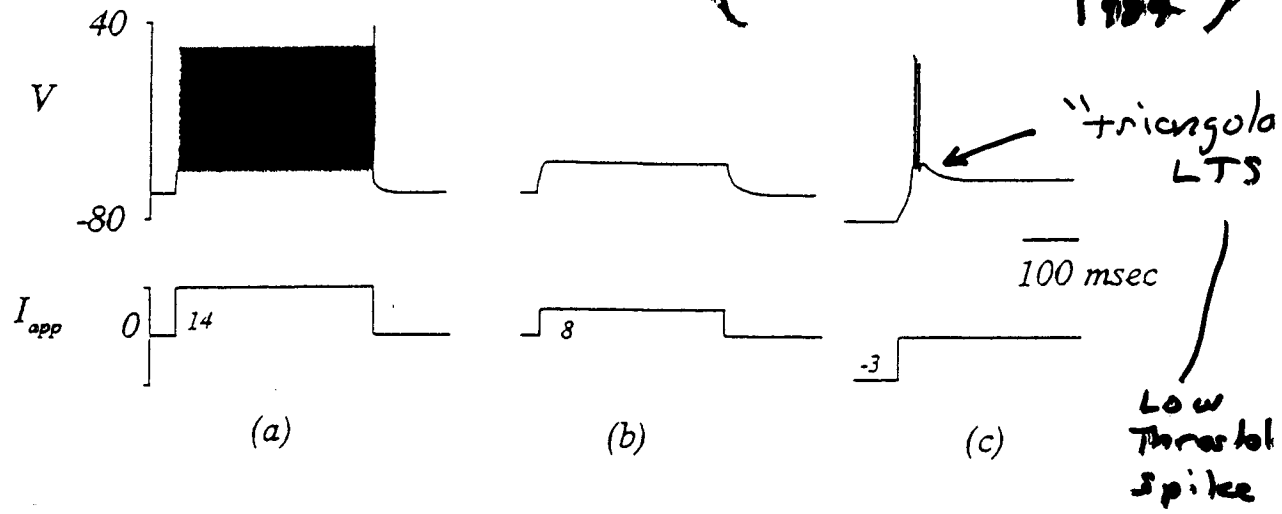

B – Transitions w/ I_{app}

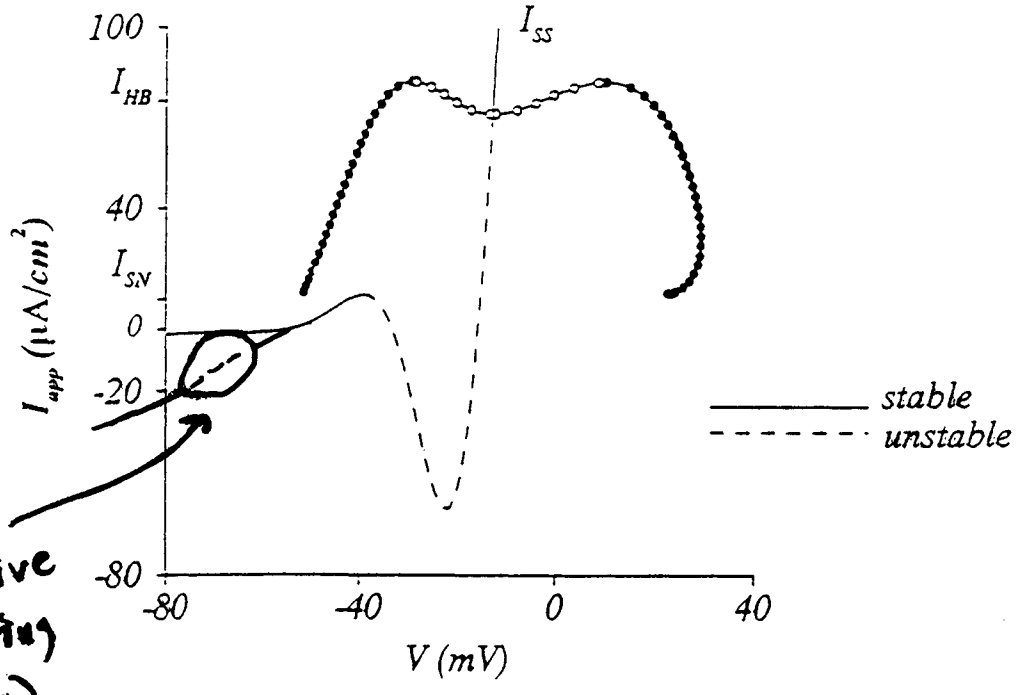

regime of repetitive LTS-bursting (schematic)

Fig. 1 -45-

Fast/Slow Dissection

Rush + Rinzel, Biol. Cybern. (1994)

LTS oscill^n w/o Na-spikes

$I_{app} < 0$

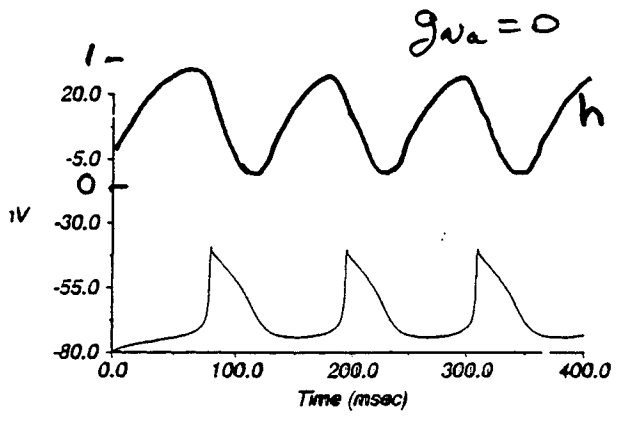

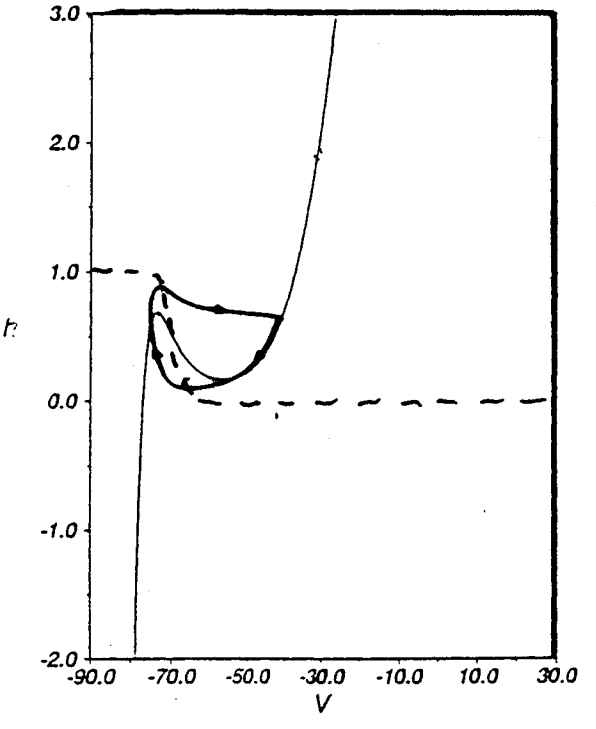

w/ Na-spikes → bursting oscill^n

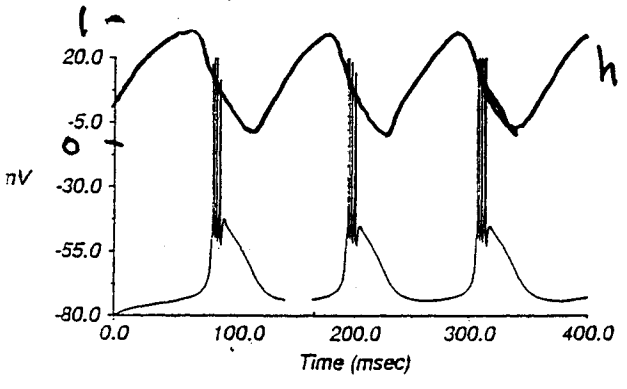

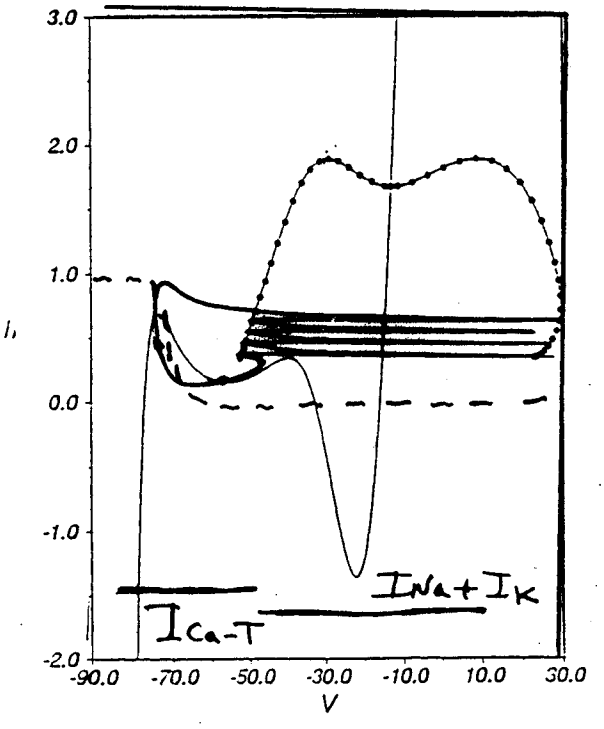

See also McCormick & Huguenard J Neurophys (1992) $+I_h$